

# Geodätisch-geophysikalische Arbeiten in der Schweiz

(Fortsetzung der Publikationsreihe  
«Astronomisch-geodätische Arbeiten in der Schweiz»)

herausgegeben von der

Schweizerischen Geodätischen Kommission  
(Organ der Akademie der Naturwissenschaften Schweiz)

**Dreiundachtzigster Band  
Volume 83**

## **Combined Analysis of Observations from Different Global Navigation Satellite Systems**

Michael Meindl

2011

Adresse der Schweizerischen Geodätischen Kommission:

Institut für Geodäsie und Photogrammetrie  
Eidg. Technische Hochschule Zürich  
ETH Zürich  
8093 Zürich  
Switzerland

Internet: <http://www.sgc.ethz.ch>

ISBN 978-3-908440-27-7

Redaktion des 83. Bandes:  
Dr. M. Meindl, Dr. B. Bürki  
Druck: Print-Atelier ADAG, Zürich

## VORWORT

Herr Michael Meindl hat sich in den letzten sechs Jahren intensiv mit der kombinierten Auswertung von mehreren globalen Satellitennavigationssystemen (GNSS) beschäftigt. Dies ist insbesondere im Hinblick auf das im Aufbau begriffene europäische Galileo und die Modernisierungsprogramme der bestehenden Systeme GPS und GLONASS ein hochaktuelles Thema.

Die Arbeit von Herrn Meindl gliedert sich in drei Teile.

Nach einer Beschreibung des Messprinzips und verschiedener Systeme widmet sich Herr Meindl im ersten Teil sehr ausführlich den vollständigen GNSS-Beobachtungsgleichungen. Dabei wird insbesondere diskutiert, welche Parameter unter welchen Voraussetzungen für die analysierten Systeme identisch und welche verschieden sind. Daraus werden die relevanten systematischen Fehler zwischen verschiedenen GNSS, Frequenzen/Signalen und Empfänger-technologien in sehr übersichtlicher Weise hergeleitet.

Im zweiten Teil hat sich Herr Meindl mit den Konsequenzen der Erweiterung eines klassischen GPS-Programmpaketes unter Verwendung zweier Frequenzen auf die flexible Mehrsystemauswertung der Zukunft auseinandergesetzt. Nach der Darstellung allgemeiner Aspekte wird die entsprechende Realisierung in der Berner Software beschrieben.

Im dritten Teil hat Herr Meindl den Einfluss von verschiedenen Längen des grundlegenden Auswertintervalls (das aus praktischen Gründen in der Regel mit 24 Stunden angenommen wird) auf die Ergebnisse von Einzel- und Mehrsystemauswertungen analysiert. Dafür hat der Autor die Beobachtungen eines globalen GNSS-Netzes von 92 GNSS-Empfängern zu den heute operationell verfügbaren Systemen GPS und GLONASS über drei Jahre verarbeitet. Zunächst werden die grundlegenden Eigenschaften (Anzahl der Beobachtungen, Wiederholungen der Satellitenkonstellation und -geometrie) in den einzelnen Lösungen analysiert. Anschliessend werden auch die Ergebnisse der Auswertung, wie etwa Stationskoordinaten und Satellitenbahnen, verglichen. Herr Meindl zeigt, dass die Kombination der GPS- und GLONASS-Messungen den jeweiligen Einzelsystemlösungen überlegen ist.

Die Schweizerische Geodätische Kommission (SGK) bedankt sich bei der Akademie der Naturwissenschaften Schweiz (ScNAT) für die Übernahme der Druckkosten.

**Prof. Dr. G. Beutler**  
Astronomisches Institut  
Universität Bern

**Prof. Dr. A. Geiger**  
ETH Zürich  
Präsident der SGK

## PREFACE

La présente publication de M. Michael Meindl est dédiée à l'analyse combinée de différents GNSS (Système Global de Navigation par Satellite). Ce sujet de recherche est en particulier important en vue du futur GNSS européen Galileo ainsi que des programmes de modernisation des systèmes existants GPS et GLONASS.

Le travail de M. Meindl se divise en trois parties.

Après la description du principe de mesure et de plusieurs systèmes, la première partie est consacrée au développement de l'équation de l'observation GNSS dans sa pleine extension. L'identification des paramètres identiques entre les systèmes considérés et ceux qui diffèrent fait l'objet d'une attention particulière. De cette discussion résulte une liste de biais entre les différents systèmes, fréquences/signaux et techniques d'acquisition des récepteurs.

Dans la seconde partie, sur la base des résultats de la première partie, M. Meindl expose les raisons de faire évoluer un logiciel GNSS capable de traiter des données GPS double fréquence uniquement vers un logiciel flexible capable de traiter de manière combinée des données de plusieurs GNSS. Une première section décrit certains aspects stratégiques d'un tel logiciel ainsi que son architecture. Une seconde section se concentre plus spécifiquement sur l'extension réalisée sur le logiciel Bernese.

Dans la troisième partie, M. Meindl a analysé l'influence de la longueur de l'intervalle de temps considéré dans le traitement des données (usuellement fixée à 24 heures pour des raisons pratiques) sur les résultats de solutions mono- et multi-GNSS. Les données d'un réseau global de 92 stations capables d'observer les deux GNSS opérationnels à ce jour, c'est-à-dire GPS et GLONASS, ont été traitées dans ce sens, sur une période de trois ans. Dans un premier temps, l'auteur analyse les caractéristiques essentielles des solutions (telles que le nombre d'observations, la vitesse de répétition des constellations et leur géométrie). Suit l'analyse des résultats tels que par exemple les coordonnées des stations ou les orbites des satellites. L'auteur démontre que l'analyse combinée de données GPS et GLONASS prévaut sur celle de données d'un système unique.

La Commission Géodésique Suisse (CGS) est reconnaissante envers l'Académie Suisse des Sciences Naturelles (ScNAT) pour avoir pris à sa charge les coûts d'impression du présent manuscrit.

**Prof. Dr. G. Beutler**  
Institut d'astronomie  
Université de Berne

**Prof. Dr. A. Geiger**  
ETH Zürich  
Président de la CGS

## FOREWORD

This publication of Mr. Michael Meindl focuses on the combined analysis of different Global Navigation Satellite Systems (GNSS). The topic is very relevant regarding the upcoming new European Galileo and the modernization programs for established systems GPS and GLONASS.

Mr. Meindl's work is divided into three parts.

After a description of the measurement principle and several systems the author develops in the first part the fully extended GNSS observation equation. Special attention is paid to which of the parameters are identical if different systems are analyzed and which of the parameters differ. From this discussion the author extracts the relevant biases between systems, frequencies/signals, and receiver tracking technologies.

In the second part Mr. Meindl draws the conclusion from the first part if a GNSS software package shall be extended from a "dual-frequency GPS-only" processing tool to a fully flexible multi-system analysis software. In a first section some strategic and design aspects are discussed whereas in a second section the realization of the extension is described in the case of the Bernese Software package.

In the third part Mr. Meindl analyzes the influence of different lengths of the basic processing interval (usually set to 24 hours for practical reasons) on the results of single- and multi-system solutions. For that purpose the author processed the observations from a global network of 92 tracking stations considering both currently operational available GNSS, namely GPS and GLONASS, for an interval of three years. First of all the author analyzes the basic characteristics (number of observations, repetition rate of the satellite constellation and geometry) of the different solutions. Afterwards, the author compares the results, e.g., for station coordinates and satellite orbits. He demonstrates that the combined GPS/GLONASS solution is preferable with respect to the single-system solutions.

The Swiss Geodetic Commission (SGC) is grateful to the Swiss Academy of Sciences (ScNAT) for covering the printing costs of this volume.

**Prof. Dr. G. Beutler**  
Astronomical Institute  
University of Bern

**Prof. Dr. A. Geiger**  
ETH Zürich  
President of SGC



# Contents

<b>List of Figures</b>	<b>v</b>
<b>List of Tables</b>	<b>vii</b>
<b>Frequently Used Acronyms</b>	<b>ix</b>
<b>1 Introduction</b>	<b>1</b>
<b>1 Global Navigation Satellite Systems</b>	<b>5</b>
<b>2 An Introduction to Global Navigation Satellite Systems</b>	<b>7</b>
2.1 Navigation Principles . . . . .	7
2.2 System Segments and Configuration . . . . .	9
2.2.1 Space Segment . . . . .	9
2.2.2 Control Segment . . . . .	10
2.2.3 User Segment . . . . .	11
2.3 Satellite Orbits and Orbital Motion . . . . .	12
2.3.1 The Equations of Motion . . . . .	12
2.3.2 The Walker Constellation . . . . .	15
2.4 Global Navigation Satellite Systems in Comparison . . . . .	18
2.4.1 Global Positioning System (GPS) . . . . .	19
2.4.2 Global'naya Nawigatsionnaya Sputnikowaya Sistema (GLONASS)	22
2.4.3 Galileo . . . . .	25
2.4.4 Compass Navigation Satellite System (CNSS) . . . . .	27
2.4.5 Comparison of GPS, GLONASS, and Galileo . . . . .	28
2.5 Motivation and Benefits of Using Different GNSS . . . . .	31
2.6 Institutions Relevant to this Work . . . . .	33
2.6.1 The International GNSS Service . . . . .	33
2.6.2 The International Laser Ranging Service . . . . .	35
2.6.3 The Center for Orbit Determination in Europe . . . . .	35
<b>3 GNSS Data Processing</b>	<b>37</b>
3.1 Fundamental Observation Equations . . . . .	37
3.1.1 Code Pseudorange Observation Equation . . . . .	38
3.1.2 Phase Observation Equation . . . . .	40

3.1.3	Satellite and Receiver Positions . . . . .	42
3.2	Linear Combinations of Observations . . . . .	42
3.3	Differences of Observations . . . . .	43
3.3.1	Single Differences . . . . .	45
3.3.2	Double Differences . . . . .	48
3.3.3	Triple Differences . . . . .	50
3.4	Biases in GNSS Data Processing . . . . .	50
3.4.1	The Single-difference Bias Term . . . . .	50
3.4.2	Code Biases . . . . .	52
3.4.3	The Conventional Differential Code Biases . . . . .	56
3.4.4	Phase Biases . . . . .	57
3.4.5	Biases in GNSS Data Analysis: A Summary . . . . .	58
3.5	Least-squares Adjustment in Overview . . . . .	59
3.5.1	Parameter Pre-elimination . . . . .	62
3.5.2	Sequential Least-squares Adjustment . . . . .	63
3.5.3	Constraining Parameters . . . . .	63
<b>II</b>	<b>Realizing a Multi-GNSS Analysis Software for Scientific Purposes</b>	<b>65</b>
<b>4</b>	<b>Concepts and Design</b>	<b>67</b>
4.1	The Bernese GPS Software . . . . .	67
4.1.1	Development History . . . . .	67
4.1.2	Main Characteristics of Version 5 . . . . .	68
4.1.3	Structure and Organization . . . . .	69
4.2	Requirements for a Multi-GNSS Software . . . . .	71
4.2.1	Scientific Requirements . . . . .	71
4.2.2	Technical Requirements . . . . .	73
4.3	Design Principles and Software Architecture . . . . .	74
4.3.1	Modularization . . . . .	75
4.3.2	Independence of External Formats . . . . .	76
4.3.3	Flexibility and Expandability . . . . .	76
<b>5</b>	<b>Practical Realization</b>	<b>79</b>
5.1	Initial Situation . . . . .	79
5.2	Software Implementations . . . . .	80
5.2.1	Harmonization and Generalization of Observation Handling . . . . .	80
5.2.2	Dynamic Memory Management and Removal of Fixed Limits . . . . .	82
5.2.3	Redesign of File Formats . . . . .	82
5.2.4	Source Code Modernization . . . . .	83
5.2.5	Secondary Issues . . . . .	84
5.3	Summary . . . . .	85

<b>III</b>	<b>Combined Analysis of Observations from GPS and GLONASS</b>	<b>87</b>
<b>6</b>	<b>Setup of Experiments</b>	<b>89</b>
6.1	Motivation . . . . .	89
6.2	Design of the Study . . . . .	90
6.2.1	Data Basis . . . . .	90
6.2.2	Characteristics of Computed Solutions . . . . .	93
6.2.3	Data Processing . . . . .	94
6.3	Summary and Key Figures . . . . .	99
6.4	Geometry-induced Variations in the Observation Material . . . . .	100
<b>7</b>	<b>Results and Discussion</b>	<b>105</b>
7.1	Station Coordinates . . . . .	105
7.1.1	Assessment of Coordinate Time Series . . . . .	105
7.1.2	Coordinate Consistency . . . . .	107
7.1.3	Coordinate Repeatabilities . . . . .	108
7.1.4	Periodic Variations in the Coordinate Residuals . . . . .	109
7.2	Orbits and Geocenter . . . . .	110
7.2.1	Overlap Differences at Session Boundaries . . . . .	111
7.2.2	Periodic Variations in the Overlap Differences . . . . .	114
7.2.3	Geocenter Coordinates . . . . .	115
7.2.4	Error Characteristics of Orbital Parameters . . . . .	117
7.3	Earth Rotation Parameters . . . . .	118
7.4	Orbit Validation with Satellite Laser Ranging . . . . .	123
<b>8</b>	<b>Summary and Conclusions</b>	<b>125</b>
<b>IV</b>	<b>Appendices</b>	<b>129</b>
<b>A</b>	<b>Tables</b>	<b>131</b>
<b>B</b>	<b>Figures</b>	<b>137</b>
	<b>Bibliography</b>	<b>143</b>



# List of Figures

2.1	Observer position represented as intersecting spherical surfaces. . . . .	7
2.2	Observer position represented as intersecting hyperbolic surfaces. . . . .	8
2.3	Division of near Earth space in orbital regions. . . . .	10
2.4	Satellites from three different GNSS. . . . .	11
2.5	The six orbital elements $a, e, i, \Omega, \omega, u_0$ . . . . .	13
2.6	Walker 56°:27/3/1 constellation. . . . .	16
2.7	Orbital plane occupancy for a Walker 56°:27/3/1 constellation. . . . .	17
2.8	Number of visible satellites and PDOP averaged over one day. . . . .	17
2.9	Orbital plane occupancy of GPS satellites, December 31, 2010. . . . .	20
2.10	GPS satellite orbits, December 31, 2010. . . . .	20
2.11	Ground tracks of the GPS satellites. . . . .	21
2.12	Orbital plane occupancy of GLONASS satellites, December 31, 2010. . . . .	23
2.13	GLONASS satellite orbits, December 31, 2010. . . . .	23
2.14	Ground tracks of the GLONASS satellites. . . . .	24
2.15	Ground tracks for a simulated nominal Galileo constellation. . . . .	26
2.16	Simulated Compass satellite orbits. . . . .	28
2.17	Visibility and PDOP for satellites above 25° for one day. . . . .	31
2.18	Mean daily PDOP for a GPS-only solution and mean PDOP improvement if GLONASS and Galileo are added. . . . .	32
2.19	PDOP amplitude spectra for single- and multi-GNSS solutions. . . . .	33
3.1	Observation configuration for 2 stations tracking 2 satellites at 2 epochs. . . . .	44
3.2	The SD bias term. . . . .	51
3.3	Receiver code ISB. . . . .	55
4.1	Flow chart of a standard processing sequence in the BSW. . . . .	70
4.2	Software design diagram. . . . .	75
5.1	Development of the BSW and programming language. . . . .	80
5.2	Observation selection in the BSW. . . . .	85
6.1	Network of tracking stations and available GPS/GLONASS observations in percent. . . . .	91
6.2	Number of tracking stations used in the data processing. . . . .	92
6.3	Number of satellites used in the data processing. . . . .	92
6.4	Flow chart of the processing steps to set up the NEQ systems. . . . .	97

6.5	Number of observations per satellite (in units of 1000). . . . .	101
6.6	Number of observations per satellite relative to the mean number of observations per satellite (in percent). . . . .	102
6.7	Stacked amplitude spectra of available observations in percent (relative to the mean number of observations per satellite). . . . .	103
7.1	Time series of coordinates (blue) for station Funchal, Portugal, and FODITS model (red) for all four solutions (session length DAY). . . . .	106
7.2	Stacked amplitude spectra of coordinate residuals for session length DAY. . . . .	110
7.3	Orbit overlap differences in radial, along-track, and cross-track directions (in cm). . . . .	111
7.4	3-D position overlap differences w.r.t. the elevation $\beta_0$ of the Sun above the orbital plane (based on single-system solutions, session length DAY). . . . .	113
7.5	Stacked amplitude spectra of 3-D position overlap differences for all four session lengths (single-system solutions). . . . .	114
7.6	Geocenter coordinates derived from GPS and GLONASS observations and elevation $\beta_0$ of the Sun above the orbital planes (session length DAY). . . . .	116
7.7	Amplitude spectra of GCC parameters for session length DAY. . . . .	116
7.8	RMS errors of 6 orbit parameters ( $a, D_0, Y_0, X_0, X_c, X_s$ ) for GLONASS satellite R20; elevation $\beta_0$ of the Sun above the orbital plane (GLONASS-only solution, 24-hour session length). . . . .	119
7.9	Difference of ERPs to IERS C04 for all solutions (session length LNG). . . . .	122
7.10	RMS errors of SLR range residuals for 2 GPS satellites and 4 GLONASS satellites observed by station Zimmerwald. . . . .	124
B.1	Stacked amplitude spectra of 3-D position overlap differences for all four session lengths (solutions CMB and NEQ). . . . .	137
B.2	Stacked amplitude spectra of GPS-only orbit overlap differences in radial (R), along-track (A), and cross-track (C) directions. . . . .	138
B.3	Stacked amplitude spectra of GLONASS-only orbit overlap differences in radial (R), along-track (A), and cross-track (C) directions. . . . .	138
B.4	RMS errors of the 6 orbital elements ( $a, e, i, \Omega, \omega, u_0$ ) and elevation $\beta_0$ of the Sun above the orbital plane (satellite R20, GLONASS-only solution, 24-hours session length). . . . .	139
B.5	RMS errors of the 6 orbital elements ( $a, e, i, \Omega, \omega, u_0$ ) and elevation $\beta_0$ of the Sun above the orbital plane (satellite G06, GPS-only solution, 24-hours session length). . . . .	140
B.6	RMS errors of the 5 dynamical parameters ( $D_0, Y_0, X_0, X_c, X_s$ ) and elevation $\beta_0$ of the Sun above the orbital plane (satellite G06, GPS-only solution, 24-hours session length). . . . .	141
B.7	Difference of ERPs to IERS C04 (from top: X-pole, Y-pole, UT1-UTC) for session lengths GPS and GLO. . . . .	142

# List of Tables

2.1	Accelerations acting on a GNSS satellite and net orbit error after one day.	14
2.2	Important parameters of GPS, GLONASS, and Galileo. . . . .	29
3.1	Properties of LCs and resulting conditions for the coefficients. . . . .	43
3.2	Maximum ambiguity initialization error for combinations of observations from GPS, GLONASS, and Galileo to ensure a SD bias below 0.1 cycles. .	52
3.3	Examples of DCB sets for a satellite. . . . .	54
3.4	Examples of DCB sets for a multi-GNSS receiver. . . . .	55
3.5	Factors for satellite-specific DCB corrections for the undifferenced observations C1, P1, C2, P2, and X2. . . . .	57
3.6	Factors for receiver-specific DCB corrections for the undifferenced observations C1, P1, C2, P2, and X2 for GPS (G) and GLONASS (R). . . . .	57
5.1	Number of programs, subroutines, and modules in BSW Versions 5 and 6.	84
6.1	Session identifiers, characteristics, and resulting number of sessions. . . . .	93
6.2	Solution identifiers and characteristics. . . . .	94
6.3	Processing details. . . . .	96
6.4	Average runtime requirement of the processing parts. . . . .	99
6.5	Averaged processing statistics for one session. . . . .	100
6.6	Main periods of the variations in the processed observation data. . . . .	103
7.1	Total number of detected events in the coordinate time series. . . . .	105
7.2	RMS errors of Helmert transformations between different solutions. . . . .	107
7.3	Median of station repeatabilities in North-, East-, Up-direction, and total (in mm). . . . .	108
7.4	Mean observed and expected improvement of coordinate repeatability. . .	109
7.5	Used satellites, planes, and maximum elevation $\beta_0$ of the Sun above the orbital plane. . . . .	111
7.6	Mean orbit 3-D position overlap difference (in cm). . . . .	112
7.7	Standard deviations of orbit overlap differences for GPS (in cm). . . . .	113
7.8	Standard deviations of orbit overlap differences for GLONASS (in cm). . .	113
7.9	Mean of X- and Y-pole differences w. r. t. IERS C04 (in $\mu\text{as}$ ). . . . .	120
7.10	Standard deviations of X- and Y-pole differences w. r. t. IERS C04 (in $\mu\text{as}$ ). .	120
7.11	Number of SLR measurements (station Zimmerwald). . . . .	123

*List of Tables*

---

A.1	Bernese GPS Software Version 6 program overview. . . . .	131
A.2	Tracking stations and data completeness. . . . .	134

# Frequently Used Acronyms

AC	Analysis center
ACC	Analysis center coordinator
AIUB	Astronomical Institute of the University of Bern
ANTEX	Antenna exchange format
ARP	Antenna reference point
ASCII	American Standard Code for Information Interchange
BKG	Bundesamt für Kartographie und Geodäsie
BPE	Bernese Processing Engine
BSW	Bernese GPS Software
C/A-code	Coarse/acquisition code
CB	Code bias
CDMA	Code division multiple access
CNSS	Compass Navigation Satellite System
CODE	Center for Orbit Determination in Europe
COM	Center of mass
DC	Data center
DCB	Differential code bias
DD	Double difference
DoD	U.S. Department of Defense
DOF	Degree of freedom
EC	European Commission
EPN	European permanent network
ERP	Earth rotation parameter
ESA	European Space Agency
EU	European Union
FDMA	Frequency division multiple access
FOC	Full operational capability
GAST	Greenwich apparent sidereal time
GCC	Geocenter coordinate
GEO	Geostationary Earth orbit
GIOVE	Galileo In-Orbit Validation Element

## *Frequently Used Acronyms*

---

GLONASS	Global'naya Nawigatsionnaya Sputnikowaya Sistema or Global Navigation Satellite System
GNSS	Global Navigation Satellite System
GPS	Global Positioning System
GSO	Geosynchronous orbit
GUI	Graphical user interface
IAG	International Association of Geodesy
IAPG	Institut für Astronomische und Physikalische Geodäsie
ICB	Inter-code bias
IERS	International Earth Rotation and Reference Systems Service
IFB	Inter-frequency bias
IGS	International GNSS Service (formerly International GPS Service for Geodynamics)
ILRS	International Laser Ranging Service
IONEX	Ionosphere map exchange format
IOV	In-orbit validation
ISB	Inter-system bias
ITRF	International Terrestrial Reference Frame
ITU	International Telecommunication Union
LC	Linear combination
LEO	Low Earth orbit
LLR	Lunar laser ranging
LSE	Least-squares estimation
MEO	Medium Earth orbit
MP	Multipath
NAVSTAR	Navigational Satellite Timing and Ranging
NEQ	Normal equation
O-C	Observed minus computed
OOP	Object-oriented programming
P-code	Precise or protected code
PB	Phase bias
PCO	Phase center offset
PCV	Phase center variation
PDOP	Position dilution of precision
PR	Pseudorange
PRN	Pseudorandom noise
RHCP	Right-handed circularly polarized
RINEX	Receiver-independent exchange format

RMS	Root mean square (error)
SBAS	Space-based augmentation system
SD	Single difference
SINEX	Solution-independent exchange format
SLR	Satellite laser ranging
SNR	Signal-to-noise ratio
SP3	Standard product 3 orbit format
SV	Space vehicle
SVN	Space vehicle number
TD	Triple difference
TUM	Technische Universität München
U.S.	United States (of America)
UNB	University of New Brunswick
USSR	Union of Soviet Socialist Republics
VMF	Vienna mapping function
ZD	Zero difference



# 1 Introduction

Global Navigation Satellite Systems (GNSS) allow it to determine instantaneously the position and the velocity of an observer in an accurate, inexpensive way anywhere on or near the Earth's surface. GNSS are not only used in military and commercial, but also in a broad spectrum of scientific applications. GNSS revolutionized the field of satellite geodesy and became an indispensable tool, in particular in geosciences, during the last two decades.

Today, the U.S. American Global Positioning System (GPS) is the best-established representative of these satellite systems. Its development started in 1973 and the first satellite was launched into orbit in 1978. In 1995, full operational capability (FOC) was declared with a constellation of 24 active satellites. From the beginning, GPS had a strong impact on science and society. Several improvements have been implemented to the GPS service over the last years to meet growing military, civil, and commercial needs.

The Global'naya Nawigatsionnaya Sputnikowaya Sistema (GLONASS) is Russia's counterpart to GPS. Its development started in the mid 1970s. The first satellite was launched in 1982 and FOC was officially declared in 1993 with only 12 satellites in orbit. The nominal constellation of 24 spaceborne satellites was reached in 1996. The number of active satellites did, however, continuously decline shortly thereafter due to funding problems and due to the short lifetime of the first satellites. After a minimum of only seven active GLONASS satellites in space in 2001, the Russian Federation decided to rebuild the system. Several new satellites were launched in recent years. As of mid 2011, there are again 24 active satellites in orbit. GLONASS is thus a fully operational system again.

There are two other GNSS to become operational in the near future: the European Galileo system as the first GNSS under full civil control, and the Chinese Compass system. Both systems are already in a late development/early deployment phase. These next-generation systems, although not yet operational, already influence the GNSS domain by triggering modernizations of existing systems, new receiver technologies, and innovations in software development.

With GPS, the rebuilt GLONASS, and the two upcoming systems Galileo and Compass, there will be at least four operational GNSS at the users' disposal in the near future. The commercial success of multi-GNSS applications and the acceptance of the new systems will be decided by the market. From a scientific point of view the use of all available systems is a "must", but the transition from single-system to multi-GNSS applications is a challenge. The field of GNSS was—and in most areas still is—dominated by the

GPS, and the technical as well as the scientific progress during the last decade(s) must be attributed to this system. The integration of all available GNSS into the scientific framework and the establishment of multi-system applications is a major task/challenge in the near future. New hardware must be developed and the tracking networks must be upgraded. Multi-GNSS capable analysis software packages, algorithms, and models must be generalized and implemented. Our work may be seen as a major step in this direction. It has the focus in particular on the theory of a combined analysis of observations from different GNSS, on corresponding software developments, and on an assessment of the characteristics and quality of various solutions from a combined analysis of GPS and GLONASS observations.

This work is structured as follows:

Chapter 2, *An Introduction to Global Navigation Satellite Systems*, recapitulates the basic principles of GNSS navigation, the main constituents of a GNSS, and the equations governing the orbital motion of satellites. Four different systems, the U.S. American GPS, the Russian GLONASS, the European Galileo, and the Chinese Compass are characterized and compared. The benefits of using different GNSS for navigation are discussed. Finally, three institutions relevant to this work are briefly introduced.

Chapter 3, *GNSS Data Processing*, summarizes the necessary knowledge to analyze observation data in a combined multi-GNSS data processing environment. Detailed versions of the observation equations are presented and the concept of linear combinations of observations is introduced. Special attention is paid to biases in GNSS data processing. The chapter ends with a brief review of the least-squares parameter estimation method.

Chapter 4, *Concepts and Design*, has the focus on the update of the Bernese GPS Software (BSW) Version 5 to a fully multi-GNSS capable analysis software system. The development history and the main characteristics of Version 5 are presented. Subsequently, a list of requirements for a multi-GNSS software is compiled, based on a scientific and a technical point of view. Three key design principles are derived from the list of requirements.

Chapter 5, *Practical Realization*, summarizes the main limitations of the old version of the BSW concerning multi-GNSS processing. The important software implementations and the necessary steps to realize the design principles in the updated version of the BSW are presented.

Chapter 6, *Setup of Experiments*, introduces the studies related to the combined data analysis of GPS and GLONASS observations. It describes the experiments, the data basis, the solutions, and the technical details concerning data processing. Periodic variations in the number of available observations are identified and explained.

---

Chapter 7, *Results and Discussion*, contains the results of the experiments. Time series of station coordinates, orbit parameters, geocenter coordinates, and Earth rotation parameters are analyzed and discussed. Special attention is paid to periodic variations in the time series. The performance of single-system solutions as compared to combined multi-GNSS solutions is studied. Finally, the estimated satellite orbits are validated using satellite laser ranging measurements.

Chapter 8, *Summary and Conclusions*, summarizes the essential results of his work and draws the conclusions.



## **Part I**

# **Global Navigation Satellite Systems**



# 2 An Introduction to Global Navigation Satellite Systems

## Satellite Systems

### 2.1 Navigation Principles

One of the main goals in navigation is the determination of position and velocity of a point of interest in a well-defined global reference frame. Global Navigation Satellite Systems (GNSS) allow it to determine these data in an accurate, inexpensive way anywhere on Earth and in real time. The GNSS are widely used for navigational tasks nowadays.

For navigation purposes, a satellite is used as fixed point in space with known coordinates. The distance between the satellite and an observer may be deduced from the travel time of a signal emitted by the satellite and received by the observer. Disregarding any errors, the signal travel time multiplied by the speed of light yields the distance between observer and satellite. The position of the observer has to lie on a spherical surface centered on the satellite with the satellite–observer distance as radius, see Fig. 2.1a. Adding a second satellite as a known point (Fig. 2.1b), the observer’s position has to lie on the intersection of two surfaces, one centered on each satellite with the respective satellite–observer distances as radii. The geometric locus of this intersection is a circle. By adding

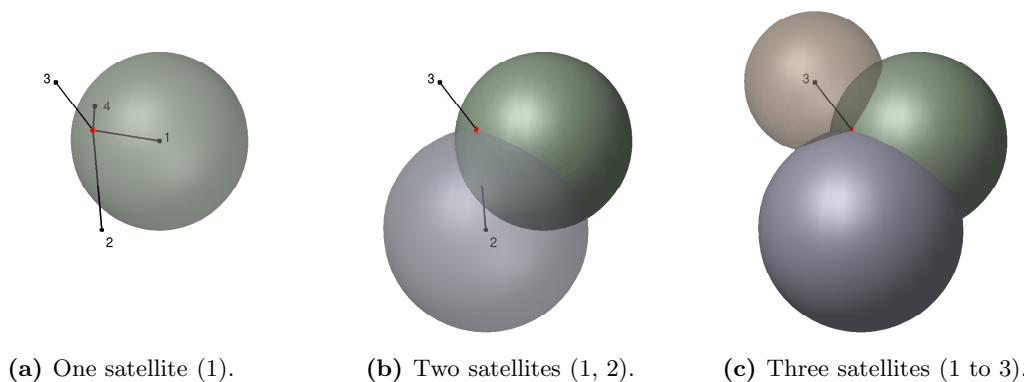


**Figure 2.1:** Observer position represented as intersecting spherical surfaces defined by the geometric distances between observer and satellites 1 to 3.

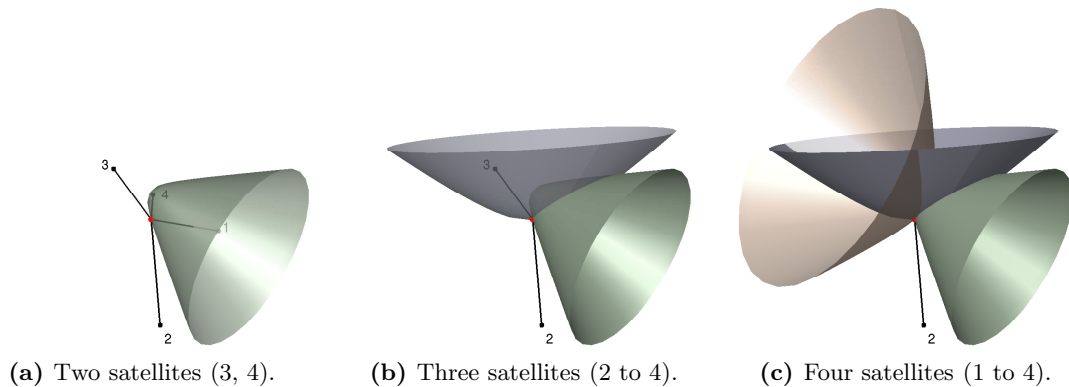


**Figure 2.2:** Observer position represented as intersecting hyperbolic surfaces each defined by two satellites.

a third satellite, the possible observer positions (now the intersection of three surfaces) are reduced to two points (Fig. 2.1c), one of which can usually be disregarded as unrealistic (far away from Earth’s surface). Therefore, only one location remains and the station position is known.

GNSS are based, however, on one-way ranges. Two clocks are involved in measuring the signal travel times: one clock on board the satellite providing the signal emission time, and one in the observer’s GNSS receiver to record the signal reception time. The difference between the readings of these two clocks would be the true travel time if both, receiver and satellite clocks, were perfectly synchronized. Each satellite carries an ensemble of very accurate atomic clocks. Synchronization errors (to GNSS time) introduced by spaceborne clocks shall be neglected in this introductory example. A typical GNSS receiver, by contrast, relies on a comparatively inaccurate internal crystal oscillator, which may considerably deviate from the reference time standard. As a consequence, all measured travel times are contaminated by clock synchronization errors. Distances computed from these biased travel times are therefore denoted as pseudoranges (PRs).

The positioning model of intersecting spheres is not valid if PRs are introduced because the radii of the spheres are biased. All travel times measured by one and the same receiver are, however, affected by one and the same clock error, implying that the bias can be eliminated by forming the difference between two PRs recorded at the same time. In other words, the difference of the measured distances between the observer and two satellites is constant. The resulting geometric locus corresponding to one PR difference is a hyperboloid of revolution with the two satellites as focal points (Fig. 2.2a). The number of independent hyperboloids defined by  $n$  PRs is always  $n - 1$ . Consequently, observations to a fourth satellite are needed to compute an unambiguous observer position from the intersection of three hyperboloids (Figs. 2.2b and 2.2c).

This positioning model explains why GNSS are sometimes called hyperbolic positioning systems. The explicit calculation of  $n - 1$  differences from  $n$  PRs (at one particular epoch) may be avoided, by keeping the  $n$  distances as parameters and introducing a receiver clock error as additional parameter.

## 2.2 System Segments and Configuration

All modern GNSS follow the same underlying navigation principles, outlined in Sect. 2.1, and are therefore rather similar in design. Although differing in realization and implementation, some principal constituents of a GNSS can be identified. All GNSS are based on three main segments, namely the space segment, the control segment, and the user segment [Hofmann-Wellenhof *et al.*, 2008].

### 2.2.1 Space Segment

The space segment contains that part of a GNSS which is located in space, i. e., the orbiting satellites, often referred to as space vehicles (SVs). The satellites of modern navigation systems are positioned in medium Earth orbits (MEOs), located between low Earth orbits (LEOs) and geosynchronous orbits (GSOs)<sup>1</sup>. This corresponds to an altitude range from about 2000 km up to approximately 36 000 km above the Earth's surface. Only a small region (a few thousand kilometers wide) around an altitude of 21 000 km is used for GNSS. Future systems, such as Compass (Sect. 2.4.4) and space-based augmentation systems (SBAS) utilize also navigation satellites positioned in the GSO, however. Figure 2.3 shows the different orbital regions true to scale. The shaded area denoted *GNSS region* is the small part of the MEO region occupied by GNSS constellations and stretches approximately from 19 000 km up to 23 500 km. Satellites in this space region revolve around the Earth with orbital periods around half a day (between 0.46 and 0.60 days).

The design of a GNSS constellation, i. e., the number of satellites and the orbit geometry, is dictated by the following considerations:

1. At least four satellites should be visible all the time at any location on (or near) the Earth's surface. Actually five or more satellites should be simultaneously visible to ensure robustness, e. g., in the case of satellite outages.
2. A low-maintenance constellation is preferred. It must be robust against satellite failures. Satellite repositionings within the constellation must be easily manageable.
3. The constellation should be stable to minimize the cost of keeping satellites at their nominal positions.

---

<sup>1</sup>The subset of GSOs with an inclination of  $i = 0^\circ$  are called geostationary Earth orbits (GEOs).

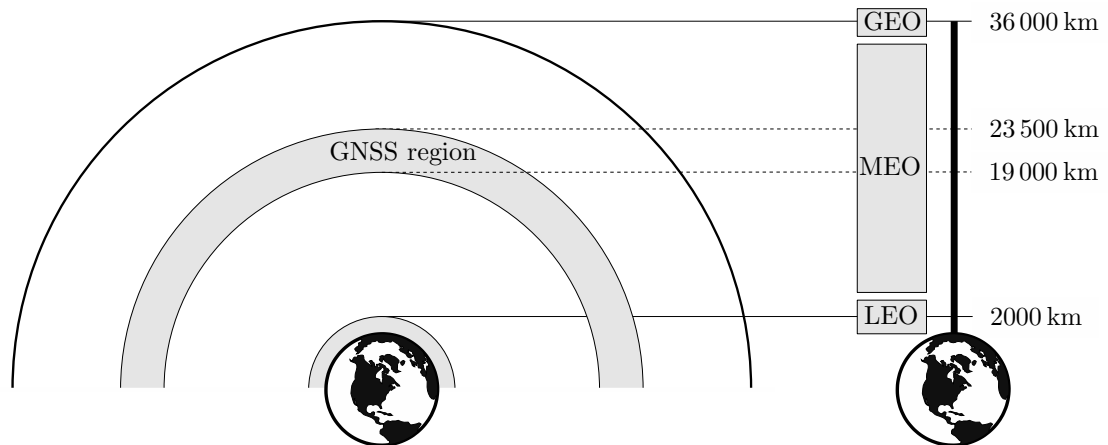


Figure 2.3: Division of near Earth space in orbital regions.

4. A good geometric distribution of the satellites in azimuth as well as in elevation must be ensured for (almost) any point on Earth to provide a good and reliable accuracy.
5. The build-up and maintenance of the constellation must be relatively cheap.

A constellation type meeting these requirements is the Walker constellation (Sect. 2.3.2) which is the basis for (or at least influenced) all GNSS with satellites in the MEO region.

A GNSS constellation is realized by the spacecrafts orbiting the Earth. A GNSS satellite carries an ensemble of atomic clocks to realize the GNSS system time on-board and to establish a reference frequency for the signal processors. It transmits several ranging codes and navigation information modulated on two or more carrier waves in the microwave band. The ranging codes may be open for public use or encrypted to restrict access to authorized users. The navigation message contains, e.g., information on the orbital positions of the satellites, clock synchronization corrections to GNSS time, and status and integrity information on the SVs.

The attitude of a satellite is governed by two basic requirements: the transmitting antenna must always point to the Earth, and the solar panels of the satellite must always be perpendicular to the line Sun–satellite. Figure 2.4 shows spacecrafts from three different GNSS.

### 2.2.2 Control Segment

The control segment contains the infrastructure for GNSS monitoring, control, and maintenance on the Earth's surface. A minimum configuration includes a number of monitor stations, a central control facility, and one up-/downlink station.

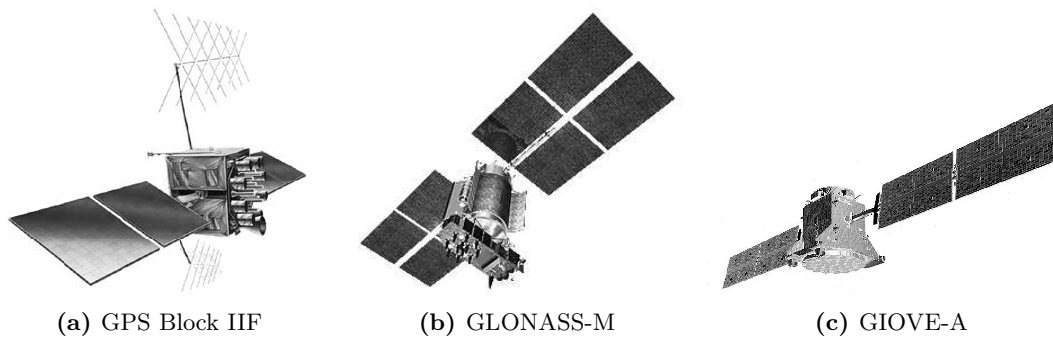


**Figure 2.4:** Satellites from three different GNSS.

The monitor stations track and record the navigation signals of all satellites of the GNSS on a continuous basis. A global uniform distribution of the monitor stations is preferable to allow for a seamless tracking of all satellites. The observation data is transferred to the control facility for further processing.

The control facility has several responsibilities. It supervises the system status and executes all necessary steering tasks to ensure full operational capability of the system. This includes, e. g., repositionings of satellites to keep them at their nominal positions or to replace unusable satellites with spares. Satellite orbits and clock corrections—and predictions thereof—are computed for all satellites based on the data recorded by the monitor stations. The tracking data may be used for integrity monitoring, as well. Finally, the control station (or a related facility) is responsible for the generation and maintenance of the system time and reference frame.

One or more up-/downlink stations equipped with antennas enable communication with the spacecrafts. The orbit and satellite clock predictions (and other auxiliary information) prepared by the control facility are uploaded to the satellites, the software of the satellites may be updated, steering signals can be sent, etc. The stations must be located on the Earth’s surface in such a way, that each satellite becomes visible at least from one of the stations in due time to receive the transmitted information.

### 2.2.3 User Segment

The user segment contains the equipment and installations necessary for accessing and using a particular GNSS. The user segment mainly consists of receivers and antennas (both, high precision as well as mass market products). In addition, augmentation systems (providing, e. g., differential corrections to GNSS observations in order to increase positioning accuracy) and supporting services like the International GNSS Service (IGS) (Sect. 2.6.1) may be included in the user segment, as well.

An antenna must be tuned to the GNSS-specific frequencies. As all GNSS transmit in the frequency band between 1 GHz and 2 GHz (microwave L-band), the construction of multi-GNSS capable antennas is greatly facilitated. Miniature antennas may be directly integrated in a receiver, which is the normal case for mass market products. External antennas usually have a higher gain and are therefore used for demanding applications requiring maximum reliability and precision. Antennas may be covered by domes in order to protect them from the environment.

Receivers may be classified according to several distinct features, such as the number of tracked frequencies, the tracking technology, or the number of GNSS tracked. Mass market receivers are usually single-system and single-frequency receivers. High-precision and scientific applications call for multi-GNSS capabilities and for a tracking of all frequencies and all different observation types.

## 2.3 Satellite Orbits and Orbital Motion

### 2.3.1 The Equations of Motion

The two-body problem is a simplified mathematical model for the motion of a satellite around the Earth. It is based on Newton's inverse square law of gravitation. Assuming a negligible mass of the satellite w.r.t. the Earth and a spherically symmetric mass distribution of the Earth, the acceleration of a satellite is given by

$$\ddot{\mathbf{r}} = -GM \cdot \frac{\mathbf{r}}{r^3} \quad (2.1)$$

with the initial conditions at epoch  $t_0$

$$\mathbf{r}(t_0) = \mathbf{r}(a, e, i, \Omega, \omega, T_0; t_0) \quad \text{and} \quad \dot{\mathbf{r}}(t_0) = \dot{\mathbf{r}}(a, e, i, \Omega, \omega, T_0; t_0), \quad (2.2)$$

where

$\mathbf{r}$  is the geocentric position vector of the satellite expressed in an inertial frame,

$r$  is the absolute value of  $\mathbf{r}$ ,

$\dot{\mathbf{r}}, \ddot{\mathbf{r}}$  are the first and second time derivatives of  $\mathbf{r}$ , i. e., the satellite's velocity and acceleration vectors in the inertial frame,

$GM$  is the product of the gravity constant  $G$  and the mass  $M$  of Earth, and

$a, e, i, \Omega, \omega, T_0$  are the orbital elements.

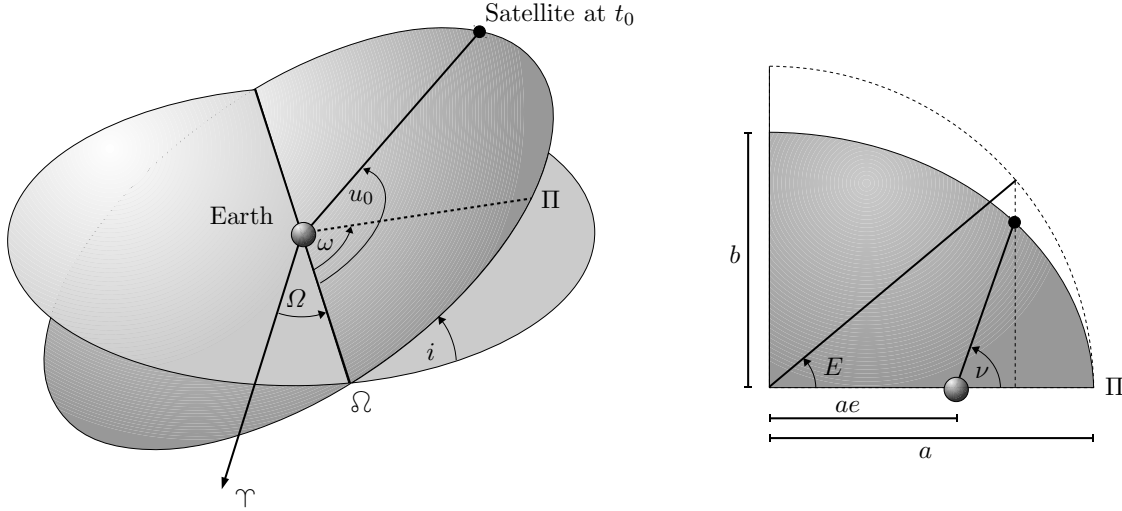


**Figure 2.5:** The six orbital elements  $a$ ,  $e$ ,  $i$ ,  $\Omega$ ,  $\omega$ ,  $u_0$ .

The vectors  $\mathbf{r}$  and  $\dot{\mathbf{r}}$  together are referred to as state vector. The equation of motion (2.1) together with a state vector represents a particular orbit for a satellite. The system of 2nd-order differential equations represented by Eq. (2.1) can be solved analytically [Beutler, 2005a]. The orbital curves related to the (unperturbed) two-body problem are conic sections. In our context, only elliptic (and as a special case circular) orbits will be considered. Hyperbolic and parabolic trajectories are not of interest.

The six orbital elements  $a$ ,  $e$ ,  $i$ ,  $\Omega$ ,  $\omega$ , and  $T_0$  are known as Kepler elements and completely characterize a particular solution of the equation of motion (2.1), i.e., the satellite's orbit. Figure 2.5 illustrates the orbital elements and shows the semi-minor axis  $b$  and the eccentric anomaly  $E$ . Size and shape of an orbit are defined by the semi-major axis  $a$  and the numerical eccentricity  $e$ , the orientation of the orbit is given by inclination  $i$ , right ascension of the ascending node  $\Omega$ , and the argument of perigee  $\omega$ . The perigee passage time  $T_0$  tells when the satellite is at perigee. The argument of perigee  $\omega$  and the perigee passage time  $T_0$  are highly correlated for nearly circular orbits. The perigee passage time is therefore sometimes replaced by the argument of latitude  $u_0 = \omega + \nu(t_0)$ , where  $\nu(t_0)$  is the true anomaly at the initial epoch  $t_0$ , to circumvent this problem. Figure 2.5 shows  $u_0$  instead of  $T_0$ . The vernal equinox, the ascending node, and the perigee of the orbit are usually associated with the symbols  $\Upsilon$ ,  $\Omega$ , and  $\Pi$ , respectively.

The model (2.1) of the two-body motion is not sufficient for satellites moving in the real force field. In addition to the term of the Earth's spherical symmetric gravity field, several perturbing accelerations must be taken into account. The equations of motion of a satellite including all perturbing forces read as

$$\ddot{\mathbf{r}} = -GM \cdot \frac{\mathbf{r}}{r^3} + \mathbf{a}(t, \mathbf{r}, \dot{\mathbf{r}}, p_1, \dots, p_n) \quad (2.3)$$

**Table 2.1:** Accelerations acting on a GNSS satellite and net orbit error after one day (based on *Beutler* [2005b]).

Perturbation caused by	Acceleration in m/s <sup>2</sup>	Net orbit error in m
Two-body term of Earth's gravity field	0.57	– <sup>a</sup>
Flattening of Earth	$5 \times 10^{-5}$	10 000
Gravitational attraction of Moon	$5 \times 10^{-6}$	3000
Gravitational attraction of Sun	$2 \times 10^{-6}$	800
Remaining terms of Earth's gravity field	$3 \times 10^{-7}$	200
Direct radiation pressure	$9 \times 10^{-8}$	200
Y-bias	$5 \times 10^{-10}$	2
Solid Earth tides	$1 \times 10^{-9}$	0.3
Ocean tides	$1 \times 10^{-10}$	0.2
Gravitational attraction of planets (Jupiter, Venus, Mars)	$1 \times 10^{-11}$	0.01

<sup>a</sup> The satellite would not be orbiting the Earth without this acceleration.

with the initial conditions (2.2), where

$\mathbf{a}$  is the perturbing acceleration,

$t$  is the time argument, and

$p_1, \dots, p_n$  are force model parameters.

The acceleration vector  $\mathbf{a}$  contains all gravitational and non-gravitational perturbing accelerations considered in the orbit model. These accelerations are described by the model parameters  $p_1, \dots, p_n$  and depend on time and the satellite's state vector. The model parameters may either be assumed to be known or may have to be estimated during an orbit determination process. Table 2.1 summarizes the most important accelerations acting on a typical GNSS satellite orbiting in the GNSS region (cf. Fig. 2.3) and gives the absolute error in orbit position after one day, i. e., the difference of the perturbed and the unperturbed orbit (referring to the initial epoch), if a particular acceleration is ignored in an initial value problem. Details on the modeling of perturbations and analytical force models may be found in, e. g., [*Rothacher*, 1992; *Beutler et al.*, 1994b; *Beutler*, 2005b]. The refined model of orbital motion (2.3) must be solved by numerically integrating the differential equations. A discussion of numerical solution methods is provided by *Beutler* [2005a].

As opposed to Eqs. (2.1), the equations of motion (2.3) are not described by a time-invariant set of orbital elements. However, for each epoch  $t$ , the state vector of the satellite's orbit can be transformed to a set of time-dependent orbital elements

$$\{ \mathbf{r}(t), \dot{\mathbf{r}}(t) \} \rightarrow \{ a(t), e(t), i(t), \Omega(t), \omega(t), T_0(t) \}. \quad (2.4)$$

The explicit transformation can be found in [Beutler, 2005a]. The time-dependent orbital elements are called osculating orbital elements and the associated orbit is the osculating orbit at the osculating epoch  $t$ . The osculating orbit is the trajectory a satellite with  $\{\mathbf{r}(t), \dot{\mathbf{r}}(t)\}$  would follow if all perturbations were switched off for  $t' \geq t$ . The real orbit and the osculating orbit are tangential at the osculating epoch. The actual orbit is the envelope of all osculating orbits.

Perturbations, especially the flattening of the Earth, lead to a drift in the satellite's node. The drift  $\dot{\Omega}$  expressed in units of degrees per day is approximated by

$$\dot{\Omega} = -\frac{10^\circ \cos i}{(1 - e^2)^2} \left(\frac{a}{a_\oplus}\right)^{-7/2}, \quad (2.5)$$

where  $a_\oplus$  is the semi-major axis of the Earth [Beutler, 2005b]. This nodal drift causes the length  $y_s$  of a "satellite year", i. e., the time interval needed by the Sun to return to the same point in space w. r. t. the satellite's node, to be not the same as the length  $y_*$  of a sidereal year. The length  $y_s$  of the satellite year in units of days is given by

$$y_s = y_* \cdot \left(1 - \frac{y_*}{360^\circ} \dot{\Omega}\right)^{-1}. \quad (2.6)$$

In our simplified unperturbed two-body model (2.1), the mean motion  $n$  of a satellite and its semi-major axis  $a$  are related by  $n^2 a^3 = GM$ . The revolution period  $U$  of the satellite is then given by

$$U = \frac{2\pi}{n}. \quad (2.7)$$

In the presence of perturbations, the orbital revolution period is no longer unique. Three revolution periods can be distinguished: (a) The anomalistic revolution period is the time interval between subsequent perigee passes. (b) The draconitic period is defined by consecutive passes through the ascending node. (c) The sidereal revolution period is the time span of a full orbit relative to the fixed stars. The differences between these revolution periods and the two-body revolution period are in the range of a few seconds for a typical GNSS MEO satellite. Detailed information on orbital revolution periods and mathematical derivations may be found in [Beutler, 2005b].

### 2.3.2 The Walker Constellation

A specific satellite constellation type introduced and described by Walker [1971] and further developed by Walker [1984] proved to be particularly well suited for GNSS purposes by meeting all requirements outlined in Sect. 2.2. This constellation is commonly called a Walker constellation.

A Walker constellation (or to be more precise, a delta pattern Walker constellation<sup>2</sup>) consists of satellites evenly distributed in several evenly spaced orbital planes in the MEO

<sup>2</sup>The delta pattern Walker constellation is also known as Ballard rosette [Ballard, 1980].

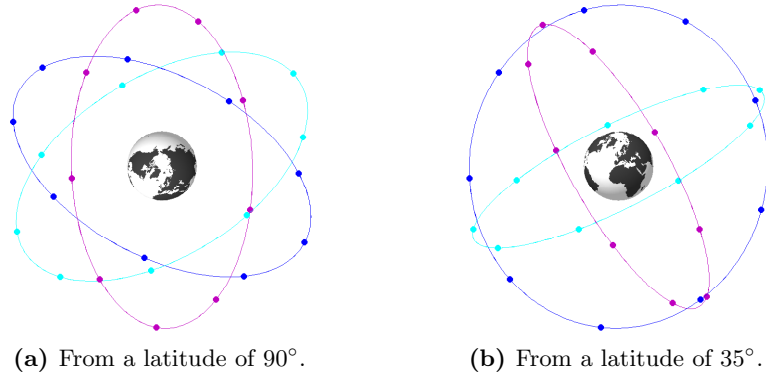


**Figure 2.6:** Walker 56°:27/3/1 constellation (semi-major axis  $a = 29\,600$  km).

region. An effective realization of this constellation type is characterized by the inclination of the orbital planes and by three numbers  $T$ ,  $P$ , and  $F$ . It follows the naming scheme Walker  $i : T/P/F$ , where

- $i$  is the inclination of the orbital planes (same for all planes),
- $T$  is the total number of satellites,
- $P$  is the number of orbital planes, and
- $F$  describes the relative positions of satellites in different planes.

The number of satellites per plane  $S$  is given by  $S = T/P$ , the in-plane spacing of the satellites by  $D_s = 360^\circ/S$ , and the spacing of the individual orbital planes in the equatorial plane by  $D_p = 360^\circ/P$ . The relative positions of the satellites in different planes are defined by  $F$ . If a satellite is in its ascending node, there is a satellite in the (eastwards) adjacent plane which has covered an orbital distance of  $D_r = F \cdot 360^\circ/T$  w. r. t. the ascending node.

Figure 2.6 shows a Walker 56°:27/3/1 constellation to illustrate a possible orbit geometry of a GNSS. The constellation is composed of 27 satellites evenly distributed in three even-spaced orbital planes. Figure 2.6a shows the constellation as viewed from a latitude of 90° (i. e., from the pole), Fig. 2.6b as viewed from 35°. Figure 2.7 shows the uniform distribution of the 27 satellites in the three orbital planes w. r. t. the right ascension of the ascending node and the argument of latitude. The satellite in-plane spacing of  $D_s = 40^\circ$  and the plane spacing of  $D_p = 120^\circ$  can be seen in the figure. Satellites in adjacent planes are shifted by  $D_r = 360^\circ/27 \approx 13.3^\circ$  in the orbital plane.

Figure 2.8a shows the satellite coverage of the Earth with an elevation mask of 5°, i. e., the number of visible satellites above 5° elevation, averaged over one day for the particular Walker constellation. At least eight satellites are visible simultaneously on the average

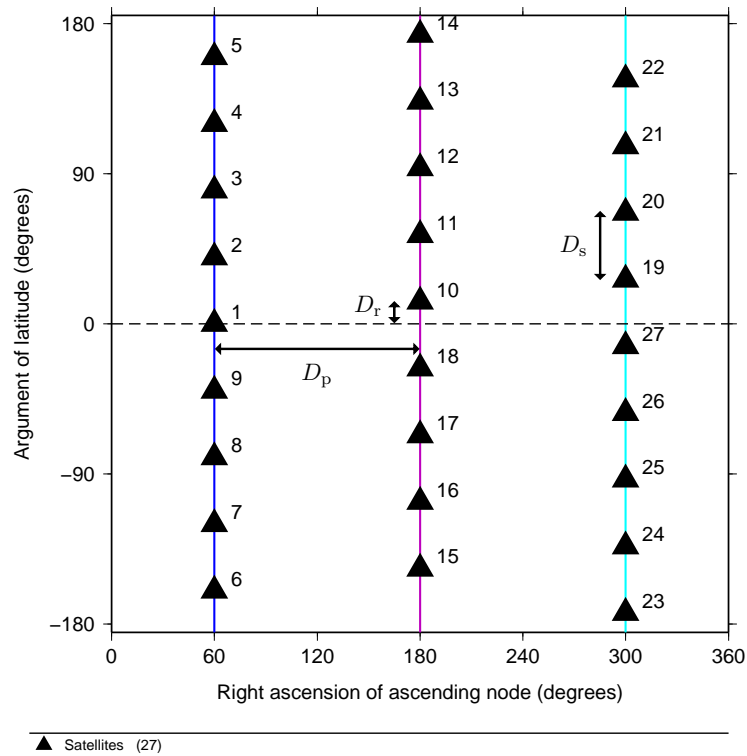


Figure 2.7: Orbital plane occupancy for a Walker  $56^\circ:27/3/1$  constellation.

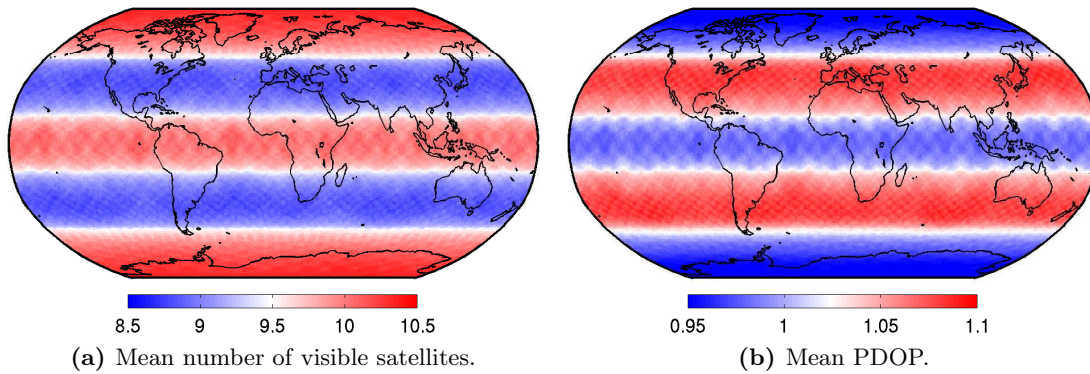


Figure 2.8: Number of visible satellites and PDOP averaged over one day (Walker  $56^\circ:27/3/1$ , semi-major axis  $a = 29\,600$  km, elevation mask  $5^\circ$ ).

from any point on the Earth, satisfying the need of four simultaneously observable satellites for navigation purposes.

The suitability of a satellite constellation for navigation purposes is, however, not only determined by the number of visible satellites but also by the receiver–transmitter geometry. The so-called position dilution of precision (PDOP) is a widely used indicator for the quality of an observation geometry in satellite navigation. A description of the PDOP may be found in many references, e. g., in [Langley, 1999] or in [Hofmann-Wellenhof et al., 2008]. Figure 2.8b shows the PDOP values (again for the same Walker constellation) averaged over one day. A PDOP value of one indicates a very good geometry, larger values indicate a degraded geometry. The mean PDOP is below 1.1 for any point on the Earth’s surface indicating that the distribution of the satellites in this Walker constellation is very well suited for a GNSS. The impact of the satellite sky distribution (for the GPS constellation) was studied in detail by *Santerre* [1991].

The satellite visibility and PDOP values shown in Fig. 2.8 represent an idealized observation scenario where the visibility of the local horizon is not limited by obstacles. The satellite visibility and PDOP may be significantly worse in unfavorable observation situations like dense urban areas or in mountainous areas. This degradation may be mitigated by observing satellites from more than one GNSS at the same time (Sect. 2.5).

## 2.4 Global Navigation Satellite Systems in Comparison

The U.S. American Global Positioning System (GPS) was the first fully operational GNSS reaching its full operational capability (FOC) in 1995 with 24 active satellites. It had a strong—in some fields even revolutionary—impact on science and society. Today, it still is the best-known GNSS with widespread military, scientific, and mass market applications.

The Russian Global’naya Nawigatsionnaya Sputnikowaya Sistema<sup>3</sup> (GLONASS) was developed and deployed in parallel to the GPS. Due to financial difficulties in the 1990s, the funding of GLONASS was significantly reduced. After a short FOC phase in 1996 the system degraded rapidly. It was in a very bad state and not nearly as popular as its American counterpart. During recent years, however, the system was built up step by step and it will soon be fully operational.

Apart from these two existing systems, there are two more GNSS to become operational in the near future: the European Galileo system as first GNSS under full civil control, and the Chinese Compass system. As of 2011, both systems are in the late development/early deployment phase. Although they will not be fully operational for some years to come,

---

<sup>3</sup>The literal translation “Global Navigation Satellite System” is incidentally the same phrase as that used to address satellite systems for navigation purposes in general.

they already influenced the GNSS domain by triggering modernizations of existing systems, new receiver technologies, innovations in software development, and by stimulating the public interest in GNSS in general.

In addition to the global systems, there are several regional satellite navigation and augmentation systems. These systems are out of the scope of this work. *Hein et al.* [2007a, 2007b] give a comprehensive overview of all major systems and technologies.

The two operational systems GPS and GLONASS and the Galileo and Compass systems are described in more detail in the following sections. Table 2.2 in Sect. 2.4.5 compares the GPS, GLONASS, and Galileo system and provides a quick overview of the GNSS. The Compass system is not included in the table as not too many assured facts are available.

### 2.4.1 Global Positioning System (GPS)

The Navigational Satellite Timing and Ranging Global Positioning System (NAVSTAR GPS), operated by the United States, was the first fully operational GNSS (although GLONASS was the first system to be officially declared fully operational, see Sect. 2.4.2). It was developed by the U.S. Department of Defense (DoD) in the 1970s. Even if the GPS was developed as military-only system, it has become a dual use system for military and civilian purposes.

The development of the GPS started in 1973, the first satellite (of type Block I) was launched five years later on February 22, 1978. Ten more Block I satellites were deployed during the following years, the last one in 1985. None of these first-generation satellites, mainly launched for concept validation, are still active today. The last one ceased operation on March 26, 1996, after having served for more than 11 years. The Block II GPS satellites were the first fully operational satellites. Nine Block II satellites were launched from February 1989 through October 1990. Step by step they were replaced by the modernized Block IIA, Block IIR (IIR-A and IIR-B), and Block IIR-M satellites. The first next generation Block IIF satellite of the GPS modernization program was successfully launched on May 27, 2010.

The initial operational capability of the system was declared on December 8, 1993, with 24 active (Block I/II/IIA) GPS satellites in orbit. FOC was officially declared about 20 months later on July 17, 1995, with 24 operational Block II/IIA satellites.

Figure 2.9 shows the GPS constellation as of December 31, 2010. The 32 active satellites are distributed in six orbital planes which are mutually separated by  $60^\circ$  in the equator. Each plane is nominally occupied by four, but actually by five or six satellites. The satellites in each plane are not evenly spaced (as opposed to a true Walker constellation) to improve satellite coverage in case of satellite failures or a reduced constellation. The satellite orbits are almost circular with semi-major axes of about 26 560 km, corresponding to an altitude of approximately 20 200 km above the Earth's surface. The orbital planes are

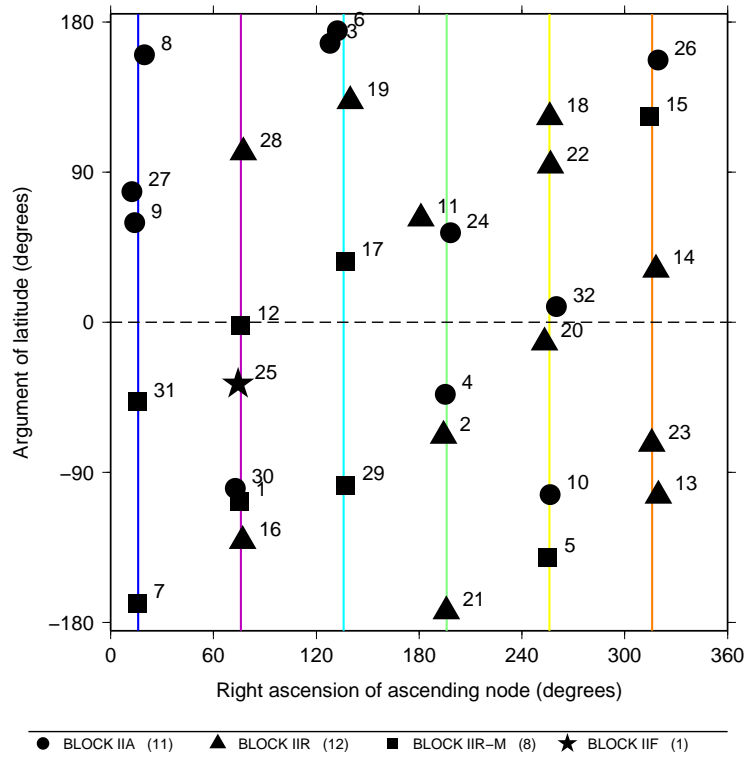


Figure 2.9: Orbital plane occupancy of GPS satellites, December 31, 2010.

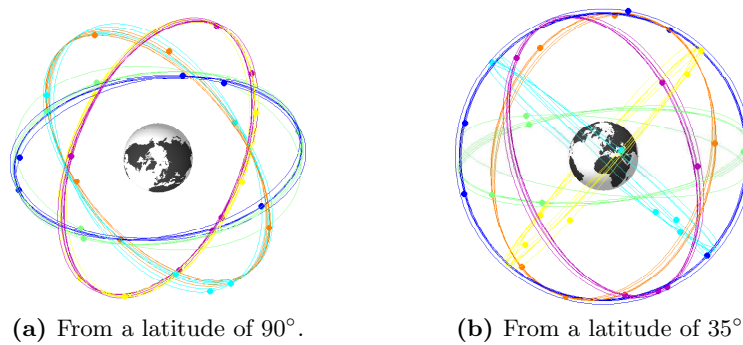
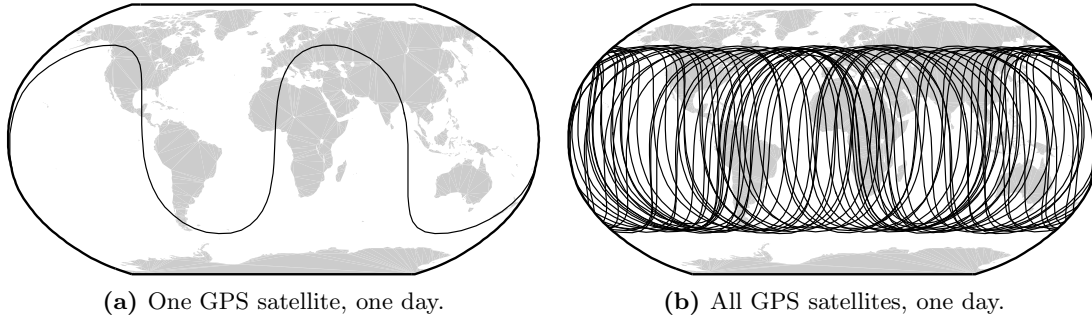


Figure 2.10: GPS satellite orbits, December 31, 2010.



**Figure 2.11:** Ground tracks of the GPS satellites.

inclined by about  $55^\circ$  w. r. t. the Earth's equator. Figure 2.10 shows the GPS constellation as seen from the north pole and from a latitude of  $35^\circ$ , respectively, to give an impression of the size and orientation of the orbits.

The orbital revolution period is 11 hours 58 minutes, corresponding almost exactly to half a sidereal day, i. e., a GPS satellite completes two full revolutions while the Earth rotates once w. r. t. the inertial coordinate system. Consequently, the sub-satellite trajectory on the Earth's surface (also called ground track) of a satellite repeats itself each sidereal day as shown in Fig. 2.11. This daily repeat cycle was advantageous in the early project phase of GPS as regular measurements and experiments were possible even with only a small number of operational GPS satellites in orbit. A consequence of this deep (2:1)-resonance of the satellites' orbital revolution period with the Earth's rotational period are pronounced secular and long-periodic perturbations in certain orbital elements [Beutler, 2005b], in particular in the semi-major axes. These perturbations cause the satellites to drift away from the nominal positions in their orbital planes. Consequently, the GPS satellites must be repositioned periodically (about once per year) in order to maintain a coherent GNSS constellation.

The GPS satellites transmit their navigation signals on two right-handed circularly polarized (RHCP) carrier waves L1 and L2. The new Block IIF satellites also transmit on a third carrier wave L5 establishing the GPS as a modernized three-frequency GNSS. The frequencies  $f_1$ ,  $f_2$ , and  $f_5$  are derived from the reference frequency  $f_0 = 10.23$  MHz as

$$\begin{aligned}
 \text{L1 : } & f_1 = 154 f_0 = 1575.42 \text{ MHz} & \lambda_1 & \approx 19.0 \text{ cm} \\
 \text{L2 : } & f_2 = 120 f_0 = 1227.60 \text{ MHz} & \text{and } \lambda_2 & \approx 24.4 \text{ cm} , \\
 \text{L5 : } & f_5 = 115 f_0 = 1176.45 \text{ MHz} & \lambda_5 & \approx 25.4 \text{ cm}
 \end{aligned} \tag{2.8}$$

where  $\lambda_1$ ,  $\lambda_2$ , and  $\lambda_5$  are the respective wavelengths. Note that the fundamental frequency  $f_0$  of the satellite clock is affected by relativistic effects [Ashby, 2003; Kouba, 2004]. The frequency of the satellite clock is corrected for a frequency shift of  $f_{\text{rel}} = -4.5674 \times 10^{-3}$  Hz [IS-GPS, 2010a] so that an observer on the Earth's surface obtains the nominal frequency of 10.23 MHz.

The GPS is based on a code division multiple access (CDMA) approach to distinguish the signals of different satellites. Each spacecraft emits on the same frequencies but uses a set of unique pseudorandom noise (PRN) codes. Apart from the space vehicle number (SVN), the PRN number is often used to identify a specific satellite. Care must be taken as different PRN numbers may be allocated to a satellite during its lifetime.

The satellites of Block IIR or previous generations modulate two PRN codes onto the carriers. The first one is the coarse/acquisition code (C/A-code) available for civil (open) use. The C/A-code is available on L1 only and has an effective wavelength of about 293 m. The second code is the precise, or protected, code (P-code) with a wavelength of about 29.3 m. It is modulated onto both carriers. The P-code is encrypted and results in the so-called Y-code, which is reserved for the U.S. military and other authorized users. Satellites of the Block IIR-M generation (which constitute currently a quarter of the GPS constellation) provide in addition some modernized M-codes and a second civil code modulated on L2 (the L2C-code). The Block IIF satellites will have in addition several new military and civil navigation codes. Apart from the navigation codes, all GPS satellites modulate a data message on all carriers, providing information on satellite clock biases, ephemerides, and system status.

Details on the GPS signal structure and the third frequency may be found in the official specification documents [*IS-GPS*, 2010a] and [*IS-GPS*, 2010b]. More information on the GPS in general may be found, e. g., in [*Kaplan and Hegarty*, 2006] or in [*Hofmann-Wellenhof et al.*, 2008]. A review of GPS history and its development is given by *Parkinson and Powers* [2010a, 2010b].

## 2.4.2 Global'naya Nawigatsionnaya Sputnikowaya Sistema (GLONASS)

The Global'naya Nawigatsionnaya Sputnikowaya Sistema or Global Navigation Satellite System (GLONASS) is the Russian counterpart of the GPS. The system development was initiated by the former USSR in the mid 1970s. Today, GLONASS is operated by the Ministry of Defense of the Russian federation. Although originally intended as a strictly military system, the system was opened for civil purposes in March 1995 by a governmental decree.

The first GLONASS satellite was launched on October 12, 1982. After several further launches the system was formally declared operational by the president of the Russian Federation on September 24, 1993. Only 12 active satellites were in space at that date. The nominal constellation with 24 satellites in orbit was established on January 18, 1996. This point in time may be viewed as the date when the FOC of GLONASS was reached.

The number of active satellites continuously declined shortly thereafter due to severe funding problems, aggravated by the short lifetime of the first generation satellites (only about three years as opposed to more than ten years for GPS satellites). After a minimum of only seven active GLONASS satellites in 2001, the Russian Federation decided to rebuild

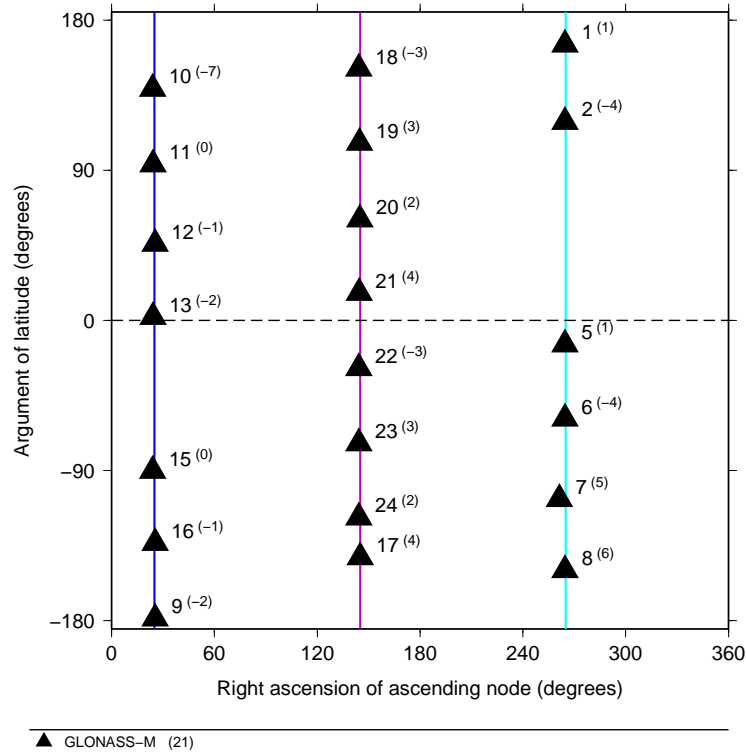


**Figure 2.12:** Orbital plane occupancy of GLONASS satellites, December 31, 2010. The superscripts correspond to the channel numbers.

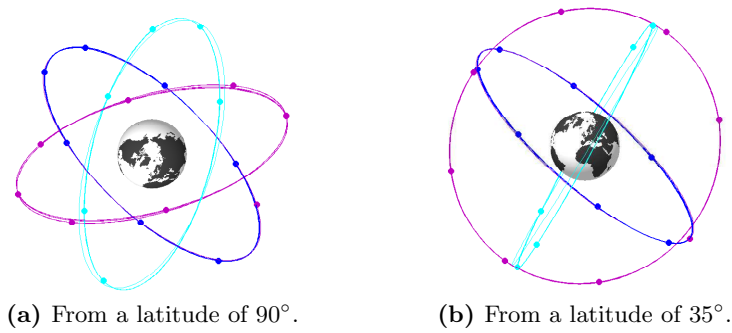


**Figure 2.13:** GLONASS satellite orbits, December 31, 2010.

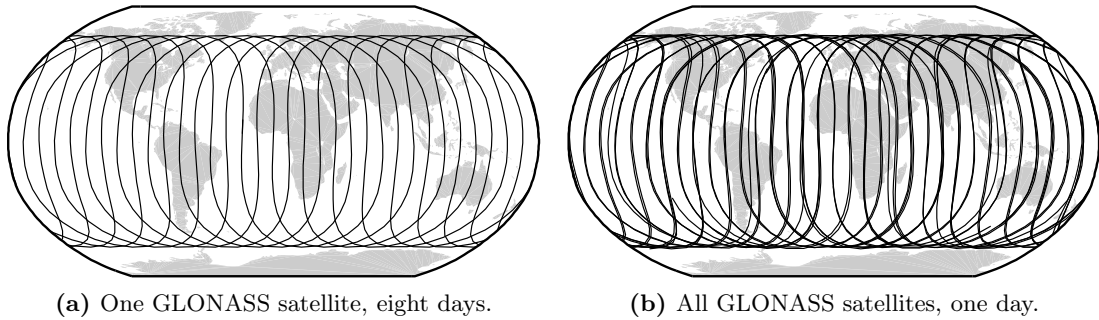


**Figure 2.14:** Ground tracks of the GLONASS satellites.

the system. A new satellite type (GLONASS-M) was developed and several satellites were launched (usually three at a time) at regular intervals.

Figure 2.12 shows the constellation as of December 31, 2010, with 21 active satellites, all of type GLONASS-M. One active GLONASS satellite does not show up in the constellation plot as it has ongoing signal problems on one frequency. The GLONASS is a realization of a Walker 64.8°:24/3/1 constellation. The satellites are arranged in three orbital planes with a nominal inclination of 64.8°. The plane spacing is  $D_p = 360^\circ/3 = 120^\circ$  and the in-plane spacing of the satellites is  $D_s = 360^\circ/8 = 45^\circ$  with eight satellites per plane. Satellites in adjacent planes are shifted by  $D_r = 360^\circ/24 = 15^\circ$  (in the argument of latitude  $u$ ). The orbits are close to circular with semi-major axes of about 25 510 km. Figure 2.13 shows the GLONASS satellite orbits from two latitudes, nicely demonstrating the regularity of the constellation.

The orbital revolution period of a GLONASS satellite is 11 hours 16 minutes, corresponding to  $8/17$  of a sidereal day. A GLONASS satellite thus completes 17 revolutions while the Earth rotates 8 times (i. e., in 8 sidereal days). Figure 2.14a shows the ground track of a GLONASS satellite over eight days to illustrate this repeat cycle. Figure 2.14b shows the trajectories of all GLONASS satellites for one day. The ground track pattern is essentially the same as for a single satellite. This feature is caused by two facts: (a) A satellite completes  $2^{1/8}$  revolutions per sidereal day, i. e., it has moved by  $45^\circ$  in orbit which is exactly the in-plane spacing  $D_s$  of the satellites of a particular plane. Therefore all satellites of a particular plane basically take the place of their in-plane neighbor after one sidereal day and follow the same ground track. (b) During  $4^{23/24}$  orbital revolutions (which is  $15^\circ$  short of five revolutions) the Earth completes exactly  $2^{1/3}$  revolutions (which corresponds to two full revolutions and an additional  $120^\circ$ ).

These numbers match exactly the plane spacing of  $D_p = 120^\circ$  and the relative satellite spacing between adjacent planes of  $D_r = 15^\circ$ . Consequently, each satellite follows the trajectory of its neighbor in the preceding orbital plane after  $4^{23/24}$  revolutions, e. g., satellite R01 would follow the trajectory of satellite R18, which in turn would follow R10

(in reference to Fig. 2.12). The small irregularity in the ground tracks in Fig. 2.14b is caused by satellites which are not exactly positioned in their nominal orbital slots.

Unlike the satellites of the GPS, the GLONASS satellites are not in a deep resonance with the Earth's rotation and maneuvers for constellation keeping are not necessary. The GLONASS is based on a frequency division multiple access (FDMA) approach. Each satellite transmits on slightly different frequencies to allow a receiver to discriminate between the different satellites. As there is no need for a separation of satellites based on signal modulation, all GLONASS satellites use the same navigation code. This approach is an alternative to the CDMA (as used by GPS), where different codes are used for the distinction of the satellites.

A GLONASS satellite transmits on two RHCP carrier waves in the microwave L-band. The nominal frequency used by a particular satellite is derived from a reference frequency  $f_0 = 178$  MHz, a frequency divisor  $\Delta f = f_0/2848 = 0.0625$  MHz, and a channel number  $m$  taking values from  $-7$  to  $6$ :

$$\begin{aligned} \text{L1: } f_1 &= 9(f_0 + m \Delta f) \approx (1598 \text{ to } 1605) \text{ MHz} & \text{and} & \lambda_1 \approx (18.8 \text{ to } 18.7) \text{ cm} \\ \text{L2: } f_2 &= 7(f_0 + m \Delta f) \approx (1243 \text{ to } 1249) \text{ MHz} & & \lambda_2 \approx (24.1 \text{ to } 24.0) \text{ cm} \end{aligned} \quad (2.9)$$

The frequency ratio  $f_1/f_2$  is constant for all satellites and with a value of  $9/7 \approx 1.2857$  very close to that of GPS with  $77/60 \approx 1.2833$ . The channel number of each GLONASS satellite is given in Fig. 2.12 as superscript to the orbital slot numbers. Note that the same channel numbers may be allocated to antipodal satellites. This allocation does not pose problems as the FDMA technique requires different frequencies only for all satellites in view.

The GLONASS satellites broadcast a C/A-code with a wavelength of about 587 m as well as a P-code with a wavelength of about 58.7 m on both carriers L1 and L2.<sup>4</sup> A navigation message is added to both carriers. As opposed to the GPS, there is no degradation or encryption of the transmitted codes.

Plans for the further development of GLONASS include new satellite types, namely GLONASS-K and GLONASS-KM, a third frequency, and new code types. Even a replacement of the FDMA technique in favor of CDMA is discussed. More information on the L1 and L2 navigational signals may be found in [ICD, 2008], details on GLONASS in general, e. g., in [Hofmann-Wellenhof et al., 2008].

### 2.4.3 Galileo

The Galileo system—still in its development phase—will be Europe's GNSS. It is a joint undertaking of the European Commission (EC) and the European Space Agency (ESA).

---

<sup>4</sup>Before the first GLONASS-M satellite was set operational in 2004, the C/A-code was only transmitted on L1.

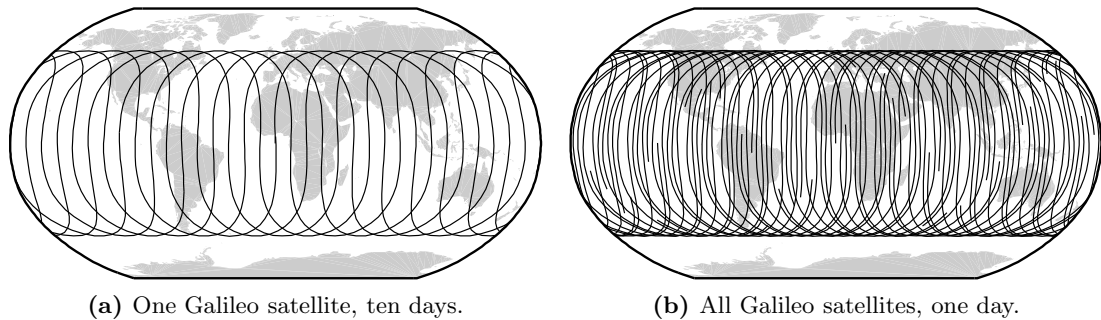


**Figure 2.15:** Ground tracks for a simulated nominal Galileo constellation.

The system is planned as a globally available, fully independent navigation satellite system promising a high level of reliability. Interoperability with existing GNSS shall be maintained. The Galileo will be under civil control.

The Galileo definition phase was approved by ESA in May 1999. As of mid 2011, the system approaches the end of its development phase and moves towards an in-orbit validation (IOV) phase with a minimum constellation of four satellites. The first 14 Galileo satellites were commissioned to the industry in January 2010.

Two Galileo test satellites have already been launched, partly to test newly developed equipment, partly to secure the transmission frequencies allocated by the International Telecommunication Union (ITU). The first Galileo In-Orbit Validation Element (GIOVE) satellite, GIOVE-A1, was launched on December 28, 2005. The second satellite, GIOVE-B, was launched on April 26, 2008.

The Galileo satellite constellation will be a Walker  $56^{\circ}:27/3/1$  constellation with an additional inactive spare satellite in each plane. The satellites orbit in an altitude of about 23 222 km above the Earth's surface, corresponding to a semi-major axis of about 29 600 km. Figure 2.7 shows the satellite plane occupancy of a simulated Galileo constellation.<sup>5</sup> An impression of the satellite orbits is given by Fig. 2.6. The figures in Sect. 2.3.2 actually show the Galileo Walker constellation.

The orbital revolution period of a Galileo satellite is 14 hours 05 minutes. A satellite completes 17 orbital revolutions in 10 sidereal days. Figure 2.15a shows the ground track for one satellite over the full repeat period of 10 days. As opposed to the GLONASS, neither satellites from the same nor from different planes follow the same ground tracks as illustrated by Fig. 2.15b. Regular repositioning maneuvers to keep the constellation will not be necessary for the Galileo satellites as the orbital revolution period is not in a deep resonance with the Earth's rotation.

---

<sup>5</sup>The right ascension of the ascending node of the first plane was chosen arbitrarily for the simulation.

The Galileo system will be based on the CDMA technique and all satellites will transmit on RHCP carrier waves of the same frequencies. All frequencies are derived from the fundamental frequency  $f_0 = 10.23$  MHz (which will be corrected for relativistic effects). The planned frequencies are:

$$\begin{aligned}
 \text{E1} & : f_1 = 154 f_0 = 1575.42 \text{ MHz} & \lambda_1 & \approx 19.0 \text{ cm} \\
 \text{E6} & : f_6 = 125 f_0 = 1278.75 \text{ MHz} & \lambda_6 & \approx 23.4 \text{ cm} \\
 \text{E5} & : f_5 = 116.5 f_0 = 1191.80 \text{ MHz} & \text{and } \lambda_5 & \approx 25.2 \text{ cm}, \\
 \text{E5a} & : f_{5a} = 115 f_0 = 1176.45 \text{ MHz} & \lambda_{5a} & \approx 25.5 \text{ cm} \\
 \text{E5b} & : f_{5b} = 118 f_0 = 1207.14 \text{ MHz} & \lambda_{5b} & \approx 24.8 \text{ cm}
 \end{aligned} \tag{2.10}$$

where E5 is split in E5a and E5b. The E1 carrier corresponds to L1 and the E5a to L5 of GPS. Galileo will thus share two frequencies with the GPS to ensure interoperability of both systems.

The signal structure of the Galileo system is rather complex including three types of ranging codes, a free open-access code, and the two encrypted commercial and public regulated codes, respectively. System integrity information as well as different navigation messages will be transmitted. More information on the Galileo signal structure may be found in the official Interface Control Document [ICD, 2010].

#### 2.4.4 Compass Navigation Satellite System (CNSS)

The People's Republic of China develops the GNSS known as Beidou-2, Compass, or Compass Navigation Satellite System (CNSS). In a first step, the Compass will provide regional service to China and neighboring countries. In its final configuration it will be a fully global navigation system.

According to [Grelrier *et al.*, 2007] and [Hofmann-Wellenhof *et al.*, 2008], the Compass constellation is expected to consist of altogether 35 satellites: (a) five satellites in the GEO placed at longitudes of about  $59^\circ$  E,  $80^\circ$  E,  $111^\circ$  E,  $140^\circ$  E, and  $160^\circ$  E; (b) three geosynchronous satellites in three evenly spaced planes with an inclination of  $55^\circ$  and a semi-major axes of about 35 785 km; (c) 27 satellites in the MEO, most probably in a Walker  $55^\circ:24/3/1$  constellation with three additional spares. The semi-major axes will be 27 840 km. As of mid 2011, the actual Compass constellation consists of four geostationary satellites G1–G4 (launched in 2009/2010), four satellites in an inclined GSO (Compass-IGSO1–IGSO4 launched in 2010/2011), and one satellite in the MEO (Compass-M1 launched in 2007). Several other Beidou test satellites have been launched in recent years. It is not known when the CNSS will be fully operational. Figure 2.16 gives an impression of how the full constellation might look like.

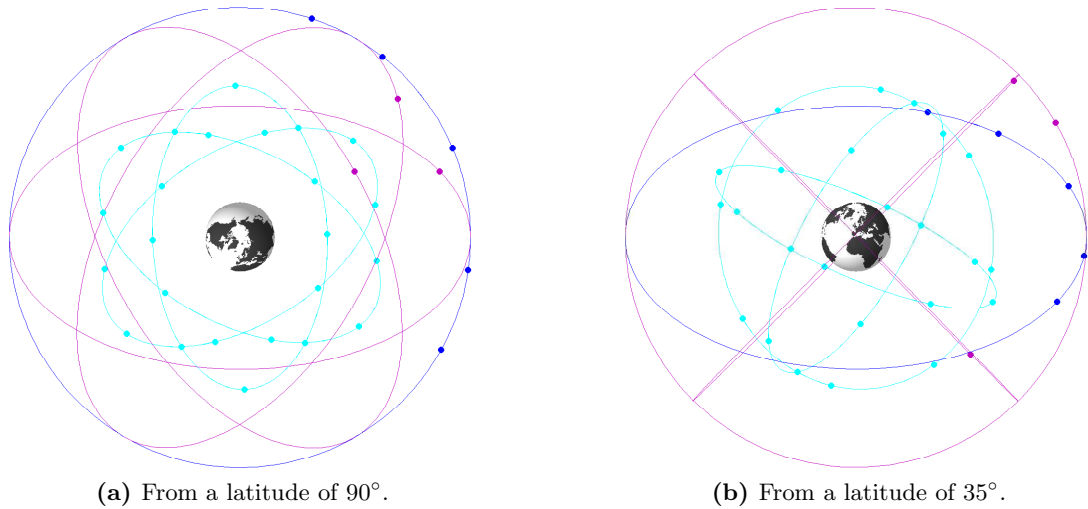


**Figure 2.16:** Simulated Compass satellite orbits.

Compass will use the CDMA technology and provide an open as well as a restricted positioning service on four frequencies:

$$\begin{array}{llll}
 \text{B1} & : f_1 & = 1561.10 \text{ MHz} & \lambda_1 \approx 19.2 \text{ cm} \\
 \text{B1-2} & : f_{1-2} & = 1589.74 \text{ MHz} & \lambda_{1-2} \approx 18.9 \text{ cm} \\
 \text{B2} & : f_2 & = 1207.14 \text{ MHz} & \lambda_2 \approx 24.8 \text{ cm} \\
 \text{B3} & : f_3 & = 1268.52 \text{ MHz} & \lambda_3 \approx 23.6 \text{ cm}
 \end{array}
 \quad \text{and} \quad (2.11)$$

The Compass signals will overlay the GPS military code as well as the publicly regulated code of Galileo in the E1/L1, L2, and E6 frequency bands.

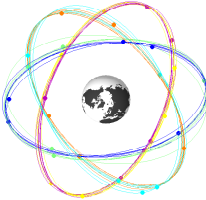
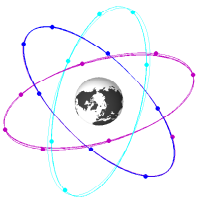
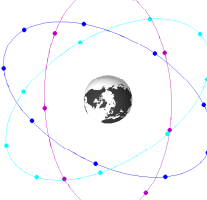
The information on Compass presented in this section reflects the state of knowledge as of mid 2011. Note that reliable information on the system is rather sparse and the final constellation design, frequencies, and signal structure may be subject to changes.

### 2.4.5 Comparison of GPS, GLONASS, and Galileo

The previous sections described the satellite systems GPS, GLONASS, Galileo, and Compass in detail. Table 2.2 summarizes the most important properties and parameters of the GNSS. Compass is not included in the comparison as there are only few assured facts known about the system.

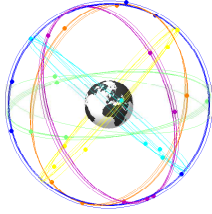
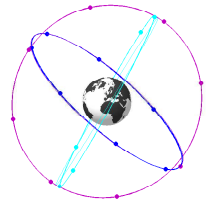
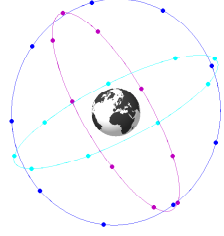
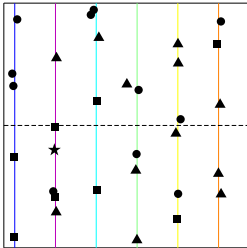
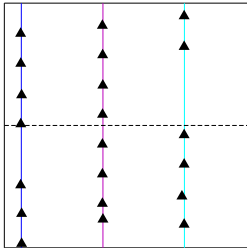
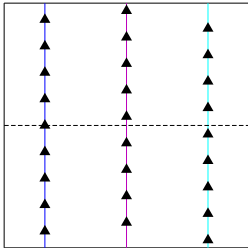
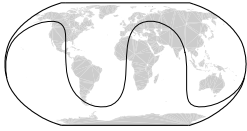
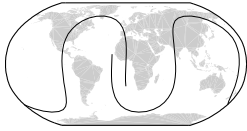
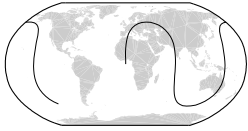
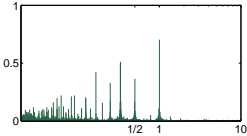
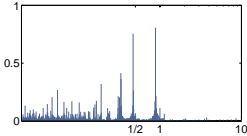
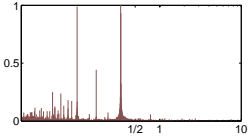
## 2.4 Global Navigation Satellite Systems in Comparison

**Table 2.2:** Important parameters of GPS, GLONASS, and Galileo.

General	GPS	GLONASS	Galileo
Operator/country	USA	Russia	EU
First launch	Feb 22, 1978	Oct 12, 1982	set for 2011 (IOV)
FOC	Jul 17, 1995	Jan 18, 1996 (Sep 24, 1993) <sup>a</sup>	—
<b>Signal characteristics</b>			
Channel access method	CDMA	FDMA	CDMA
Number of frequencies	3	2 base frequencies	5
Reference frequency $f_0$	10.23 MHz	178 MHz	10.23 MHz
Frequency divisor $\Delta f$	—	0.0625 MHz	—
Multipliers $n$	154, 120, 115	9, 7	154, 125, 116.5, 115, 118
Channel numbers $m$	—	-7 to 6	—
Frequency computation	$n f_0$	$n (f_0 + m \Delta f)$	$n f_0$
<b>Orbit characteristics</b>			
Walker designation	—	64.8°: 24/3/1	56°: 27/3/1
Orbital planes	6	3	3
Spacing of planes	60°	120°	120°
Semi-major axis	26 560 km	25 510 km	29 600 km
Inclination	55°	64.8°	56°
Nodal drift $\dot{\Omega}$ per day	-0.0384°	-0.0336°	-0.0260°
Length of GNSS year	351.5 days	353.2 days	355.6 days
SVs current (nominal)	32 (24)	21 (24)	— (27)
SVs per plane	5/6/5/5/6/5	7/8/6	9/9/9
SV in-plane spacing	irregular	45°	40°
SV phase, adjacent plane	irregular	15°	13.3°
Satellite constellation (from 90°)			

*continued next page*

**Table 2.2:** Important parameters of GPS, GLONASS, and Galileo (*continued*).

	GPS	GLONASS	Galileo
Satellite constellation (from 35°)			
Plane occupancy			
Ground tracks			
Revolution period	11 h 58 min $\frac{1}{2}$ sidereal day	11 h 16 min $\frac{8}{17}$ sidereal days	14 h 05 min $\frac{10}{17}$ sidereal days
Repeat cycle	1 sidereal day	8 sidereal days	10 sidereal days
Repeat orbits	2	17	17
Ground track for one day			
Amplitude spectrum of satellite visibility <sup>b</sup>			

<sup>a</sup> Official declaration of FOC with only 12 active satellites in orbit.

<sup>b</sup> Position: Zimmerwald, Switzerland, 46.9° N, 7.5° E; elevation mask: 5°.

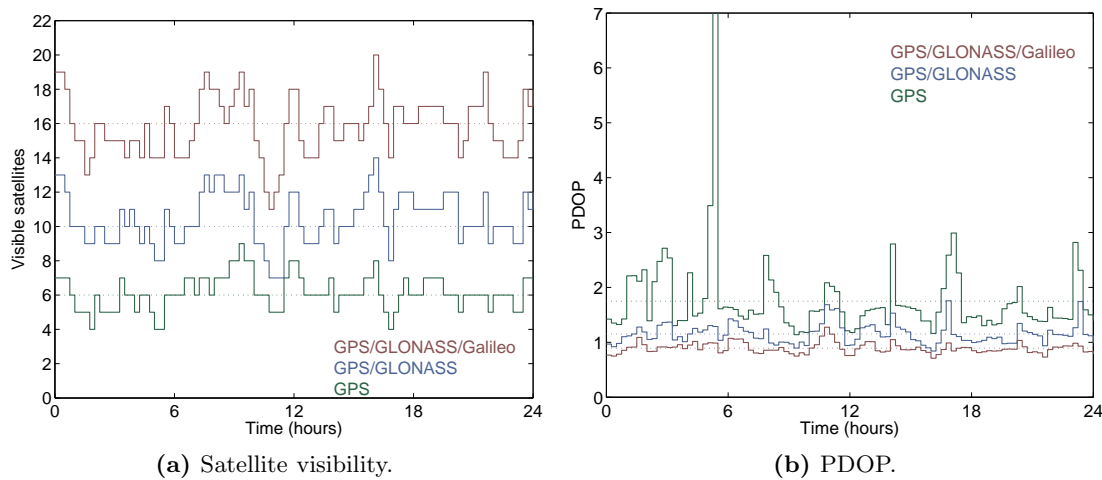


**Figure 2.17:** Visibility and PDOP for satellites above  $25^\circ$  for one day (station Zimmerwald).

## 2.5 Motivation and Benefits of Using Different GNSS

A GNSS user may ask the question why several different systems are needed and whether the benefits of using multiple GNSS counterbalance the investment in more expensive multi-GNSS capable equipment. A data analyst may ask the question whether it is worthwhile to include all available systems and multi-GNSS capabilities in the data processing software. The accuracies achievable with GPS alone are good enough for most navigational purposes, after all. But there are several good reasons for using all available systems and to consequently follow a multi-GNSS approach.

The number of simultaneously visible satellites and the observation geometry are two crucial factors for the quality of a (high-rate) positioning solution—especially under unfavorable observation conditions with a restricted horizon visibility. The number of available satellites is also crucial for applications like atmosphere tomography using GNSS signals. Figures 2.17a and 2.17b show the number of visible satellites and corresponding PDOP values during one day for a mid-latitude station (Zimmerwald, Switzerland,  $46.9^\circ$  N,  $7.5^\circ$  E).<sup>6</sup> An elevation mask of  $25^\circ$  is applied, i. e., only satellites with an elevation of at least  $25^\circ$  are considered, to simulate an observation scenario with obstacles restricting the satellite visibility.

The number of visible satellites varies between four and nine if only GPS is considered; six satellites are visible on the average. The PDOP is about two but reaching values of three several times a day; the maximum PDOP is about seven. According to *Hofmann-Wellenhof et al.* [2008], a PDOP below three indicates a good observation geometry. The

<sup>6</sup>Throughout this section, all values for GPS and GLONASS are computed for the constellations as of December 31, 2010. The values for Galileo are computed from a simulated constellation.

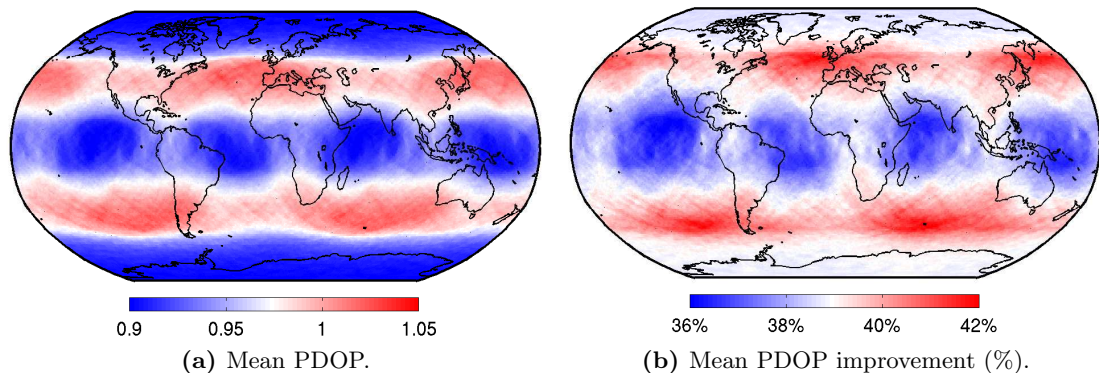


**Figure 2.18:** Mean daily PDOP for a GPS-only solution and mean PDOP improvement if GLONASS and Galileo are added.

situation immediately improves if GLONASS is considered, too. The number of satellites increases on the average by four with a minimum of seven observable satellites. The PDOP is now around 1.2 and the daily variations are greatly reduced. Adding Galileo observations still significantly improves the results. There are now 16 satellites visible on the average (with a minimum of 11 and a maximum of 20). The PDOP shows almost no daily variations and the mean value of 0.9 promises very good positioning results during the entire day.

Figure 2.18a shows the average daily PDOP for a GPS-only solution (using a  $5^\circ$  elevation mask). The PDOP varies between 0.9 to 1.05 reaching its maximum values in mid-latitudes. Figure 2.18b shows the mean PDOP improvement if GLONASS and Galileo are considered, too. The improvement ranges from 35% to 45%. The main improvement is achieved in the mid-latitude regions. As these regions encompass Europe, Asia, North America, and Australia, many users might benefit from a multi-GNSS solution [Springer and Dach, 2010].

Another important advantage of using multiple GNSS is the mitigation of periodic variations in the quality of a positioning solution. The periods of the variations are system-specific and depend on the geometric properties of the constellations. Figure 2.19 shows the amplitude spectrum of the PDOP for station Zimmerwald for periods up to 20 days. The amplitudes are computed from 60 days of data for satellites seen above  $5^\circ$  (the lines for GPS, GLONASS, and Galileo are shifted each by 0.05 for display purposes).

The PDOP spectra of the single systems clearly show constellation-specific signals: the beat frequencies (and harmonics thereof) when sampling the orbital revolution period by one sidereal day, namely 1 sidereal day for GPS and about 0.9 sidereal days for GLONASS; and the number of orbital planes (GLONASS and Galileo). The uniform distributions of the satellites in the orbital planes in the case of GLONASS and Galileo lead to more pronounced periods and in turn to larger amplitudes in the corresponding spectra. The

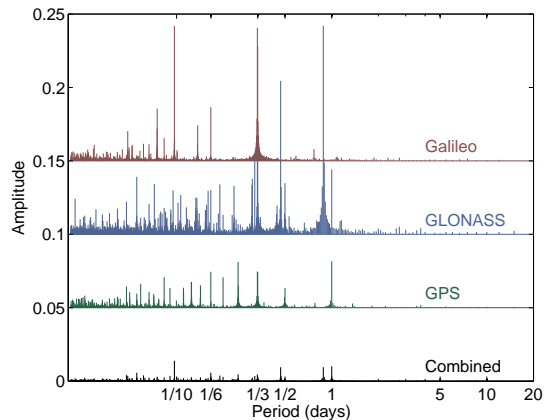


**Figure 2.19:** PDOP amplitude spectra for single- and multi-GNSS solutions (for station Zimmerwald, spectra are shifted by 0.05 for display purposes).

spectral lines for the combined GPS/GLONASS/Galileo multi-GNSS approach are significantly reduced. No pronounced periods remain in PDOP spectrum of the multi-GNSS solutions, promising positioning results of a high and consistent quality in time.

The increased number of satellites and the improved observation geometry are very interesting for navigational applications as the overall performance and quality of a positioning solution might be significantly improved. The use of multiple GNSS is especially beneficial in mid-latitude regions and in difficult environments with a restricted view of the sky. From a scientific point of view, these geometric considerations are not very important. The quality of a scientific GNSS analysis is nowadays not limited by the number of satellites but rather by modeling deficiencies. One may not expect that the results improve following the square root law<sup>7</sup> if the number of satellites or GNSS is increased. However, additional (new) navigation signals on varying frequencies create room for innovation in data processing and will help to improve results. Moreover, combining GNSS with different orbital characteristics will offer opportunities to separate system-specific variations in parameter time series and to sophisticate system- or satellite-specific processing models (e.g., orbit models).

## 2.6 Institutions Relevant to this Work

### 2.6.1 The International GNSS Service

The International GNSS Service (IGS) is a nonprofit voluntary collaboration of over 200 institutions and agencies around the world [Beutler *et al.*, 1999; Dow *et al.*, 2009]. The

<sup>7</sup>The precision of a sample mean improves with the square root of the sample size.

IGS is committed to providing the highest-quality GNSS tracking data, orbits, and other products to promote and facilitate the use of GNSS in Earth sciences.

The first ideas to establish a service for GPS users with highest accuracy requirements were brought forwards at the International Association of Geodesy (IAG) Scientific Assembly in Edinburgh in 1989. After a call for participation in 1991, a three month test campaign was started on June 21, 1992. The test was successful beyond expectations, which is why the service did not cease its operations after the three months period. In 1993, the IGS—originally known as *International GPS Service for Geodynamics* at that time—was officially recognized by the IAG. It started its operation as an IAG service on January 1, 1994, providing GPS products to the scientific community [Beutler *et al.*, 1994a]. In 2005 it was renamed as *International GNSS Service* in order to recognize the importance of the combination of GNSS other than GPS.

The 2008–2012 strategic plan [IGS, 2008] states the mission of the IGS:

The International GNSS Service provides the highest-quality GNSS data, products, and services in support of the terrestrial reference frame; Earth observations and research; Positioning, Navigation, and Timing; and other applications that benefit the scientific community and society.

In 2011, the permanent GNSS tracking network of the IGS consists of more than 300 active stations all around the world. More and more tracking stations are upgraded from GPS-only to multi-GNSS capability. The tracking data is gathered, archived, and made available for online access by regional and global data centers (DCs). The raw tracking data is one of the core products of the IGS.

The tracking data is processed by presently ten IGS analysis centers (ACs). The AC-specific products are combined by the analysis center coordinator (ACC) to generate the official IGS products:

- GPS satellite ephemerides and clock corrections,
- station clock corrections,
- GLONASS satellite ephemerides,
- coordinates and velocities of more than 250 IGS tracking stations, and
- Earth rotation parameters (polar motion coordinates and length-of-day).

Atmospheric parameters, namely station-specific tropospheric zenith path delays and ionosphere maps, are provided by dedicated IGS working groups. The GPS products and the Earth rotation parameters are created and delivered in three product lines, namely the ultra-rapid (with a latency of 3 to 9 hours), the rapid (with a latency of 1 to 2 days), and the final products (with a delay of about 11 to 17 days). The GLONASS orbits presently are contained only in the final product. An ultra-rapid GLONASS product is under development and already available as experimental product.

Further details on the IGS, its structure, and products is given, e. g., by *Dow et al.* [2009]. The IGS online publication archive<sup>8</sup> is a comprehensive source of information.

The raw IGS GNSS tracking data is used as basis for the experiments presented in Part III of this work.

### 2.6.2 The International Laser Ranging Service

The International Laser Ranging Service (ILRS) is (like the IGS) one of the space geodetic services of the IAG. It was established in September 1998 to support geophysical research and to participate in the maintenance of an accurate International Terrestrial Reference Frame (ITRF) [*Pearlman et al.*, 2002; *Gurtner et al.*, 2004].

The ILRS collects, archives, and distributes satellite laser ranging (SLR) and lunar laser ranging (LLR) observations from a global tracking network of about 40 stations. Two data products are generated by the ILRS based on the observation data: (a) coordinates and velocities for the tracking stations; (b) Earth rotation parameters (polar motion, length-of-day). In addition, the ILRS develops SLR-related standards and specifications and promotes an adoption of these standards in the international scientific community.

Even if the main focus lies on dedicated SLR satellites like LAGEOS or ETALON, about 15 SLR tracking stations routinely observe GNSS satellites, too. Tracking of the two GPS satellites (equipped with a retro-reflector) began in 1993 and 1994, respectively. Tracking of the GLONASS satellites was initiated in 1990. More than 25 different GLONASS satellites have been observed until now, although only a maximum of six at a time.

The ILRS web site<sup>9</sup> provides detailed information on the ILRS, its organization, products, technologies, and satellite missions. The SLR observations used to validate the orbit quality (Sect. 7.4) were provided by the ILRS.

### 2.6.3 The Center for Orbit Determination in Europe

The Center for Orbit Determination in Europe (CODE) is a joint venture of four institutions:

- the Astronomical Institute of the University of Bern (AIUB), Bern, Switzerland;
- the Federal Office of Topography (swisstopo), Wabern, Switzerland;
- the Bundesamt für Kartographie und Geodäsie (BKG), Frankfurt a. M., Germany;
- the Institut für Astronomische und Physikalische Geodäsie (IAPG), Technische Universität München (TUM), Munich, Germany.

---

<sup>8</sup><http://www.igs.org> (accessed June 2011)

<sup>9</sup><http://ilrs.gsfc.nasa.gov> (accessed June 2011)

The operational processing of CODE is carried out at the AIUB and uses the latest version of the Bernese GPS Software (BSW) [*Dach et al.*, 2007] for all GNSS-related computations (see Sect. 4.1 for details concerning the BSW).

The CODE presently contributes to three services: as an AC to the IGS; as a local AC to the EUREF, the IAG reference frame sub-commission for Europe; and as an associated AC to the ILRS.

Since the IGS pilot service in 1992, CODE reliably delivers a complete GNSS product set to the IGS and to the user community. Wherever possible, CODE products are used for the experiments in this work.

More information on CODE and available products may be found in the CODE annual and technical reports [*Hugentobler et al.*, 2006] or on the AIUB home page<sup>10</sup>. A recent description of CODE's efforts in multi-GNSS analysis is given by *Dach et al.* [2009], details on the processing strategy in general are provided by the analysis strategy summary [*Schaer et al.*, 2008].

---

<sup>10</sup><http://www.aiub.unibe.ch> (accessed June 2011)

## 3 GNSS Data Processing

This chapter summarizes the necessary facts to consistently analyze observations from different GNSS. Detailed versions of the underlying observation equations are presented in Sect. 3.1. Linear combinations and differences of observations are introduced in Sects. 3.2 and 3.3. Relevant biases are introduced and discussed in Sect. 3.4. Finally, the least-squares parameter estimation method is briefly summarized in Sect. 3.5.

### Notation and Formalism

The observation equations get more and more complicated when increasing the level of details. We will keep the equations as simple and readable as possible without losing information or generality. Our notation is based on a few principles:

1. All quantities in the observation equations get symbols from the *Latin alphabet*.
2. Generally accepted symbols are used for physical quantities.
3. Vectors and matrices are typeset in a *bold font*.
4. *Capital letters* are used for station-specific quantities.
5. *Lower case letters* are used for satellite-specific quantities.
6. Capital letters in a *calligraphic font* are used for quantities specific to both, stations and satellites.

Extensive indexing is avoided and indices are omitted if no danger of confusion arises. Numeric subscripts are used as generic observation designators. Subscripts with capital letters are used to distinguish observations from different stations, superscripts in lower case refer to satellites.

### 3.1 Fundamental Observation Equations

GNSS observations are one-way ranges deduced from the comparison of a signal generated and transmitted by a satellite with a reference signal generated by a receiver. The satellite and receiver clocks used for signal generation contain errors, which in turn bias the measured range observation. The observations are therefore called pseudoranges (PRs). PRs can be deduced from navigation codes modulated on a carrier wave or more directly

from the phase of the carrier wave itself. Following customary nomenclature, the term pseudorange is associated only with code but not with the phase observations.

### 3.1.1 Code Pseudorange Observation Equation

The code PR observation  $\mathcal{C}$  of a navigation code transmitted by a satellite at emission time  $t'$  and recorded by a receiver at reception time  $T'$  is given in units of length by

$$\mathcal{C} = c(T' - t') = c\mathcal{D}', \quad (3.1)$$

where

- $\mathcal{C}$  is the code PR measured by the receiver,
- $c$  is the vacuum speed of light (being 299 792 458 m/s),
- $T'$  is the receiver clock reading at signal reception time,
- $t'$  is the signal transmission time as given by the satellite clock, and
- $\mathcal{D}'$  is the signal travel time.

Referring both clock readings  $T'$  and  $t'$  to a common—in principle arbitrary—timescale and introducing the corresponding synchronization errors, Eq. (3.1) may be written as

$$\mathcal{C} = c((T + S) - (t + s)) = c\mathcal{D} + cS - cs, \quad (3.2)$$

where

- $T, t$  are the signal reception and emission time referring to a common timescale,
- $S, s$  are the station and satellite clock synchronization errors so that  $T' = T + S$  and  $t' = t + s$ , and
- $\mathcal{D}$  is the clock-bias free signal travel time, i. e.,  $\mathcal{D} = \mathcal{D}' - S + s$ .

Usually, the GPS system time as maintained by the master control station (see Sect. 2.2) is used as timescale. This approach is reasonable in a GPS-only analysis. In a GLONASS-only scenario, one must refer the time to the GLONASS time. In multi-GNSS applications, however, the choice of a reference timescale is a matter of convention.

The term  $c\mathcal{D}$  in Eq. (3.2) does not only represent the geometric distance between receiver and satellite but also contains signal delays, e. g., due to the Earth's atmosphere. A more

detailed version of the observation equation is established by explicitly splitting up  $c \mathcal{D}$  into its constituents and adding an error term. A refined version of Eq. (3.2) is

$$\begin{aligned} \mathcal{C} = & |(\mathbf{R} + \mathbf{E} + \mathbf{Y}) - (\mathbf{r} + \mathbf{e} + \mathbf{y})| \\ & + cS - cs + cB - cb + \mathcal{T} + \mathcal{I} \\ & + \mathcal{U} + \mathcal{Q} + \mathcal{V}, \end{aligned} \quad (3.3)$$

where

- $\mathbf{R}$  is the geocentric position vector of the station reference point in an Earth-fixed frame at observation time,
- $\mathbf{r}$  is the geocentric position vector of the center of mass (COM) of the satellite in the same Earth-fixed reference frame at observation time (see Sect. 3.1.3 for the transformation between the inertial and the Earth-fixed frame),
- $\mathbf{E}$  is the station antenna eccentricity, i. e., the vector pointing from the station reference point to the antenna reference point (ARP),
- $\mathbf{e}$  is the satellite antenna eccentricity vector pointing from COM to ARP,
- $\mathbf{Y}, \mathbf{y}$  are the antenna phase center vectors of the station and the satellite w. r. t. the respective ARP, i. e., vectors pointing from ARP to the antenna phase center,
- $B, b$  are code biases (CBs) caused by receiver and satellite hardware delays of the ranging code signal,
- $\mathcal{T}$  is the signal delay due to the Earth's troposphere,
- $\mathcal{I}$  is the ionospheric signal delay caused by the Earth's ionosphere,
- $\mathcal{U}$  is a correction term due to relativistic effects,
- $\mathcal{Q}$  is the code multipath (MP) caused by reflected signals, and
- $\mathcal{V}$  contains all remaining unmodeled effects and the observation noise.

The position vector  $\mathbf{R}$  contains all relevant displacements due to plate tectonics, solid Earth tides, pole tides, ocean loading, atmospheric loading, post-glacial rebound, etc. *Petit and Luzum* [2010] and *Dong et al.* [2002] list and describe many displacement effects.

The transmission and reception points of a carrier wave are defined by the electromagnetic properties of the antennas. The antenna phase center vectors  $\mathbf{Y}$  and  $\mathbf{y}$  are sometimes split up in phase center offsets (PCOs) and phase center variations (PCVs). The offsets are the difference of the ARP to the mean electromagnetic reference point. They depend on antenna hardware and carrier frequency. The position of the actual phase center of an

antenna additionally depends on the direction (azimuth and elevation) of the signal and is modeled by the PCVs. Detailed information on modeling and calibrating antenna phase centers is provided, e. g., by *Rothacher et al.* [1996], *Mader* [1999], *Schmid and Rothacher* [2003], or *Görres et al.* [2006].

The signal delays caused by the troposphere and ionosphere are extensively discussed in the GNSS literature, e. g., in [*Teunissen and Kleusberg*, 1998]. Up-to-date troposphere models are provided by *Böhm et al.* [2006a, 2006b]. *Schaer* [1999] provides a deep insight into ionosphere modeling and *Petrie et al.* [2011] give a comprehensive review of higher order ionospheric effects. As opposed to the tropospheric refraction the ionospheric signal delay depends on the frequency  $f$  of the underlying carrier ( $\mathcal{I} \sim f^{-2}$ ).

Modern GNSS provide several navigation codes on different carrier waves. Frequency-dependent satellite hardware signal delays for the individual code types are responsible for the satellite biases  $b$ . Some of the codes are encrypted by the system operators for security reasons. A direct tracking of these code types is thus not possible for unauthorized users. However, several methods (receiver tracking modes) have been developed to circumvent this problem. These modes may lead to different signal hardware delays in the receiver. Consequently, the receiver bias  $B$  depends not only on the code type but also on the particular tracking mode. The receiver biases are in addition frequency dependent. The frequency dependence is important when observations on different carriers are combined or if FDMA systems like GLONASS are tracked. An overview of the most popular tracking technologies is given by *Hofmann-Wellenhof et al.* [2008].

The correction term  $\mathcal{U}$  contains effects due to special and general relativity. These effects are relevant for signal propagation as well as for satellite and receiver clocks. An extensive discussion of the relevant relativistic effects is provided in [*Ashby*, 2003; *Kouba*, 2004].

The multipath error  $\mathcal{Q}$  is caused by the interference of direct and reflected signals at the receiving antenna. *Bilich and Larson* [2009] give an introduction to MP, its connection to the signal-to-noise ratio (SNR), and to some applications. The effect of signal scattering is investigated in [*Elósegui et al.*, 1995] and methods to mitigate MP are summarized in [*Hofmann-Wellenhof et al.*, 2008].

### 3.1.2 Phase Observation Equation

The phase observation  $\mathcal{P}$  emerges from the comparison of a received carrier wave with a reconstructed one in the receiver. The difference between these carrier waves (beat phase) yields a fractional part and an integrated integer number of phase cycles. The unknown initial number of integer cycles between the satellite and receiver carriers is called initial phase ambiguity  $\mathcal{N}$ .

The phase observation equation (in units of length) has the same structure as the code observation equation (3.3) with additional phase-related parameters:

$$\begin{aligned} \mathcal{P} = & |(\mathbf{R} + \mathbf{E} + \mathbf{Y}) - (\mathbf{r} + \mathbf{e} + \mathbf{y})| \\ & + cS - cs + cA - ca + \mathcal{T} - \mathcal{I} \\ & + \lambda(P - p) + \lambda\mathcal{N} + \lambda\mathcal{W} + \mathcal{U} + \mathcal{M} + \mathcal{E}, \end{aligned} \quad (3.4)$$

where

- $A, a$  are phase biases (PBs) caused by receiver and satellite hardware delays of the carrier wave,
- $\lambda$  is the carrier wavelength,
- $P, p$  are the initial phase readings of receiver and satellite at an arbitrary start epoch,
- $\mathcal{N}$  is the initial phase ambiguity,
- $\mathcal{W}$  is the phase polarization effect (also known as phase wind-up),
- $\mathcal{M}$  is the phase multipath, and
- $\mathcal{E}$  contains all remaining unmodeled effects and the observation noise.

The phase ambiguity  $\mathcal{N}$  is constant as long as the signal is continuously tracked. A new ambiguity must be set up if the signal is re-acquired after a loss of lock or if a cycle slip (jump in the number of cycles caused by an interruption of the tracking) occurred. The ambiguity  $\mathcal{N}$  is an integer number of cycles by construction. Determining the correct integer values (ambiguity resolution) and introducing the values as known (ambiguity fixing) strengthens the solution [Mervart, 1995]. *Teunissen and Kleusberg [1998]* provide a thorough introduction to the field of ambiguity resolution.

The initial phase readings of the receiver and satellite are constant as long as the equipment is not reset or restarted.

The receiver phase bias  $A$  depends on the carrier frequency and on the GNSS. Additionally, it depends on the tracking mode just as the receiver bias  $B$  in Eq. (3.3). The satellite bias  $a$ —unlike its analog in the code equation—only depends on the frequency carrier wave but not on code type.

The phase wind-up  $\mathcal{W}$  is relevant for circularly polarized carrier waves (as commonly used by GNSS). A change in the orientation of the satellite’s antenna with respect to the receiving antenna (a rotation) is manifested either as carrier phase advance or delay. More information concerning this topic may be found in [*Wu et al., 1993*].

As opposed to the ionospheric signal delay for code observations we have a phase advance due to the ionospheric refraction, reflected by the opposite signs for the term  $\mathcal{I}$  in Eqs. (3.3) and (3.4).

### 3.1.3 Satellite and Receiver Positions

The receiver position  $\mathbf{R}$  and the satellite position  $\mathbf{r}$  in Eqs. (3.3) and (3.4) must be provided in one and the same reference frame. As the receiver position is usually available in the Earth-fixed frame and the satellite position in the inertial frame, we have to transform either the receiver position to the inertial or the satellite position to the Earth-fixed frame. The transformations are given by

$$\mathbf{R}' = \mathbf{P}(T) \mathbf{N}(T) \mathbf{R}_3(-\Theta) \mathbf{R}_1(y_p) \mathbf{R}_2(x_p) \mathbf{R} \quad \text{and} \quad (3.5a)$$

$$\mathbf{r} = \mathbf{R}_2(-x_p) \mathbf{R}_1(-y_p) \mathbf{R}_3(\Theta) \mathbf{N}^{-1}(t) \mathbf{P}^{-1}(t) \mathbf{r}', \quad (3.5b)$$

where

$\mathbf{R}', \mathbf{r}'$  are the receiver and satellite positions in the inertial frame at observation times  $T$  and  $t$ , respectively,

$\mathbf{P}, \mathbf{N}$  are the precession and nutation matrices,

$\mathbf{R}_n(\alpha)$  characterizes a particular rotation around axis  $n$  by a rotation angle  $\alpha$ ,

$\Theta$  is the Greenwich apparent sidereal time (GAST), and

$x_p, y_p$  are the polar coordinates.

The transformation quantities  $\mathbf{P}, \mathbf{N}, \Theta, x_p$ , and  $y_p$  provide the link between the terrestrial and inertial reference frame [*Petit and Luzum, 2010; Capitaine et al., 2002*].

The position vector  $\mathbf{r}'$  of the satellite's COM is a particular solution of the equations of motion (2.3) as presented in Sect. 2.3. It is a function of the orbital elements and the parameters of the force models (e. g., parameters related to radiation pressure).

## 3.2 Linear Combinations of Observations

Modern geodetic GNSS receivers aiming at highest accuracy record (a substantial subset of) all signals transmitted by the satellites. Phase and code observations are available for more than one carrier frequency; different code types may be available. All these observations to one and the same satellite can be combined to yield new observations, commonly called linear combinations (LCs).

**Table 3.1:** Properties of linear combinations and resulting conditions for the coefficients.

Property of linear combination	Condition for coefficients
Elimination of frequency-independent parameters	$\sum \mathbf{c}_i + \sum \mathbf{p}_j = 0$
Preservation of frequency-independent parameters	$\sum \mathbf{c}_i + \sum \mathbf{p}_j = 1$
Elimination of (1st-order) ionospheric delay	$\sum (\mathbf{c}_i f_i^{-2}) - \sum (\mathbf{p}_j f_j^{-2}) = 0$

Let all available code and phase observations of a station to one satellite at one observation epoch be  $\mathcal{C}_i$  and  $\mathcal{P}_j$  with  $i = 1, \dots, n$  and  $j = 1, \dots, m$ . Any particular linear combination  $\mathcal{L}$  can be represented as

$$\mathcal{L} = \sum_{i=1}^n \mathbf{c}_i \mathcal{C}_i + \sum_{j=1}^m \mathbf{p}_j \mathcal{P}_j, \quad (3.6)$$

where

$\mathbf{c}_i$  are the LC factors for the code observations  $\mathcal{C}_i$  and

$\mathbf{p}_j$  are the LC factors for the phase observations  $\mathcal{P}_j$ .

A linear combination is unambiguously described by a set of coefficients  $\mathbf{c}_i$  and  $\mathbf{p}_j$ . Equation (3.6) is the general case of a so-called mixed LC, i. e., an observation combining code and phase observations. Pure code- and phase-only LCs can easily be created by setting either all  $\mathbf{p}_j$  or all  $\mathbf{c}_i$  to zero.

The noise  $\sigma_{\mathcal{L}}$  of a linear combination follows from the law of error propagation as

$$\sigma_{\mathcal{L}}^2 = \sum_{i=1}^n (\mathbf{c}_i \sigma_{\mathcal{C}_i})^2 + \sum_{j=1}^m (\mathbf{p}_j \sigma_{\mathcal{P}_j})^2, \quad (3.7)$$

where the observation noise of its single constituents ( $\sigma_{\mathcal{C}_i}$  and  $\sigma_{\mathcal{P}_j}$ ) is assumed to be uncorrelated.

A “reasonable” linear combination must have advantageous characteristics as compared to the original observations. Particular features of a LC put constraints on the selection of the coefficients  $\mathbf{c}_i$  and  $\mathbf{p}_j$ . Table 3.1 lists important LC characteristics and the resulting conditions for the coefficients. Several well-established linear combinations are in use today, each of them serving a special purpose like, e. g., eliminating terms common to all involved observations to facilitate preprocessing or ambiguity resolution.

### 3.3 Differences of Observations

Several terms in the GNSS observation equations (3.3) and (3.4) only depend on the station or on the satellite. A receiver clock error, for example, introduces the same error

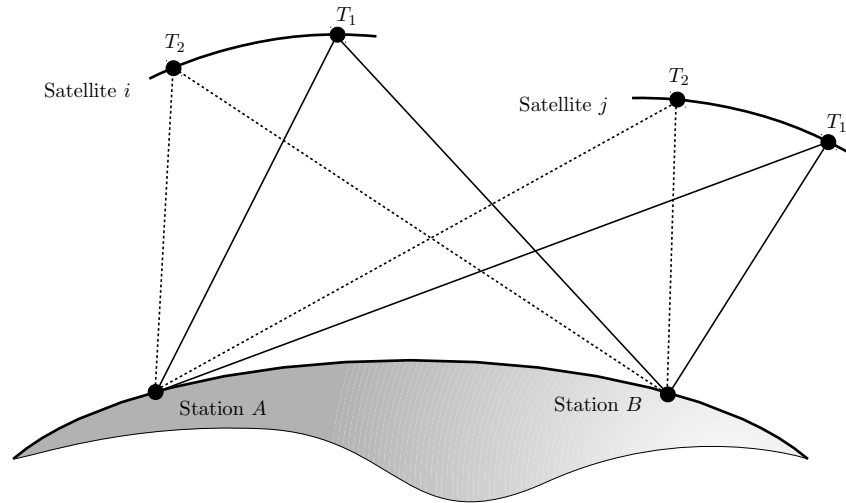


**Figure 3.1:** Observation configuration for 2 stations tracking 2 satellites at 2 epochs (12 SDs, 6 DDs, and 1 TD can be formed from the 8 observations).

in all observations taken by the receiver. This fact is exploited by forming differences between observations where such terms are eliminated.

A difference may be formed for any two observations but preferably the observations vary in only one characteristic, namely either in station, satellite, or epoch. Three types (or degrees) of differences are commonly used in GNSS analysis:

**Single differences (SDs)** are derived from two original observations. A particular SD involves either two stations, or two satellites, or two—in most cases consecutive—observation epochs.

**Double differences (DDs)** are created by taking the difference of two single differences. The involved SDs have either the station pair, the satellite pair, or the observation epoch in common.

**Triple differences (TDs)** are differences of double differences. A TD involves exactly two stations, two GNSS satellites, and two (usually subsequent) observation epochs.

The classification of observations in linear combinations on one hand and differences on the other hand is redundant because the differences between stations, satellites, and epochs can easily be represented by the LC equation (3.6), if the observations  $\mathcal{C}_i$  and  $\mathcal{P}_j$  are not restricted to one and the same station, satellite, and epoch. However, the classification is well-established and can be used without loss of generality.

Figure 3.1 illustrates the tracking situation for two stations observing the same two satellites at two observation epochs. Twelve single differences and six double differences can be created from the eight original observations. One triple difference may be retrieved from

the double differences. The original observations (3.3) and (3.4) are commonly referred to as zero differences (ZDs) or undifferenced observations in this context.

The noise of a differenced observation increases following the law of error propagation. The noise of a SD, DD, and TD is a factor of  $\sqrt{2}$ ,  $\sqrt{4}$ , and  $\sqrt{8}$  higher as compared to the undifferenced observations (assuming independence of all original observations and the same basic noise). Finally it should be mentioned that all differenced observations derived from a basic set of original observations are mathematically correlated. These correlations must be taken into account when striving for the highest precision. *Beutler et al.* [1987] and *Hofmann-Wellenhof et al.* [2008] explain the correlations in detail.

From this point onwards, some simplifications of the observation equations are made for the sake of readability and to keep the focus on parameters relevant for this work:

1. The antenna eccentricities  $\mathbf{E}$  and  $\mathbf{e}$  are constant for all types of observations and will be included in the geocentric positions by setting  $\mathbf{R} \stackrel{\text{def}}{=} \mathbf{R} + \mathbf{E}$  and  $\mathbf{r} \stackrel{\text{def}}{=} \mathbf{r} + \mathbf{e}$ .
2.  $\mathcal{R}$  is introduced as geometric receiver–satellite distance whenever compact equations are required:  $\mathcal{R} \stackrel{\text{def}}{=} |(\mathbf{R} + \mathbf{Y}) - (\mathbf{r} + \mathbf{y})|$ .
3. The relativistic term  $\mathcal{U}$  and the phase wind-up  $\mathcal{W}$  are omitted because these effects are usually not estimated but captured by models.
4. We consider multipath as an unmodeled effect contributing to the error budget of an observation. Therefore it is included in the error term, so that  $\mathcal{V} \stackrel{\text{def}}{=} \mathcal{V} + \mathcal{Q}$  and  $\mathcal{E} \stackrel{\text{def}}{=} \mathcal{E} + \mathcal{M}$ .
5. All single error terms  $\mathcal{V}_i$  and  $\mathcal{E}_j$  are merged into one term  $\mathcal{V}$  or  $\mathcal{E}$  when forming LCs or differences of observations.

### 3.3.1 Single Differences

The most general code single-difference observation equation based on two observations  $\mathcal{C}_1$  and  $\mathcal{C}_2$  is described by

$$\begin{aligned} \mathcal{C}_1 - \mathcal{C}_2 = & |(\mathbf{R}_1 + \mathbf{Y}_1) - (\mathbf{r}_1 + \mathbf{y}_1)| - |(\mathbf{R}_2 + \mathbf{Y}_2) - (\mathbf{r}_2 + \mathbf{y}_2)| \\ & + \mathcal{T}_1 - \mathcal{T}_2 + \mathcal{I}_1 - \mathcal{I}_2 \\ & + c S_1 - c S_2 - c s_1 + c s_2 + c B_1 - c B_2 - c b_1 + c b_2 + \mathcal{V}. \end{aligned} \quad (3.8)$$

Accordingly, the phase single difference reads as

$$\begin{aligned} \mathcal{P}_1 - \mathcal{P}_2 = & |(\mathbf{R}_1 + \mathbf{Y}_1) - (\mathbf{r}_1 + \mathbf{y}_1)| - |(\mathbf{R}_2 + \mathbf{Y}_2) - (\mathbf{r}_2 + \mathbf{y}_2)| \\ & + \mathcal{T}_1 - \mathcal{T}_2 - \mathcal{I}_1 + \mathcal{I}_2 \\ & + c S_1 - c S_2 - c s_1 + c s_2 + c A_1 - c A_2 - c a_1 + c a_2 \\ & + \lambda_1 (P_1 - p_1) + \lambda_1 \mathcal{N}_1 - \lambda_2 (P_2 - p_2) - \lambda_2 \mathcal{N}_2 + \mathcal{E}. \end{aligned} \quad (3.9)$$

The most important differences between the two SDs are the phase ambiguities  $\mathcal{N}$  and the initial phase terms  $(P - p)$ , which are only present in the phase equation, and the opposite signs of the ionospheric correction terms  $\mathcal{I}$  in the two equations.

Both equations can formally be simplified without loss of information by introducing the single-difference symbols  $(\cdot)_{\alpha\beta} \stackrel{\text{def}}{=} (\cdot)_{\alpha} - (\cdot)_{\beta}$  and  $(\cdot)^{\alpha\beta} \stackrel{\text{def}}{=} (\cdot)^{\alpha} - (\cdot)^{\beta}$ . Indices may be omitted if there is no danger of confusion.

The reduced general SD equations for code and phase are then given by

$$\mathcal{C}_{12} = \mathcal{R}_{12} + \mathcal{T}_{12} + \mathcal{I}_{12} + c S_{12} - c s_{12} + c B_{12} - c b_{12} + \mathcal{V} \quad \text{and} \quad (3.10a)$$

$$\begin{aligned} \mathcal{P}_{12} = \mathcal{R}_{12} + \mathcal{T}_{12} - \mathcal{I}_{12} + c S_{12} - c s_{12} + c A_{12} - c a_{12} \\ + \lambda_1 (P_1 - p_1) - \lambda_2 (P_2 - p_2) + \lambda_1 \mathcal{N}_1 - \lambda_2 \mathcal{N}_2 + \mathcal{E}. \end{aligned} \quad (3.10b)$$

### Station differences

This type of SD is derived from observations from two stations tracking the same signal of the same satellite at a quasi-simultaneous epoch. Code type and tracking mode may be different for the two observations.

Observations from two receivers are usually not recorded at exactly the same epoch ( $T_A \neq T_B$ ) due to the receiver clock errors and to the differences in the signal travel time. Modern GNSS receivers, however, continuously update the internal clock. The resulting clock corrections therefore remain comparatively small and the assumption  $T_A \approx T_B$  is sufficiently accurate to allow some simplifications in Eqs. (3.10). Together with the fact that the difference in travel time  $\mathcal{D}_A$  and  $\mathcal{D}_B$  is always below 0.05 seconds, it is justified to assume that the satellite clock correction  $s$  and the satellite phase bias  $a$  are constant over the very short time interval  $T_A - T_B$ .

Let  $\mathcal{C}_A$ ,  $\mathcal{P}_A$ ,  $\mathcal{C}_B$ , and  $\mathcal{P}_B$  be (quasi-) simultaneous observations of the same signal of one satellite recorded by two receivers  $A$  and  $B$ . The satellite clock correction  $s$ , the satellite phase bias  $a$ , and the initial phase reading  $p$  are the same for both observations ( $s_A = s_B$ ,  $a_A = a_B$ , and  $p_A = p_B$ ). Signal frequency  $f$  and wavelength  $\lambda$  are identical, as well ( $f = f_A = f_B$ ,  $\lambda = \lambda_A = \lambda_B$ ).

The general SD equations (3.10) are therefore reduced to

$$\mathcal{C}_{AB} = \mathcal{R}_{AB} + \mathcal{T}_{AB} + \mathcal{I}_{AB} + c S_{AB} + c B_{AB} - c b_{AB} + \mathcal{V} \quad \text{and} \quad (3.11a)$$

$$\begin{aligned} \mathcal{P}_{AB} = \mathcal{R}_{AB} + \mathcal{T}_{AB} - \mathcal{I}_{AB} + c S_{AB} + c A_{AB} \\ + \lambda P_{AB} + \lambda \mathcal{N}_{AB} + \mathcal{E}. \end{aligned} \quad (3.11b)$$

The presence of the satellite code bias term  $b_{AB}$  in Eq. (3.11a) is an important difference between the phase and code SD observation. As opposed to its phase analog it only

cancels, if the same code type is tracked by both receivers. Code and phase biases are discussed in detail in Sects. 3.4.2 and 3.4.4.

### Satellite differences

The second possibility to create a SD involves observations  $\mathcal{C}^i$ ,  $\mathcal{P}^i$ ,  $\mathcal{C}^j$ , and  $\mathcal{P}^j$  to two satellites  $i$  and  $j$  recorded by one station at the same epoch. Both observed carriers should ideally—but not necessarily—have the same frequency. This is, however, not always possible, e. g., in the case of cross-GNSS differences or for satellites from an FDMA-based system.

The code and phase SDs are given by

$$\mathcal{C}^{ij} = \mathcal{R}^{ij} + \mathcal{T}^{ij} + \mathcal{I}^{ij} - c s^{ij} + c B^{ij} - c b^{ij} + \mathcal{V} \quad \text{and} \quad (3.12a)$$

$$\begin{aligned} \mathcal{P}^{ij} = & \mathcal{R}^{ij} + \mathcal{T}^{ij} - \mathcal{I}^{ij} - c s^{ij} + c A^{ij} - c a^{ij} \\ & + \lambda^i (P - p^i) - \lambda^j (P - p^j) + \lambda^i \mathcal{N}^i - \lambda^j \mathcal{N}^j + \mathcal{E}. \end{aligned} \quad (3.12b)$$

The station clock synchronization terms  $S^i$  and  $S^j$  are the same for both observations and cancel. The initial phase  $P$  is the same for all observations of a particular receiver ( $P = P^i = P^j$ ).

Further simplifications can be made if the observations are identical in frequency, code type, and tracking mode: the receiver code bias difference  $B^{ij}$  is zero; the initial phase terms are reduced to  $-\lambda p^{ij}$ ; and the ambiguity difference  $\lambda^i \mathcal{N}^i - \lambda^j \mathcal{N}^j$  can be represented by an integer SD ambiguity  $\lambda \mathcal{N}^{ij}$ . The receiver phase bias difference  $A^{ij}$  cancels only if the two observed satellites belong to the same GNSS.

### Epoch differences

This type of SD is created from observations of one station to a satellite at two epochs  $T_1$  and  $T_2$ . Frequency  $f$ , wavelength  $\lambda$ , code type, and tracking mode are the same for both observations. The phase ambiguities  $\mathcal{N}$  are eliminated as long as no cycle slip occurs. The phase terms  $P$  and  $p$  cancel, as well. The receiver and satellite code and phase biases  $B$ ,  $b$ ,  $A$ , and  $a$  can be treated as constant if  $T_1$  and  $T_2$  are close (e. g., consecutive epochs with a spacing of 30 seconds) and are therefore eliminated.

The code and phase epoch SDs are

$$\mathcal{C}(T_{12}) = \mathcal{R}(T_{12}) + \mathcal{T}(T_{12}) + \mathcal{I}(T_{12}) + c S(T_{12}) - c s(T_{12}) + \mathcal{V} \quad \text{and} \quad (3.13a)$$

$$\mathcal{P}(T_{12}) = \mathcal{R}(T_{12}) + \mathcal{T}(T_{12}) - \mathcal{I}(T_{12}) + c S(T_{12}) - c s(T_{12}) + \mathcal{E}. \quad (3.13b)$$

The epoch differences contain only the variations of the parameters in time.

### 3.3.2 Double Differences

A code double-difference observation is the difference between two SDs  $\mathcal{C}_{12}$  and  $\mathcal{C}_{34}$  and is thus composed of four ZD observations. A phase DD observation accordingly contains four ZD phase observations  $\mathcal{P}_1$ ,  $\mathcal{P}_2$ ,  $\mathcal{P}_3$ , and  $\mathcal{P}_4$ .

The general phase and code DD observations read as

$$\begin{aligned} \mathcal{C}_{12} - \mathcal{C}_{34} = & \left| (\mathbf{R}_1 + \mathbf{Y}_1) - (\mathbf{r}_1 + \mathbf{y}_1) \right| - \left| (\mathbf{R}_2 + \mathbf{Y}_2) - (\mathbf{r}_2 + \mathbf{y}_2) \right| \\ & - \left| (\mathbf{R}_3 + \mathbf{Y}_3) - (\mathbf{r}_3 + \mathbf{y}_3) \right| + \left| (\mathbf{R}_4 + \mathbf{Y}_4) - (\mathbf{r}_4 + \mathbf{y}_4) \right| \\ & + \mathcal{T}_1 - \mathcal{T}_2 - \mathcal{T}_3 + \mathcal{T}_4 + \mathcal{I}_1 - \mathcal{I}_2 - \mathcal{I}_3 + \mathcal{I}_4 \\ & + c S_1 - c S_2 - c S_3 + c S_4 - c s_1 + c s_2 + c s_3 - c s_4 \\ & + c B_1 - c B_2 - c B_3 + c B_4 - c b_1 + c b_2 + c b_3 - c b_4 + \mathcal{V} \quad \text{and} \end{aligned} \quad (3.14a)$$

$$\begin{aligned} \mathcal{P}_{12} - \mathcal{P}_{34} = & \left| (\mathbf{R}_1 + \mathbf{Y}_1) - (\mathbf{r}_1 + \mathbf{y}_1) \right| - \left| (\mathbf{R}_2 + \mathbf{Y}_2) - (\mathbf{r}_2 + \mathbf{y}_2) \right| \\ & - \left| (\mathbf{R}_3 + \mathbf{Y}_3) - (\mathbf{r}_3 + \mathbf{y}_3) \right| + \left| (\mathbf{R}_4 + \mathbf{Y}_4) - (\mathbf{r}_4 + \mathbf{y}_4) \right| \\ & + \mathcal{T}_1 - \mathcal{T}_2 - \mathcal{T}_3 + \mathcal{T}_4 - \mathcal{I}_1 + \mathcal{I}_2 + \mathcal{I}_3 - \mathcal{I}_4 \\ & + c S_1 - c S_2 - c S_3 + c S_4 - c s_1 + c s_2 + c s_3 - c s_4 \\ & + c A_1 - c A_2 - c A_3 + c A_4 - c a_1 + c a_2 + c a_3 - c a_4 \\ & + \lambda_1 (P_1 - p_1) - \lambda_2 (P_2 - p_2) - \lambda_3 (P_3 - p_3) + \lambda_4 (P_4 - p_4) \\ & + \lambda_1 \mathcal{N}_1 - \lambda_2 \mathcal{N}_2 - \lambda_3 \mathcal{N}_3 + \lambda_4 \mathcal{N}_4 + \mathcal{E}. \end{aligned} \quad (3.14b)$$

A DD observation is usually not created from two arbitrary SDs but from SDs of the same type, i. e., either from station, satellite, or epoch differences.

#### Station and satellite differences

This type of DD observations involves exactly two stations ( $A$ ,  $B$ ), two satellites ( $i$ ,  $j$ ), and one observation epoch. It is created either from two simultaneous station-difference SDs to two satellites or from two simultaneous satellite-differences from two stations.

The satellite and receiver clock offsets  $s$  and  $S$ , the satellite phase biases  $a$ , and the initial phase readings  $p$  are eliminated. The code DD observation equation (3.14a) then reads as

$$\mathcal{C}_{AB}^{ij} = \mathcal{R}_{AB}^{ij} + \mathcal{T}_{AB}^{ij} + \mathcal{I}_{AB}^{ij} + c B_{AB}^{ij} + c b_{AB}^{ij} + \mathcal{V}. \quad (3.15a)$$

The DD phase observation is given by

$$\begin{aligned} \mathcal{P}_{AB}^{ij} = & \mathcal{R}_{AB}^{ij} + \mathcal{T}_{AB}^{ij} - \mathcal{I}_{AB}^{ij} + c A_{AB}^{ij} \\ & + \lambda^i P_{AB}^i - \lambda^j P_{AB}^j + \lambda^i \mathcal{N}_{AB}^i - \lambda^j \mathcal{N}_{AB}^j + \mathcal{E}. \end{aligned} \quad (3.15b)$$

The satellite CB terms  $b$  in Eq. (3.15a) are eliminated only if the same code types are observed by both receivers. The receiver CBs  $B$  are eliminated if a receiver uses the same code type and tracking mode for both code measurements.

The difference  $\lambda^i \mathcal{N}_{AB}^i - \lambda^j \mathcal{N}_{AB}^j$  yields an integer DD ambiguity (see Sect. 3.4.1) if the carrier wavelength is the same for all observations ( $\lambda = \lambda^i = \lambda^j$ ). The initial phase terms  $P$  in Eq. (3.15b) cancel in that case, as well. The receiver PBs  $A$  are only eliminated, if frequency and GNSS are the same for both satellites.

The main advantage of this particular DD is the absence of all clock corrections  $S$  and  $s$ . This DD is advantageous if the clocks are not stable enough to be modeled accurately. The number of parameters to be estimated is greatly reduced in that case.

### Epoch differences

Two types of epoch-difference DDs are possible:

1. A DD involving two stations and one satellite. It may be created from two station-difference SDs, e. g.,  $\mathcal{C}_{AB}(T_1)$  and  $\mathcal{C}_{AB}(T_2)$ , or from two epoch-difference SDs, e. g.,  $\mathcal{C}_A(T_{12})$  and  $\mathcal{C}_B(T_{12})$ .
2. A DD involving one station but two satellites. This type may be obtained from either two satellite-difference SDs, e. g.,  $\mathcal{C}^{ij}(T_1)$  and  $\mathcal{C}^{ij}(T_2)$ , or from two epoch-difference SDs, e. g.,  $\mathcal{C}^i(T_{12})$  and  $\mathcal{C}^j(T_{12})$ .

The difference of the two observation epochs  $T_1$  and  $T_2$  is assumed to be small. Frequency, wavelength, code type, and tracking mode must be the same for both epochs. Receiver and satellite biases are eliminated. The phase ambiguities  $\mathcal{N}$  and initial phase readings  $P$  and  $p$  cancel, as well.

The code and phase observation equations for the first DD type read as

$$\mathcal{C}_{AB}(T_{12}) = \mathcal{R}_{AB}(T_{12}) + \mathcal{T}_{AB}(T_{12}) + \mathcal{I}_{AB}(T_{12}) + c S_{AB}(T_{12}) + \mathcal{V} \quad \text{and} \quad (3.16a)$$

$$\mathcal{P}_{AB}(T_{12}) = \mathcal{R}_{AB}(T_{12}) + \mathcal{T}_{AB}(T_{12}) - \mathcal{I}_{AB}(T_{12}) + c S_{AB}(T_{12}) + \mathcal{E}. \quad (3.16b)$$

The observations of the second DD type are given by

$$\mathcal{C}^{ij}(T_{12}) = \mathcal{R}^{ij}(T_{12}) + \mathcal{T}^{ij}(T_{12}) + \mathcal{I}^{ij}(T_{12}) + c s^{ij}(T_{12}) + \mathcal{V} \quad \text{and} \quad (3.16c)$$

$$\mathcal{P}^{ij}(T_{12}) = \mathcal{R}^{ij}(T_{12}) + \mathcal{T}^{ij}(T_{12}) - \mathcal{I}^{ij}(T_{12}) + c s^{ij}(T_{12}) + \mathcal{E}. \quad (3.16d)$$

### 3.3.3 Triple Differences

A triple difference is created by subtracting two DDs, i. e., it is based on eight ZD observations. In the most general case, a TD observation involves eight stations, eight satellites and eight observation epochs. The general observation equation is not explicitly given. It can easily be derived by subtracting eight observation equations of type (3.3) or (3.4).

In practice, a TD observation involves exactly two stations ( $A, B$ ), two satellites ( $i, j$ ), and two observation epochs ( $T_1, T_2$ ), i. e., the two underlying DDs are of the same type. The code and phase TD observations are then given by

$$\mathcal{C}_{AB}^{ij}(T_{12}) = \mathcal{R}_{AB}^{ij}(T_{12}) + \mathcal{T}_{AB}^{ij}(T_{12}) + \mathcal{I}_{AB}^{ij}(T_{12}) + \mathcal{V} \quad \text{and} \quad (3.17a)$$

$$\mathcal{P}_{AB}^{ij}(T_{12}) = \mathcal{R}_{AB}^{ij}(T_{12}) + \mathcal{T}_{AB}^{ij}(T_{12}) - \mathcal{I}_{AB}^{ij}(T_{12}) + \mathcal{E}. \quad (3.17b)$$

The main advantage of the triple differences is the absence of any clock synchronization terms, receiver and satellite biases, initial phase readings, and ambiguities. They are—like all epoch differences—very well suited for preprocessing purposes because cycle slips and gross outliers can easily be identified.

## 3.4 Biases in GNSS Data Processing

### 3.4.1 The Single-difference Bias Term

The single-difference bias term, as introduced, e. g., in [Habrich, 1999], appears in the DD phase observation equation as soon as observations with different wavelengths are involved. This may either happen if observations of satellites of an FDMA-based GNSS or from two different GNSS are combined.

The relevant term in the DD observation equation (3.15b) in this context is the ambiguity difference

$$\lambda^i \mathcal{N}_{AB}^i - \lambda^j \mathcal{N}_{AB}^j. \quad (3.18)$$

The wavelength  $\lambda^j$  can always be expressed as  $\lambda^i + \lambda^{ij}$  and the ambiguity term can be rewritten as

$$\lambda^i (\mathcal{N}_{AB}^i - \mathcal{N}_{AB}^j) - \lambda^{ij} \mathcal{N}_{AB}^j = \lambda^i \mathcal{N}_{AB}^{ij} - \lambda^{ij} \mathcal{N}_{AB}^j, \quad (3.19)$$

where  $\mathcal{N}_{AB}^{ij}$  is the DD ambiguity and  $\lambda^{ij} \mathcal{N}_{AB}^j$  the single-difference bias term. The SD bias is proportional to the wavelength difference  $\lambda^{ij}$  of the two involved carriers and moreover to the initial SD phase ambiguity  $\mathcal{N}_{AB}^j$ . Figure 3.2 visualizes the SD bias and its proportionality for an (exaggerated) wavelength difference  $\lambda^{ij}$  and three SD ambiguities  $\mathcal{N}_{AB}^j = 5, 10, \text{ and } 20$ .

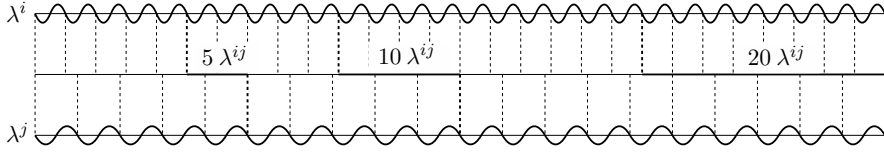


**Figure 3.2:** The SD bias term for a wavelength difference  $\lambda^{ij}$  and three SD ambiguities  $\mathcal{N}_{AB}^j = 5$ , 10, and 20.

Equation (3.19) makes it clear that the ambiguity term (3.18) is no longer an integer in the presence of the SD bias term. The SD bias complicates—or even prohibits—attempts to determine the correct integer cycle value of the DD ambiguity. The additional single-difference term  $\mathcal{N}_{AB}^j$  in the DD observation equation prohibits a strictly DD-based treatment of ambiguity parameters. Consequently, ambiguities must be handled on the SD level if different wavelengths are involved. The implications of the SD bias on ambiguity resolution are investigated in [Habrich, 1999] for satellites of the FDMA-based GLONASS system.

In the presence of a SD bias, the DD ambiguity  $\mathcal{N}_{AB}^{ij}$  may still be correctly determined, if the SD bias is sufficiently small, e. g., below 0.1 cycles. A good measure for the practicability of ambiguity resolution is the accuracy level to which the SD ambiguity must be initialized (i. e., known a priori) to keep the SD bias below the desired limit. According to Habrich [1999] the SD ambiguity must be known to an uncertainty better than 285 cycles for two GLONASS satellites with the minimum channel number difference  $i - j = 1$  and better than 22 cycles for the maximum difference  $i - j = 13$  to ensure a SD bias smaller than 0.1 cycles in absolute value.

The frequency difference  $f^{ij}$  can, however, be considerably larger than the GLONASS frequency increment ( $\Delta f = 0.0625$  MHz, see Sect. 2.4.2), if two different GNSS are involved. Table 3.2 lists the maximally allowed uncertainty of the SD ambiguity (i. e., the maximum initialization error) for all possible combinations of observations from GPS, GLONASS<sup>1</sup>, and Galileo. The adopted threshold for the single-difference bias term was 0.1 cycles.

The GPS and Galileo have two frequencies in common, namely the L1/E1 and the L5/E5a. This is indicated by the “ $\infty$ ” symbols in the table. No SD bias appears in the case of GPS/Galileo L1–E1 or L5–E5a cross-system differences and ambiguities can be resolved without problems. A value of zero indicates combinations for which ambiguity resolution is not possible at all (the ambiguity would have to be initialized with its true value). All other combinations require an a priori knowledge of the SD ambiguity with an uncertainty of below 8 cycles (about 2 meters) in the optimal setting. The availability of very precise code PR measurements might help to fulfill these demanding requirements.

<sup>1</sup>For each combination, the satellite-specific wavelength yielding the smallest  $\lambda^{ij}$  was selected, i. e., the best possible case was assumed.

**Table 3.2:** Maximum ambiguity initialization error for combinations of observations from GPS, GLONASS, and Galileo to ensure a SD bias below 0.1 cycles.

GPS	GLONASS		Galileo				
	L1	L2	E1	E5a	E5b	E5	E6
L1	7	0	$\infty$	0	0	0	1
L2	0	8	0	2	6	3	2
L5	0	2	0	$\infty$	4	8	1
		L1	7	0	0	0	1
		L2	0	2	3	2	4

In practice, cross-system ambiguity resolution is only possible for frequencies shared by both systems (like the GPS/Galileo L1–E1 and L5–E5a). The determination of correct integer values is not realistic for all other combinations (GPS/GLONASS, GLONASS/Galileo). However, a significant receiver phase bias  $A_{AB}^{ij}$  may be present in the observation equation (3.15b), if two different GNSS are involved. This bias may prevent cross-system ambiguity resolution in general. The GNSS-specific sets of resolved ambiguities must remain independent and (at least) one SD reference ambiguity per GNSS must be left unresolved.

### 3.4.2 Code Biases

Code biases are caused by signal delays in the satellite and receiver hardware. They are due to the specific design and electronic properties of the signal processing units. In the most general case, code biases (CBs) depend on the code type, the receiver tracking mode, and on the frequency of the carrier (which implies a GNSS dependency as well). Code biases appear in the ZD observation equation (3.3) explicitly and as differences in the SD and DD equations (3.10a) and (3.14a), respectively.

A rearranged version of the code ZD observation equation, well suited in the context of code biases, is

$$\mathcal{C} = \mathcal{R} + \mathcal{T} + \mathcal{I} + c(S + B) - c(s + b), \quad (3.20)$$

where the error term  $\mathcal{V}$  is neglected.

According to Eq. (3.6), a LC of undifferenced code observations is then defined by

$$\mathcal{L} = \sum_{i=1}^n \mathbf{c}_i (\mathcal{R}_i + \mathcal{T}_i + \mathcal{I}_i) + cS \sum_{i=1}^n \mathbf{c}_i + c \sum_{i=1}^n \mathbf{c}_i B_i - c s \sum_{i=1}^n \mathbf{c}_i - c \sum_{i=1}^n \mathbf{c}_i b_i. \quad (3.21)$$

Both equations show that no absolute values of the CB parameters  $B$  and  $b$  can be determined as they are correlated with the receiver and satellite clock corrections  $S$  and  $s$ ,

respectively. The code biases and clock corrections cannot be separated if only observations of the same tracking mode, code type, and frequency are involved in the estimation process. If code observations with different characteristics are combined, it is, however, possible to estimate differences between the involved biases. These differences are called differential code biases (DCBs).

As the biases appear only as differences in the observation equations, one particular code bias—or a linear combination of code biases—must be selected as reference if clock corrections are estimated. All estimated clock corrections then contain (or refer to) this reference code bias. The estimated clock corrections are therefore not  $S$  and  $s$  but

$$S' \stackrel{\text{def}}{=} S + \sum_{i=1}^n \mathbf{c}_i B_i \quad \text{and} \quad s' \stackrel{\text{def}}{=} s + \sum_{i=1}^n \mathbf{c}_i b_i, \quad (3.22)$$

where the  $\mathbf{c}_i$  are the coefficients of the selected reference LC. This is—for all practical purposes—the same as defining the reference bias to be zero. The selection of the reference bias is not completely arbitrary, but restricted by the requirement that this reference bias appears in at least one observation equation in the parameter estimation process.

The resulting DCB correction term for a ZD observation can be derived by introducing  $S'$  and  $s'$  instead of the original clock corrections  $S$  and  $s$  in Eq. (3.20). The explicit transformation of the relevant receiver-specific term is

$$S + B = S + \sum_{i=1}^n \mathbf{c}_i B_i - \sum_{i=1}^n \mathbf{c}_i B_i + B = S' - \sum_{i=1}^n \mathbf{c}_i B_i + B. \quad (3.23)$$

Keeping in mind that code biases appear as ordinary differences (e. g.,  $B_A - B_B$ ) in the SD and DD observation equations, it makes sense to rely on this type of differences in the ZD case, as well. This can be achieved by requesting that  $\sum_{i=1}^n \mathbf{c}_i = 1$ , i. e., that the selected reference combination of biases is geometry-conserving (cf. Tab. 3.1). The bias  $B$  can then be included in the sum yielding

$$S + B = S' + \sum_{i=1}^n \mathbf{c}_i (B - B_i), \quad (3.24)$$

where the differences  $B - B_i$  are the DCBs and the  $\mathbf{c}_i$  are the LC factors of the selected reference bias. The satellite-specific DCBs—derived analogous to the receiver biases—are given by

$$s + b = s' + \sum_{i=1}^n \mathbf{c}_i (b - b_i). \quad (3.25)$$

The required DCB correction for an arbitrary linear combination of observations is simply the linear combination of the corrections of the involved original observations. A set of DCBs can easily be transformed to another set of differences by the relations

$$B - B_i = (B - B_j) - (B_i - B_j) \quad \text{and} \quad b - b_i = (b - b_j) - (b_i - b_j). \quad (3.26)$$

**Table 3.3:** Examples of DCB sets for a satellite.

Set	DCB type		
	IFB	ICB	mixed CB
1	$b_{X1} - b_{X2}$	$b_{X1} - b_{Y1}$	$b_{X1} - b_{Z2}$
	$b_{X1} - b_{X3}$		$b_{X1} - b_{Z3}$
2	$b_{X1} - b_{X2}$	$b_{X1} - b_{Y1}$	
	$b_{X1} - b_{X3}$	$b_{X2} - b_{Z2}$	
	$b_{Z2} - b_{Z3}$		

Note that the receiver bias  $B$  of a specific station is assumed to be the same for all observed satellites ( $B = B^i = B^j$ ). The treatment of biases parameters gets more complicated if this assumption does not hold.

### Satellite-specific differential code biases

A set of  $n - 1$  linearly independent DCBs can be established for a satellite with  $n$  different code-type-carrier combinations. Let us assume a satellite transmitting three navigation codes (X, Y, Z) on three carriers (1, 2, 3): code X on all three carriers (X1, X2, X3); code Y only on carrier 1 (Y1); and code Z on carriers 2 and 3 (Z2, Z3). An overall of five DCBs must be defined to take into account all code-carrier combinations. Table 3.3 lists two possible DCB sets. The DCBs can be classified into three groups, namely inter-frequency biases (IFBs), inter-code biases (ICBs), and a mixture of both (mixed CBs).

Different sets of DCBs can be established for a given satellite configuration and there is usually no best set. The DCBs must be selected in a “best possible adaption to a given problem”-way. It is, however, reasonable to avoid mixed CBs (as present in set 1 in Tab. 3.3) in order to reduce the number of involved DCB types.

### Receiver-specific differential code biases

Receiver-specific code biases can be dealt with in exactly the same way as satellite code biases as long as the receivers exclusively track one GNSS (e.g., GPS-only receivers). The same DCB types can be distinguished. Note that receiver IFBs include the biases of FDMA-based systems, as well.

An additional bias type—an inter-system bias (ISB)—must be introduced, if more than one GNSS is tracked by a multi-GNSS receiver. An ISB is the difference between code biases from signals of two different GNSS. All GNSS-specific DCBs are usually of the same order of magnitude; ISBs, however, may show much larger values depending on the receiver design. Large values occur, if all the biases of one GNSS are significantly larger than the biases of another system as demonstrated by Fig. 3.3.

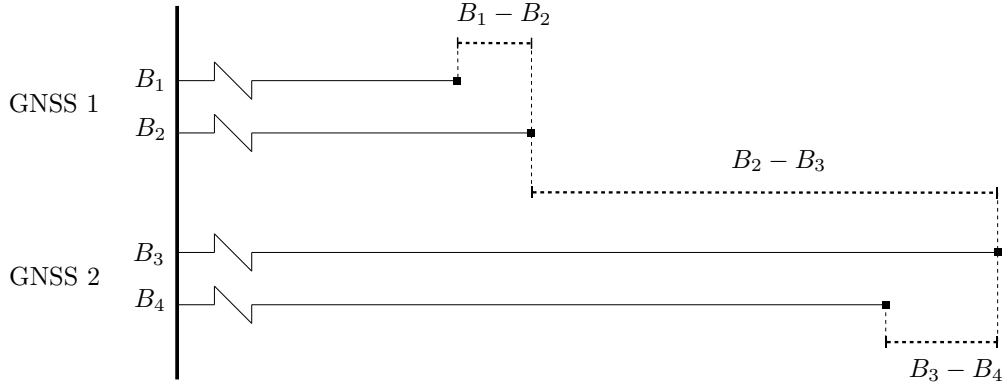


**Figure 3.3:** Receiver code ISB  $B_2 - B_3$ .

**Table 3.4:** Examples of DCB sets for a multi-GNSS receiver.

Set	DCB type		
	IFB	ICB	ISB
1	$B_{X1}^G - B_{X2}^G$	$B_{X1}^G - B_{Y1}^G$	$B_{X1}^G - B_{X1}^R$
		$B_{X2}^G - B_{Y2}^G$	$B_{X2}^G - B_{X2}^R$
			$B_{Y1}^G - B_{Y1}^R$
			$B_{Y2}^G - B_{Y2}^R$
2	$B_{X1}^G - B_{X2}^G$ $B_{X1}^R - B_{X2}^R$	$B_{X1}^G - B_{Y1}^G$	$B_{X1}^G - B_{X1}^R$
		$B_{X2}^G - B_{Y2}^G$	
		$B_{X1}^R - B_{Y1}^R$	
		$B_{X2}^R - B_{Y2}^R$	

Let us assume a multi-GNSS receiver tracking two ranging code types (X, Y) on two carriers (1, 2) for two GNSS (G, R). Table 3.4 shows two possible sets of DCBs for this receiver. The DCB set 1 in Tab. 3.4 shows that all biases from one system (GNSS R) can be represented by inter-system biases, only. This setup is not ideal as the selected DCB set cannot be used in a single-system analysis of data exclusively from GNSS R.

It therefore makes sense to minimize the number of inter-system bias components of the DCB set. Set 2 in Tab. 3.4 shows a different setup with independent GNSS-specific groups of biases and only one inter-system bias linking the biases from both systems. This DCB set can be used in single-system as well as in multi-GNSS applications without the need of redefining its components.

### 3.4.3 The Conventional Differential Code Biases

The IGS is based on a world-wide GNSS tracking network to generate precise GNSS (currently GPS and GLONASS) products. Differential code biases for satellites have to be taken into account by the IGS ACs to ensure the best possible consistency for orbit and clock products [Ray, 2000].

The satellite as well as the receiver DCB correction terms relevant in a fully consistent multi-GNSS data analysis are derived as shown in Sect. 3.4.2. They comply to the IGS recommendations.

According to [Ray, 2000] four different types of code observations must be distinguished for GPS: the C/A-code on the first frequency (C1), P-codes on both frequencies (P1 and P2), and a P2-like observation X2 on the second frequency ( $X2 = C1 + P2 - P1$ ). In 2005, the first block IIR-M GPS satellite was launched. This satellite provides a civil code on the second frequency, adding a fifth code type to be considered (C2). In the case of GLONASS there are four observations types available, namely C1, P1, C2, and P2.

Let  $\mathcal{C}_1$  and  $\mathcal{C}_2$  be two P-code observations of a station to a GPS satellite on carriers L1 and L2. The IGS adopts the ionosphere-free linear combination of P1 and P2 GPS observations as reference, i. e., this particular observation is assumed to be code-bias free. The corresponding LC factors are given by  $\mathbf{c}_1 = f_1^2/(f_1^2 - f_2^2)$  and  $\mathbf{c}_2 = -f_2^2/(f_1^2 - f_2^2)$ , respectively. The factors meet the requirement  $\mathbf{c}_1 + \mathbf{c}_2 = 1$ , so that Eqs. (3.24) and (3.25) hold. The resulting receiver and satellite DCB correction terms for an original ZD observation are then given by

$$S + B = S' - (B_{P1} - B) + \mathbf{c}_2 (B_{P1} - B_{P2}) \quad \text{and} \quad (3.27a)$$

$$s + b = s' - (b_{P1} - b) + \mathbf{c}_2 (b_{P1} - b_{P2}). \quad (3.27b)$$

The clock corrections  $S'$  and  $s'$  contain the reference biases ( $\mathbf{c}_1 B_{P1} + \mathbf{c}_2 B_{P2}$ ) and ( $\mathbf{c}_1 b_{P1} + \mathbf{c}_2 b_{P2}$ ), respectively.

Table 3.5 lists the factors with which the satellite DCBs must be taken into account to render the five basic ZD observation equations consistent to the selected DCB reference. The necessary DCB factors for a combined GPS/GLONASS receiver are listed in Tab. 3.6. The satellite bias correction for X2 is computed by  $b_{X2} = b_{C1} + b_{P2} - b_{P1}$ , based on the definition of the X2 observation, the receiver bias correction is computed accordingly. Two possible DCBs w. r. t. C2 observations are  $(b_{P2} - b_{C2})$  and  $(B_{P2} - B_{C2})$  or  $(b_{C1} - b_{C2})$  and  $(B_{C1} - B_{C2})$ . As there is no recommendation yet, the DCBs  $(b_{P2} - b_{C2})$  and  $(B_{P2} - B_{C2})$  are used in Tabs. 3.5 and 3.6 for demonstration purposes.

Table 3.6 shows that an inter-system code biases must be taken into account as soon as observations from two or more GNSS are used in a common analysis, e. g.,  $(B_{P1}^G - B_{P1}^R)$  in the case of a combined GPS/GLONASS analysis.

**Table 3.5:** Factors for satellite-specific DCB corrections for the undifferenced observations C1, P1, C2, P2, and X2.

DCB	C1	P1	C2	P2	X2
$(b_{P1} - b_{P2})$	$+\mathbf{c}_2$	$+\mathbf{c}_2$	$-\mathbf{c}_1$	$-\mathbf{c}_1$	$-\mathbf{c}_1$
$(b_{P1} - b_{C1})$	-1	0	0	0	-1
$(b_{P2} - b_{C2})$	0	0	-1	0	0

**Table 3.6:** Factors for receiver-specific DCB corrections for the undifferenced observations C1, P1, C2, P2, and X2 for GPS (G) and GLONASS (R).

DCB	GPS					GLONASS			
	C1	P1	C2	P2	X2	C1	P1	C2	P2
$(B_{P1}^G - B_{P2}^G)$	$+\mathbf{c}_2$	$+\mathbf{c}_2$	$-\mathbf{c}_1$	$-\mathbf{c}_1$	$-\mathbf{c}_1$	$+\mathbf{c}_2$	$+\mathbf{c}_2$	$+\mathbf{c}_2$	$+\mathbf{c}_2$
$(B_{P1}^G - B_{C1}^G)$	-1	0	0	0	-1	0	0	0	0
$(B_{P2}^G - B_{C2}^G)$	0	0	-1	0	0	0	0	0	0
$(B_{P1}^G - B_{P1}^R)$	0	0	0	0	0	-1	-1	-1	-1
$(B_{P1}^R - B_{P2}^R)$	0	0	0	0	0	0	0	-1	-1
$(B_{P1}^R - B_{C1}^R)$	0	0	0	0	0	-1	0	0	0
$(B_{P2}^R - B_{C2}^R)$	0	0	0	0	0	0	0	-1	0

The necessary DCB correction for any LC of the basic observations is simply the corresponding linear combination of the correction terms in Tabs. 3.5 and 3.6. The corrections for SD, DD, and TD observations are obtained by forming the corresponding differences of the table values.

### 3.4.4 Phase Biases

Hardware biases do not only exist for code but also for phase observations. These phase biases  $A$  and  $a$  appear explicitly in the ZD phase observation equation:

$$\mathcal{P} = \mathcal{R} + \mathcal{T} - \mathcal{I} + c(S + A) - c(s + a) + \lambda(P - p) + \lambda\mathcal{N}. \quad (3.28)$$

It is not possible to estimate the absolute biases due to the linear dependence of the biases, clock corrections, initial phases, and ambiguities in Eq. (3.28). The absolute biases are of no concern if the ambiguities are estimated as real values or if a LC is used where the ambiguities are no integers at all.

The PBs (or differences thereof) must be estimated if ambiguities should be fixed to their integer values. This is of particular importance if the PBs are not constant over the analyzed time interval (or at least over the mean validity interval of an ambiguity),

because only a time-invariant part may be compensated by the constant ambiguities. Time-variable PBs must be modeled and estimated. The impact of (inter-system) PBs and implications for ambiguity resolution have been studied by *Dach et al.* [2010].

Although several attempts were made to calibrate receiver and satellite phase biases, e. g., [*Banville et al.*, 2008; *Ge et al.*, 2008], there is no widely accepted method to deal with these biases, yet.

### 3.4.5 Biases in GNSS Data Analysis: A Summary

#### Single-difference bias term

The SD bias term appears in SD and DD observation equations as soon as observations with different carrier wavelengths are combined. The bias term can be written as  $\lambda^{ij} \mathcal{N}_{AB}^j$  where  $\lambda^{ij}$  is the wavelength difference and  $\mathcal{N}_{AB}^j$  a SD ambiguity. The SD bias destroys the integer nature of the DD ambiguities, but ambiguity resolution is still possible, provided  $\mathcal{N}_{AB}^j$  is known with adequate accuracy. The required degree of accuracy for cross-system ambiguity resolution can, however, not be achieved easily due to comparatively large differences  $\lambda^{ij}$ . Ambiguity resolution between different GNSS is only feasible for frequencies shared by both systems and if no large receiver PBs prevent ambiguity resolution.

#### Hardware biases

The biases caused by signal delays in receiver and satellite hardware depend on the characteristics of the observation type, i. e., on signal frequency, code type, and receiver tracking mode. A basic distinction can be made between code biases and phase biases.

Absolute CBs appear in the ZD observation equation and are inseparably linked to clock synchronization terms. Satellite biases can be estimated on a differential level, if the satellites are tracked by receivers using different tracking technologies. Receiver DCBs can be estimated, if a receiver tracks different satellites in different modes (and on different frequencies). This is always the case for multi-GNSS receivers tracking satellites from more than one GNSS. An inter-system DCB must be taken into account as soon as satellites from different GNSS are involved.

The clock synchronization parameters absorb a reference CB, as only bias differences can be estimated. Observation equations must thus be corrected accordingly, if clock corrections are estimated based on a mix of observations (different code types and tracking modes) or if code-based clock estimates (from a separate analysis or an external source) are introduced as known.

In the case of single or higher differences of the observations equations, the CBs enter on a differential level (so-called DCBs). They completely cancel in CDMA-based single-system

applications, if only one observation type is used. In all other cases (FDMA-based GNSS, multi-GNSS applications or mixed observation types) they must be accounted for.

Phase biases are—in a conceptual sense—very similar to the CBs. As opposed to the CBs they are not only directly correlated with clock correction parameters, but also with the phase ambiguities. As the ambiguities are by definition integer numbers, they can absorb a part of the PBs corresponding to integer multiples of the wavelength, but not the fractional parts. The PBs therefore do not only contaminate the correct ambiguity values, they also destroy the integer nature of the ambiguities.

Satellite PBs—as opposed to their code counterparts—always cancel, if SDs or DDs are formed. Receiver PBs cancel under the same conditions as the CBs. An inter-system PB must always be taken into account in multi-GNSS applications.

Phase biases are of no major concern, if ambiguities are estimated as real values or if a LC with real-valued ambiguities is used (as long as the PBs can be assumed to be constant at least over the mean validity time of an ambiguity). If the biases are time variable, this dependency must be taken into account by modeling the biases accordingly (e. g., as piecewise linear functions).

Code biases may appear in ZD or SD phase observation equations, if code-based clock estimates are introduced as known quantities. Introducing the estimated clock synchronization errors  $S'$  and  $s'$ , as defined by Eq. (3.22), in the phase ZD equation (3.28) yields

$$\mathcal{P} = \mathcal{R} + \mathcal{T} - \mathcal{I} + c(S' + A - \sum_{i=1}^n c_i B_i) - c(s' + a - \sum_{i=1}^n c_i b_i) + \lambda(P - p) + \lambda\mathcal{N},$$

and adopting the IGS DCB conventions from Sect. 3.4.3 gives

$$\begin{aligned} \mathcal{P} = \mathcal{R} + \mathcal{T} - \mathcal{I} + c(S' - s') - c((B_{P1} - A) - c_2(B_{P1} - B_{P2})) \\ + c((b_{P1} - a) - c_2(b_{P1} - b_{P2})) + \lambda(P - p) + \lambda\mathcal{N}, \end{aligned}$$

where not only the CBs appear but also a difference between a code and a phase bias, i. e., a bias between two different measurement types. This differential code-phase bias makes the phase observation consistent with the selected reference DCB contained in  $S'$  and  $s'$ .

### 3.5 Least-squares Adjustment in Overview

Parameter estimation in GNSS data analysis can basically be reduced to solving a system of observation equations. The system is overdetermined and mathematical methods must be applied to find an unique and optimum solution. Least-squares adjustment is exclusively used throughout this work. It is briefly summarized in this section. More details on parameter estimation are provided, e. g., in [Koch, 1999].

The observations recorded by GNSS receivers are modeled by a set of observation equations as presented in Sects. 3.1 through 3.3. The exact functional specification of these equations defines the mathematical model  $\Psi$ . The equation system is not consistent if the number of observations  $n$  is larger than the number of unknowns  $u$ . Corrections to the observations must be allowed to re-establish system consistency. The observation equation system is defined by

$$\mathbf{L} + \mathbf{y} = \Psi(\mathbf{X}) \quad (3.29)$$

with the  $n \times 1$  vectors

- $\mathbf{L}$  of the actual observations,
- $\mathbf{y}$  of the corrections to the observations, and
- $\mathbf{X}$  of the unknown parameters.

The observation equations are usually nonlinear. Applying a 1st-order linearization to the model  $\Psi$ , the equation system (3.29) can be written as

$$\mathbf{L} + \mathbf{y} = \Psi(\mathbf{X}_0) + \mathbf{A} \mathbf{x}, \quad (3.30)$$

where

- $\mathbf{X}_0$  is the array of approximations of the unknown parameters  $\mathbf{X}$ ,
- $\mathbf{x}$  are the unknown corrections w. r. t.  $\mathbf{X}_0$  so that  $\mathbf{X} = \mathbf{X}_0 + \mathbf{x}$ , and
- $\mathbf{A}$  is the first design matrix.

The  $n \times u$  matrix  $\mathbf{A}$  contains the partial derivatives of the observation equations w. r. t. the unknown model parameters  $\mathbf{X}$  evaluated at  $\mathbf{X}_0$ . The elements of  $\mathbf{A}$  are defined by

$$\mathbf{A} = \left. \frac{\partial \Psi(\mathbf{X})}{\partial \mathbf{X}} \right|_{\mathbf{X}=\mathbf{X}_0}.$$

Solving the linearized equation system (3.30) for the correction vector  $\mathbf{y}$  gives

$$\mathbf{y} = \mathbf{A} \mathbf{x} - (\mathbf{L} - \Psi(\mathbf{X}_0)) = \mathbf{A} \mathbf{x} - \mathbf{l}, \quad (3.31)$$

where  $\mathbf{l} = \mathbf{L} - \Psi(\mathbf{X}_0)$  is the difference between the observations and the mathematical model evaluated at  $\mathbf{X}_0$ . This term is often called “observed minus computed” and abbreviated by O-C.

The statistical properties of the observations are described by the stochastic model

$$\mathbf{P} = \mathbf{Q}_l^{-1} = \sigma_0^2 \mathbf{C}_l^{-1}, \quad (3.32)$$

where

- $\mathbf{P}$  is the weight matrix of the observations,
- $\mathbf{Q}_l$  is the cofactor matrix of the observations,
- $\sigma_0$  is the a priori standard deviation of unit weight, and
- $\mathbf{C}_l$  is the covariance matrix of the observations.

Off-diagonal elements in the cofactor matrix indicate that the observations are correlated. The correlations may either be mathematical (e. g., by forming differences) or physical in nature. In the special case of uncorrelated observations, the matrix  $\mathbf{Q}_l$  (and thus also the weight matrix  $\mathbf{P}$ ) is a diagonal matrix. The elements of  $\mathbf{P}$  are then given by  $P_{ii} = \sigma_0^2/\sigma_i^2$ , where  $P_{ii}$  is the diagonal element number  $i$ , and  $\sigma_i$  is the a priori standard deviation of the corresponding observation  $i$ .

The system of observation equations (3.30) can be solved by following the least-squares estimation (LSE) principle of minimizing the weighted sum of squared residuals  $\mathbf{y}^\top \mathbf{P} \mathbf{y}$ , i. e., by demanding that  $\frac{d}{dx}(\mathbf{y}^\top \mathbf{P} \mathbf{y}) = 0$ . This request leads to the normal equation (NEQ) system

$$(\mathbf{A}^\top \mathbf{P} \mathbf{A}) \mathbf{x} - \mathbf{A}^\top \mathbf{P} \mathbf{l} \stackrel{\text{def}}{=} \mathbf{N} \mathbf{x} - \mathbf{b} = \mathbf{0}, \quad (3.33)$$

where

- $\mathbf{N} = \mathbf{A}^\top \mathbf{P} \mathbf{A}$  is the symmetric  $u \times u$  normal equation matrix and
- $\mathbf{b} = \mathbf{A}^\top \mathbf{P} \mathbf{l}$  is a  $u \times 1$  vector defining the right-hand side of the normal equation system.

The solution vector  $\mathbf{x}$  follows from Eqs. (3.33) as

$$\mathbf{x} = (\mathbf{A}^\top \mathbf{P} \mathbf{A})^{-1} \mathbf{A}^\top \mathbf{P} \mathbf{l} = \mathbf{N}^{-1} \mathbf{b}. \quad (3.34)$$

The cofactor matrix  $\mathbf{Q}_x$  of the estimated parameters  $x$  follows from (3.34) by the law of error propagation as

$$\mathbf{Q}_x = (\mathbf{N}^{-1} \mathbf{A}^\top \mathbf{P}) \mathbf{Q}_l (\mathbf{N}^{-1} \mathbf{A}^\top \mathbf{P})^\top = \mathbf{N}^{-1}. \quad (3.35)$$

The estimated a posteriori standard deviation of unit weight  $m_0$  is given by

$$m_0 = \sqrt{\frac{\mathbf{y}^\top \mathbf{P} \mathbf{y}}{n - u}} \quad (3.36)$$

if  $n - u > 0$ . The quantity  $f = n - u$  is called degree of freedom (DOF) of the least-squares adjustment. The sum of squared residuals  $\mathbf{y}^\top \mathbf{P} \mathbf{y}$  can either be computed from Eq. (3.31) in a straight-forward manner or more efficiently from

$$\mathbf{y}^\top \mathbf{P} \mathbf{y} = \mathbf{l}^\top \mathbf{P} \mathbf{l} - \mathbf{x}^\top \mathbf{b}. \quad (3.37)$$

The covariance matrix of the estimated parameters is given by

$$\mathbf{C}_x = m_0^2 \mathbf{Q}_x = m_0^2 \mathbf{N}^{-1} \quad (3.38)$$

and the mean errors of the estimated parameters  $i = 1, \dots, u$  are

$$m_i = \sqrt{C_{x,ii}} = m_0 \sqrt{Q_{x,ii}}, \quad (3.39)$$

where  $C_{x,ii}$  and  $Q_{x,ii}$  are the diagonal elements of the respective matrices.

### 3.5.1 Parameter Pre-elimination

The pre-elimination of parameters is a useful tool to reduce the size of normal equation systems. It offers the possibility to remove the explicit appearance of selected parameters without losing their statistical influence on the remaining system.

Splitting the vector of unknowns  $\mathbf{x}$  in two parts  $\mathbf{x}_1$  and  $\mathbf{x}_2$ , the normal equation system (3.33) may be rewritten as

$$\begin{pmatrix} \mathbf{N}_{11} & \mathbf{N}_{12} \\ \mathbf{N}_{21} & \mathbf{N}_{22} \end{pmatrix} \begin{pmatrix} \mathbf{x}_1 \\ \mathbf{x}_2 \end{pmatrix} = \begin{pmatrix} \mathbf{b}_1 \\ \mathbf{b}_2 \end{pmatrix}, \quad (3.40)$$

where  $\mathbf{N}_{11}$ ,  $\mathbf{N}_{22}$ , and  $\mathbf{N}_{12} = \mathbf{N}_{21}^\top$  are the parts of  $\mathbf{N}$  corresponding to only  $\mathbf{x}_1$ , only  $\mathbf{x}_2$ , and to a mixture of both. The parameters  $\mathbf{x}_2$  can be eliminated by multiplying the second line of system (3.40) with  $-\mathbf{N}_{12}\mathbf{N}_{22}^{-1}$ . Assuming matrix  $\mathbf{N}_{22}$  to be regular, the resulting equation can be simplified to

$$(\mathbf{N}_{11} - \mathbf{N}_{12}\mathbf{N}_{22}^{-1}\mathbf{N}_{21}) \mathbf{x}_1 = \mathbf{b}_1 - \mathbf{N}_{12}\mathbf{N}_{22}^{-1}\mathbf{b}_2, \quad (3.41)$$

which in turn can be abbreviated by

$$\tilde{\mathbf{N}} \mathbf{x}_1 = \tilde{\mathbf{b}}, \quad (3.42)$$

where

$\tilde{\mathbf{N}} = \mathbf{N}_{11} - \mathbf{N}_{12}\mathbf{N}_{22}^{-1}\mathbf{N}_{21}$  is the reduced normal equation for parameters  $\mathbf{x}_1$  and

$\tilde{\mathbf{b}} = \mathbf{b}_1 - \mathbf{N}_{12}\mathbf{N}_{22}^{-1}\mathbf{b}_2$  is the corresponding right-hand side of the reduced system.

The new weighted sum of squared residuals  $\mathbf{y}^\top \mathbf{P} \mathbf{y}$  must be adjusted based on Eq. (3.37):

$$\mathbf{y}^\top \mathbf{P} \mathbf{y} = \mathbf{l}^\top \mathbf{P} \mathbf{l} - \mathbf{x}_1^\top \tilde{\mathbf{b}} - \mathbf{b}_2^\top \mathbf{N}_{22}^{-1} \mathbf{b}_2. \quad (3.43)$$

The reduced normal equation system does no longer explicitly contain  $\mathbf{x}_2$ , but the corresponding statistical information is preserved by the correction terms  $-\mathbf{N}_{12}\mathbf{N}_{22}^{-1}\mathbf{N}_{21}$ ,  $-\mathbf{N}_{12}\mathbf{N}_{22}^{-1}\mathbf{b}_2$ , and  $-\mathbf{b}_2^\top \mathbf{N}_{22}^{-1} \mathbf{b}_2$ , respectively. The results for the parameters  $\mathbf{x}_1$  are not affected by the pre-elimination of  $\mathbf{x}_2$ .

### 3.5.2 Sequential Least-squares Adjustment

Sequential least-squares adjustment is a technique, where the observations are split up and processed in independent LSE batches and then combined in a subsequent step. The results are the same as if all observations would have been used in one LSE, provided the separate observation series are independent [Brockmann, 1997].

Let us assume two statistically independent equation systems containing only common parameters. There are no—or only pre-eliminated—system-specific parameters. In this scenario, the observation equations are given by

$$\begin{aligned} \mathbf{y}_1 &= \mathbf{A}_1 \mathbf{x}_1 - \mathbf{l}_1 \quad \text{and} \\ \mathbf{y}_2 &= \mathbf{A}_2 \mathbf{x}_2 - \mathbf{l}_2, \end{aligned} \tag{3.44}$$

where the  $\mathbf{x}_i$  represent the common parameters  $\mathbf{x}_c$  satisfying system  $i$ . The resulting combined normal equation system

$$\mathbf{N}_c \mathbf{x}_c = \mathbf{b}_c \tag{3.45}$$

is simply the superposition of the individual normal equation systems with

$$\begin{aligned} \mathbf{N}_c &= \mathbf{N}_1 + \mathbf{N}_2 = \mathbf{A}_1^\top \mathbf{P}_1 \mathbf{A}_1 + \mathbf{A}_2^\top \mathbf{P}_2 \mathbf{A}_2 \quad \text{and} \\ \mathbf{b}_c &= \mathbf{b}_1 + \mathbf{b}_2 = \mathbf{A}_1^\top \mathbf{P}_1 \mathbf{l}_1 + \mathbf{A}_2^\top \mathbf{P}_2 \mathbf{l}_2. \end{aligned} \tag{3.46}$$

The weighted sum of squared residuals is obtained from the superposition

$$\mathbf{y}^\top \mathbf{P} \mathbf{y} = (\mathbf{l}_1^\top \mathbf{P}_1 \mathbf{l}_1 + \mathbf{l}_2^\top \mathbf{P}_2 \mathbf{l}_2) - \mathbf{x}_c^\top (\mathbf{A}_1^\top \mathbf{P}_1 \mathbf{l}_1 + \mathbf{A}_2^\top \mathbf{P}_2 \mathbf{l}_2). \tag{3.47}$$

Equations (3.46) and (3.47) show that combining two observation series on the normal equation level is achieved by a simple addition of the corresponding terms from the individual solutions. This is, however, only true if the two original systems are statistically independent from each other. The above technique of combining parameters from individual systems is also known as parameter stacking.

### 3.5.3 Constraining Parameters

Sometimes it is useful, or even necessary, to include additional information concerning parameters in a normal equation system, e. g., to prevent weakly observed parameters from taking unreasonable values. This may be achieved by introducing fictitious observations (also called pseudo-observations) with a certain given variance.

A model parameter  $X_i$  may be constrained to its a priori value  $X_{0,i}$  by assuming the corresponding correction  $x_i$  to be zero within the limits  $\pm\sigma_{\text{abs}}$  in the least-squares sense (absolute constraining). The value of O-C is zero in that special case and the weight

$$P = \frac{\sigma_0^2}{\sigma_{\text{abs}}^2} \tag{3.48}$$

has to be added only to the corresponding diagonal element  $N_{ii}$  of the original normal equation  $\mathbf{N}$ .

Two parameters  $i$  and  $j$  may be constrained relative to each other by assuming the difference of the corresponding corrections  $x_i - x_j$  to be zero (relative constraining). The weight matrix

$$\mathbf{P} = \begin{pmatrix} P & -P \\ -P & P \end{pmatrix} \quad \text{with} \quad P = \frac{\sigma_0^2}{\sigma_{\text{rel}}^2} \quad (3.49)$$

must be added to the normal equation  $\mathbf{N}$ , i. e.,  $P$  must be added to the diagonal elements  $N_{ii}$  and  $N_{jj}$  and  $-P$  to the off-diagonal elements  $N_{ij}$  and  $N_{ji}$ , respectively. Relative constraints are very well suited to limit the variability of parameters with a high temporal resolution.

Note that the number of observations and the DOF must be incremented by 1 for each pseudo-observation introduced. Constraining is not limited to absolute and relative constraints. Several other options are discussed by *Brockmann* [1997].

## **Part II**

# **Realizing a Multi-GNSS Analysis Software for Scientific Purposes**



# 4 Concepts and Design

## 4.1 The Bernese GPS Software

The Bernese GPS Software (BSW) is a scientific tool to analyze GNSS observations meeting highest quality standards. It offers high-performance data post-processing on the highest possible precision level with full control over all relevant processing options. A very high degree of automation facilitates in particular the analysis of data from large permanent observation networks and long surveying campaigns.

The BSW is commercially available and used at about 400 universities and research institutions worldwide. The software is developed, maintained, and refined by the staff of the Astronomical Institute of the University of Bern (AIUB). Currently<sup>1</sup>, Version 5.0 [Dach *et al.*, 2007] is available.

A project, realized jointly with the Bundesamt für Kartographie und Geodäsie (BKG), was initiated in January 2005 with the goal to update the BSW from a dual-frequency GPS/GLONASS to a full multi-GNSS software. The extension should not only focus on Galileo but should prepare the software for any upcoming GNSS and all modernizations of already existing systems. Special attention was paid to a software design allowing it to easily include new technologies (e. g., new carriers, LCs, observation types) without rewriting major parts of the source code. The software should be capable of a single-system as well as a fully consistent multi-GNSS data analysis, taking into account all relevant biases. The current development version of the BSW, as used at the AIUB, served as the basis for the update. Subsequently, the old version is called BSW Version 5, the updated software BSW Version 6.

### 4.1.1 Development History

The foundations of the Bernese GPS Software were laid back in 1983/84 when *Beutler et al.* [1984] developed a software package to process double-differenced GPS carrier phase observations. The software was realized in 1983/84 by Beutler at the University of New Brunswick (UNB) in Fredericton, Canada, to estimate coordinates and orbital parameters based on single-frequency measurements from Macrometer V-1000 GPS receivers.

---

<sup>1</sup>As of June 2011.

This experimental version of a GPS data analysis software was re-organized, generalized, and extended in the following year. The resulting program package was called Bernese Second Generation GPS Software [Gurtner *et al.*, 1985]. It consisted of three main parts: a data preprocessor, a program to convert orbit information from various sources to a standardized format, and a parameter estimation program. Single- and dual-frequency data from different receiver types could be processed to estimate station coordinates, phase ambiguities, receiver clock corrections, orbital elements, and ionospheric parameters.

In March 1988, the BSW Version 3.0—a totally revised version of the Second Generation Software—was released. The program parts were restructured and extended to five parts (transfer, orbit, processing, simulation, and service parts), new linear combinations were implemented, and several new parameter types were added (e. g., troposphere parameters). In addition, Version 3.0 was delivered with an ASCII-based menu system for easy (easier) user interaction. Five updated versions were released during the following years to keep track of the rapid developments in the field of GPS applications. The last Version 3.5 was issued in February 1995.

In September 1996 Version 4.0 of the BSW was finished. It was based on the previous version and offered several new components, including a new parameter estimation program using normal equation systems as input and the Bernese Processing Engine (BPE) to automate predefined processing sequences. Version 4.2 was released three years later in November 1999 offering the possibility to analyze data from GLONASS [Habrich, 1999] as well as SLR measurements to GNSS satellites. The transition from a single-system to a GPS/GLONASS capable software package was made.

Version 5.0, released in April 2004, was an important milestone in the development history of the software package. The previous ASCII-based interface was replaced by a graphical user interface (GUI), considerably improving the user friendliness. The BPE was completely rewritten and the normal equation manipulation program was replaced by a more sophisticated and much more powerful version.

### 4.1.2 Main Characteristics of Version 5

The BSW Version 5.0 is capable of post-processing GPS and GLONASS microwave observations either in a system-specific or in a combined mode. Code and phase data of two frequencies—L1 and L2 as defined by Eqs. (2.8) and (2.9)—can be processed in a zero- or double-difference approach. Additionally, SLR measurements can be analyzed. The software can handle observation data from static, kinematic, and spaceborne receivers on LEO satellites.

The software adheres to internationally approved standards. It is compliant to the conventions adopted by the International Earth Rotation and Reference Systems Service (IERS), in particular to the issue 2003 [McCarthy and Petit, 2004]. Adequacy of models is guaranteed by a continuous development and by periodic software updates.

The mathematical modeling of the observations is based on equations very similar to the observation equations presented in Sect. 3. As scientific analysis software, the BSW does not only allow it to estimate the most prominent parameters (like station coordinates or troposphere parameters) but also all other parameters appearing in the observation equations. This includes, e.g., osculating orbital elements for the satellites, stochastic pulses, geocenter coordinates (GCCs), Earth rotation parameters (ERPs), antenna phase center offsets and patterns, ionosphere maps, and DCBs. A comprehensive list of parameters is provided in [Dach et al., 2007]. All parameters can individually be estimated or taken into account by introduced a priori information. Time-dependent parameters may either be estimated for each single epoch or they may be represented by piece-wise linear, continuous functions.

All results may be stored in dedicated files. These files may be used later on to re-introduce parameter estimates as a priori information. Apart from software-specific file formats, all major international file formats are supported for data input and/or output. The software in particular supports the receiver-independent exchange format (RINEX) [Gurtner and Mader, 1990; Gurtner and Estay, 2009], the solution-independent exchange format (SINEX) [Blewitt et al., 1994; Rothacher and Thaller, 2006], the antenna exchange format (ANTEX) [Rothacher and Mader, 2003; Schmid and Khachikyan, 2010], the ionosphere map exchange format (IONEX) [Schaer et al., 1998], and the extended standard product 3 orbit format (SP3-c) [Hilla, 2010].

### 4.1.3 Structure and Organization

The BSW can be subdivided into the six main parts: the orbit part, simulation part, transfer and conversion part, processing part, service part, and last, but not least, the Bernese Processing Engine. Figure 4.1 illustrates these parts by a flow chart of a standard processing sequence. Each part is dedicated to a particular topic and consists of a set of stand-alone programs customized for specific sub-tasks. All programs are listed in Tab. A.1 in Appendix A, grouped according to the software parts.

The programs of the orbit part handle tasks related to satellite orbits and ERPs. This includes the generation of a software-specific orbit representation (standard orbits) based on a numerical integration of the equations of motion using as input either precise ephemerides, broadcast navigation messages, or orbital elements estimated in a precedent orbit improvement step. Concatenation and comparison of orbit files, format conversions, and extraction of pole information are additional features.

The data conversion and transfer part includes programs for the conversion and import of all types of RINEX files (observations, navigation messages, meteorological measurements, clock corrections) into Bernese format and vice versa. The files can be merged or cut; important meta data may be extracted. Observations are preprocessed on the RINEX-level.

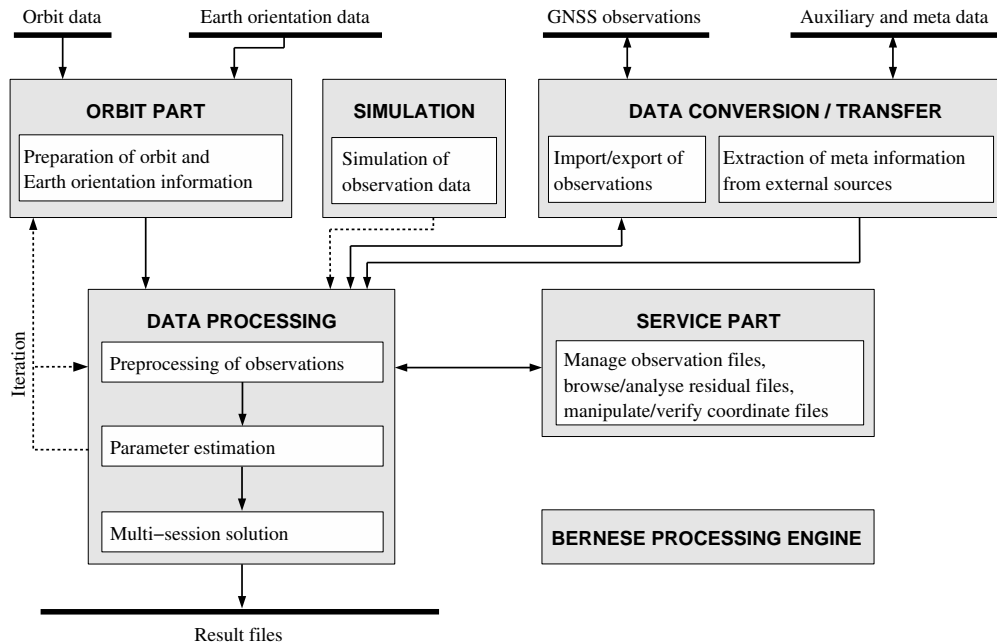


**Figure 4.1:** Flow chart of a standard processing sequence in the BSW.

The simulation part allows it to generate synthetic GNSS (GPS/GLONASS) observations for terrestrial as well as for LEO satellites. The models applied in the simulator are identical to those used in data processing. So-called “zero-tests” are thus possible if exactly the same geometry and options were used in the simulation and the processing program. However, this is only true if the data was simulated error-free. More realistic data can be retrieved by adding (normal distributed) observation noise and cycle slips to the simulated data.

The main analysis programs are the nucleus of the processing part. The programs cover the receiver clock synchronization based on undifferenced code observations, the creation of single differences (baselines), data preprocessing (including cycle slip detection and repair), parameter estimation, and the manipulation and combination of normal equation systems.

The service part contains a large collection of tools to browse binary observation files, screen residuals, compare and manipulate coordinate files for automated processing, extract information from output files, and several other auxiliary programs.

The BPE has a special status as the associated programs do not deal with data analysis. They offer means and tools to completely automate entire processing sequences. This includes, e.g., tools to create processing schemes, to control running processes, and to manage available hard- and software resources.

## 4.2 Requirements for a Multi-GNSS Software

The first step of developing (or of expanding an existing software package to) a scientific multi-GNSS analysis tool is the definition of a set of fundamental requirements. This set is the basis for the following design and development process. Due to the high rate of new developments in the field of GNSS, the list of requirements is not static, but subject to change during and after the development process. A competitive software package must therefore offer the possibility to flexibly react on yet unknown requirements.

### 4.2.1 Scientific Requirements

New GNSS and the modernization of operational systems offer many new features and challenges. A combined, fully consistent, and highly accurate analysis of tracking data from all GNSS is essential in order to extract maximum scientific benefit from the systems. Moreover, the software should not impose processing restrictions whatsoever on the data analyst; the software must be a flexible tool allowing an easy adaption to varying experimental setups. The scientific requirements are as follows:

#### **Adherence to up-to-date standards and models**

A scientific GNSS data analysis software package must always adhere to the latest accepted standards and incorporate the most recent parameter models. Apart from an overall improvement of the results, there are mainly two reasons for this requirement: (a) Many scientifically interesting effects are of a very small order of magnitude and only detectable if a sufficient level of sophistication is reached. With continuous enhancements of the models, the threshold for the detection and the study of such small effects is more and more advanced. (b) Parameter estimates and time series of parameters are the basis for subsequent scientific research work. It is therefore necessary that the parameters only contain the signal of interest. As parameter estimates may absorb unmodeled effects, the interesting effects may not be detectable. Improved models help to better separate different effects.

#### **Possibility of customizing all relevant processing options**

The data analyst must have full control over all relevant processing options of the software. As a matter of principle, the software design should not impose restrictions—even if some options are not useful or even harmful in standard applications. The possibility of changing and optimizing all settings facilitates scientific work.

#### **Allowance for consistent single- and multi-GNSS analysis in all possible combinations**

The analysis software must be able to consistently analyze data from the GNSS in arbitrary combinations, e. g., GPS/GLONASS combined, Galileo/GLONASS combined, or

Galileo only. There should be no preference for any system. This is of particular importance for the selection of references such as the time system for clock corrections. A fully consistent analysis must be possible on the observation level as well as on the normal equation level.

### **Easy and flexible handling of observations**

An obvious, but nevertheless important, innovation offered by modern GNSS is the transmission of new and improved navigation codes on more than two carrier waves. Established and new linear combinations may be formed using all available carriers and signals. A GNSS data analyst will be faced with a multitude of new observations such as LCs with more than the customary two constituents or combinations of different code types on the same carrier. Even if not all combinations make sense, the software must be able to handle all possible combinations in an easy and flexible way.

### **Correct accounting for receiver tracking technology and related biases**

Modern GNSS receivers utilize different modes (e.g., direct tracking or semi-codeless tracking) to track the GNSS navigation signals. These modes may cause specific signal delays in the receiver, and the recorded observations are consequently affected by varying biases, as described in Sects. 3.4.2 and 3.4.4. Moreover, the biases may also depend on signal frequency, GNSS, and time.

Information on observation type and tracking mode finds its way into data analysis by exchanging observation data based on RINEX Version 3 [Gurtner and Estay, 2009]. The correct and consistent handling of the observation types and all resulting biases is an important issue especially for a multi-GNSS software.

### **Customized parameter setup**

The characteristics of different GNSS may help to understand the relationship between specific observation scenarios and parameter estimates, or to identify model deficiencies. Combining systems with different orbital revolution periods, e.g., may help to understand periodic non-physical variations in time series of parameters.

A GNSS-specific parameter setup is desirable for investigations in this field, e.g., to keep the ERP estimates independent for each GNSS in order to analyze the spectral properties of the resulting time series. However, the software should also offer the possibility to combine these GNSS-specific parameters into a single system-independent parameter on the normal equation level.

### **Provision of extensive statistics and processing protocols**

The software must not only be able to produce highly accurate results but also to provide comprehensive reports and statistics. This includes in particular GNSS-specific statistics

for each parameter type. In addition, all processing options should be documented in detail to provide information on how the results were generated and to facilitate an identical reproduction of a specific program run.

### 4.2.2 Technical Requirements

The inclusion of new and upgraded GNSS is not only challenging from the scientific point of view but involves in addition a number of technical challenges, mainly caused by two factors:

1. Any modern multi-GNSS software must be open for future developments without the need of extensive code modifications or changes in its internal structure. It must be as open to new developments as possible (e.g., to new LCs) and at the same time as self-contained as necessary to guarantee a high level of independence from external factors (like changing and evolving file formats).
2. The software must be able to easily cope with continuously growing numbers of satellites, observations, and parameters. The inclusion of a fully deployed GNSS in the CODE IGS processing adds about 1100 parameters to be estimated<sup>2</sup>, raising the total number of parameters by about 20% w.r.t. an analysis situation based on 50 GPS and GLONASS satellites and a network of 240 receivers. The inclusion of new tracking sites will significantly let these numbers grow, as well. The software must be ready to deal with high requirements in memory, file size, and computational power. Available hardware resources should be used optimally.

These issues affect the software design process, as they ask for elementary decisions, e.g., the selection of a programming language. The technical approach must be well defined and all structure-related decisions must have been made before a line of code is written. It is usually difficult to change basic structure deficits afterwards without rewriting significant parts of the source code. The most important technical requirements are related to:

#### Programming language

An object-oriented programming (OOP) language is preferable, as some basic OOP concepts like classes, inheritance, or encapsulation are well-suited to meet the needs of a complex GNSS software package. If compatibility with already existing program parts is required (e.g., if an existing software should be updated), the programming language is usually given and not freely selectable.

In either case, high-level capabilities like dynamic memory management are absolutely mandatory. The computation speed of real-valued numerical calculations and task parallelization capabilities should be considered in the decision process, as well.

---

<sup>2</sup>30 satellites with 18 orbit and 19 antenna parameters, each. Additional introduced biases and ambiguities are not considered in this context but would add to these numbers, too.

### **Memory management and size limitations**

The source code should not contain hard-wired size limitations like maximum dimensions of arrays. This is especially important for the maximum number of satellites, observations, and parameters as these will significantly grow with the inclusion of each new GNSS.

Memory should be allocated as needed to ensure easy expandability without running into size-exceeding problems. A rigorous dynamic memory management is mandatory. Nevertheless, a resource control mechanism might be foreseen to limit the allocated memory to a reasonable size.

### **File formats**

Information to be stored in software-specific files should be limited as little as possible by corresponding file formats. The software-specific format definitions should be as flexible and expandable as possible to ensure an easy adaption to future needs.

### **Future software enhancements and extensions**

A modern GNSS software must keep up with the ongoing developments in the field of GNSS hardware and new applications. The internal parts and structures of the software (like objects representing observation types) must be generic and flexible to facilitate the inclusion of new components. This is in particular true for software parts dealing with carrier frequencies, observations, LCs, biases, parameter types, and satellite systems as a whole.

The software package must be easily expandable to future extensions and upgrades. An easy integration of new tools, programs, or program parts must be possible throughout the software package. This also calls for the maintenance of well-defined communication channels between different program parts. The GUI must be easily adaptable to new programs, as well.

## **4.3 Design Principles and Software Architecture**

Before writing a complex software package (or updating an existing one), the fundamental software architecture and some basic design principles must be specified. The available infrastructure, programming environment, and the list of requirements compiled in the previous section are the starting point for these tasks.

Figure 4.2 shows the conceptual software design for the updated BSW realizing a high degree of modularization, expandability, and flexibility. The main processing programs should be kept independent of external factors to the extent possible (indicated by the dashed rectangle). These programs communicate with the “outside” world only via well-defined interface routines (bold black arrows). Shared data, specifications, file formats,

and definitions are organized and encapsulated in core modules together with the methods and functions operating on these data. External files are always converted to software-internal formats. The GUI is a separate, independent program part.

Three basic design principles have been identified as particularly important to meet the list of requirements and to realize the software architecture, namely modularization, independence from external formats, and high flexibility and expandability. These principles should be strictly observed, guaranteeing a comprehensible and consistent design.

### 4.3.1 Modularization

The software must be highly modular to be able to react to yet unforeseen developments without rewriting a significant portion of the source code.

The functionality of the software package is subdivided in independent sub-tasks (e.g., data conversion, preprocessing, parameter estimation). Each task is realized in a specialized self-contained program. Single programs may be changed or even removed without side-effects on the remaining software package. New programs can be easily included, if needed. The information exchange between different programs is based on intermediate software-internal files. All processing programs depend on various specialized core modules. The processing programs realize the mathematical models for, e.g., data screening or parameter estimation. They do in particular not contain any GNSS-specific information.

The core modules, on the other hand, contain all the shared data, definitions, and information needed by the processing programs to execute their tasks. This includes GNSS-

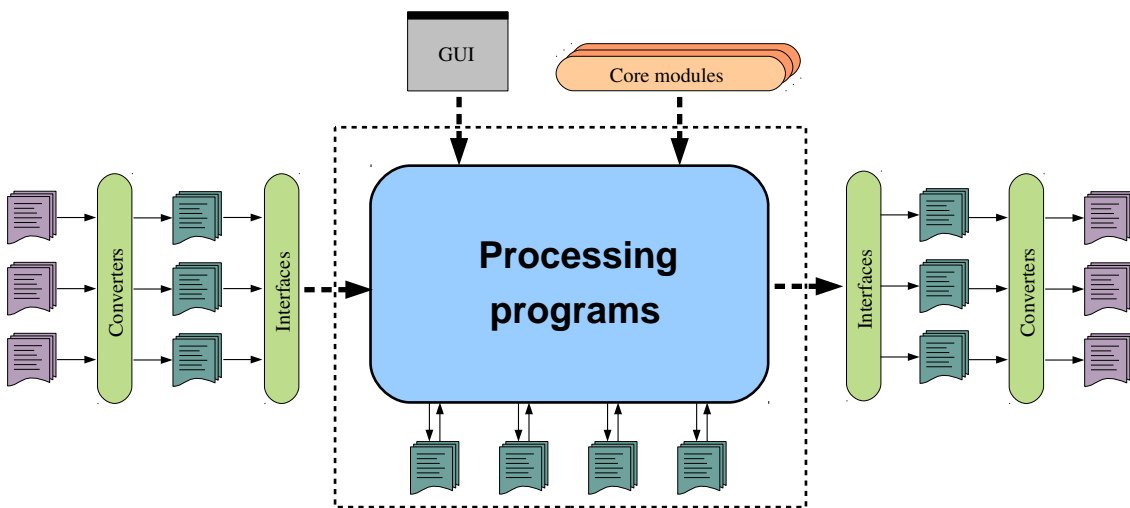


Figure 4.2: Software design diagram.

specific information (such as the number of carriers, the associated frequencies, or the number and type of ranging codes), receiver-specific information (e. g., available tracking modes, trackable GNSS), observation type definitions (like rules for creating LCs), and general information like time-system definitions. The processing programs can access the module data only via dedicated interface routines. These routines are defined and coded in the corresponding core modules. The programs do not need knowledge of implementation details, only the interfaces must be available.

This approach greatly facilitates new implementations, especially of new frequencies or LCs. As long as the interface does not change, only the corresponding core modules must be adapted. The changes are then immediately available throughout the entire software package.

### 4.3.2 Independence of External Formats

The independence of the processing programs from external file formats is another important aspect. The main programs use solely software-internal file formats and naming conventions. Data is exchanged between individual programs via internal files, as well.

Information from external files (e. g., observation data from RINEX files) is first converted to a software-internal file format using a collection of dedicated interface routines (converters). File format specifications, definitions, and conversion, access, and manipulation routines are encapsulated in the corresponding modules. External nomenclature (e. g., the observation codes as defined in RINEX 3) is translated by the interface routines (usually during a conversion step) to a set of internal global identifiers. These are defined in the core modules and are used in all programs.

Only the corresponding module, especially the conversion routines, must be adapted in the case of changes or updates of external file formats or nomenclature. As long as the interfaces do not change, external file formats do not have any direct impact on the core processing programs.

Nomenclature for software output files (such as the abbreviations for observation types) are defined in core modules, as well. The names can be accessed by the processing programs only via the interface routines. A consistent naming for all output files is thus guaranteed. Should it be necessary, e. g., to change the name of a linear combination, only one module must be changed.

### 4.3.3 Flexibility and Expandability

In view of future developments and the increasing pace of scientific innovations in the field of GNSS and space geodesy, special attention must be paid to flexibility and expandability of a software package.

There should be no absolute limitations such as array sizes, file lengths, or maximum dimensions (e. g., maximum allowed number of satellites or stations) in the software. This calls for a purely dynamic memory management, facilitated by modern programming languages. Without program-internal limitations it is, however, left to the developer to foresee a number of security mechanisms to keep the memory use and computation time within reasonable limits.

Internal file formats and the corresponding interface routines should be as generic, flexible, and expandable as possible. Files are stored in binary format, if file size and access time are important issues, otherwise the ASCII format is preferred. Easy readability of ASCII files should be maintained wherever possible but not at the expense of storing additional information.

The graphical user interface of the software is separated from the processing programs. A dedicated GUI program displays option panels, reads user input, and prepares information for further use. The processing programs access user input (e. g., selected files and options) only by a set of input routines. These input routines may already validate the user input, thus minimizing runtime errors. A redesign of the GUI or the implementation of new options does not require changes in the processing programs (the programs must of course be adapted to make use of the new options).



# 5 Practical Realization

## 5.1 Initial Situation

The Bernese GPS Software package consists of 101 programs, about 60 modules, and more than 1200 subroutines; this equals more than 400 000 lines of source code.<sup>1</sup> About 80 software-specific file formats are supported [Dach *et al.*, 2007]. Most formats may be accessed by specialized editing and conversion tools. The BSW was originally coded in FORTRAN 77 [ANSI, 1978]. Linear programming predominates and FORTRAN 77 does not offer the functionality of modern functional or OOP languages. The transition to Fortran 90 [ANSI, 1992] was initiated in the year 2000 allowing for a module-based programming style. Figure 5.1 shows the creation dates and programming language of the BSW programs in chronological order. The solid line gives the total number of programs contained in the BSW package.

Although Fortran 90 is solely used since 2000, existing programs have not been updated. About half of the programs were created in the years before 1996 and are coded in FORTRAN 77 (with all accompanying restrictions). However, old routines were translated to Fortran 90 whenever advanced programming features were needed. About 30% of the BSW programs are older than 20 years. Several key processing programs are among the oldest programs of the software package, namely the program for code-based clock synchronization CODSP from 1987, the data preprocessor MAUPRP from 1988, SNGDIF to create SD observation files from 1987, and the main parameter estimation program GPSEST from 1987 (see Tab. A.1 in Appendix A).

The BSW was initially designed to process dual-frequency carrier phase and pseudorange GPS data. In 1999, the GLONASS capability was added by adapting the already existing software structures and algorithms. GLONASS was in essence treated as a “GPS with some peculiarities”. This approach was feasible, because GLONASS is quite similar to GPS in terms of system design, models, and algorithms. The dual-frequency design of GLONASS with satellite-specific carrier frequencies was, however, a crucial point.

The upcoming next-generation GNSS and improvements of existing systems generally offer more than two frequencies and new observation types. The number of satellites, observations, and parameters to be estimated is growing significantly. These issues together with the old age of the main processing programs and outdated programming technologies

---

<sup>1</sup>As of June 2011

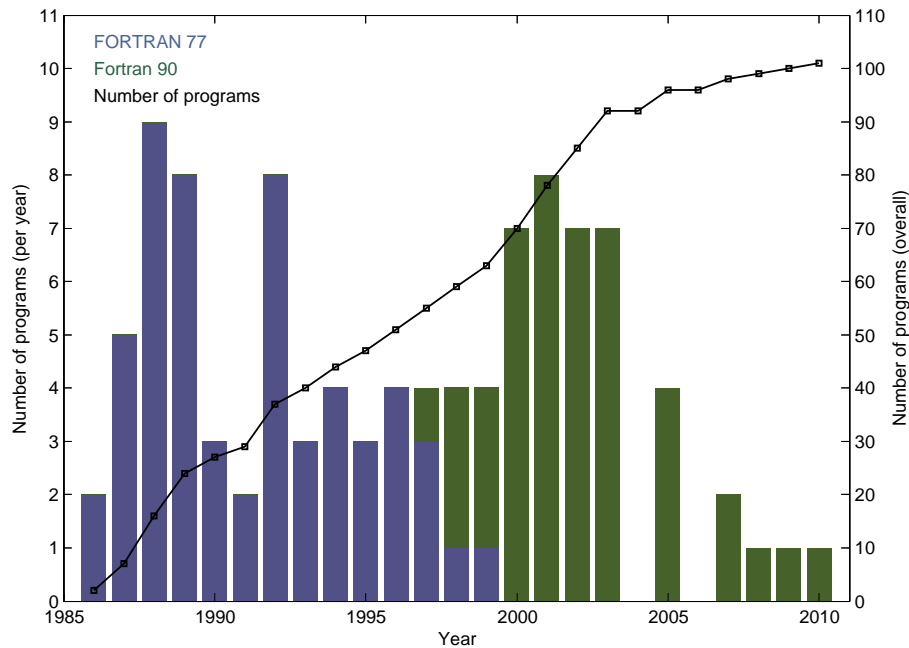


Figure 5.1: Development of the BSW and programming language.

render a straight-forward implementation, as performed in the case of GLONASS, impossible. A radical redesign of the BSW—adhering to the principles stated in the previous sections—was necessary to implement true multi-GNSS capabilities.

## 5.2 Software Implementations

### 5.2.1 Harmonization and Generalization of Observation Handling

The redesign and implementation of the observation management was one of the most important and labor-intensive tasks of the update. The main problem of the old BSW version were the restrictions to two carriers, two code types, and a certain number of linear combinations. All array sizes and maximum dimensions were set independently in all individual programs. Furthermore, the rules for creating LCs were not centralized but explicitly coded in several different programs. An update to three or more carriers and new LCs was not feasible under these circumstances.

The management of observations was completely removed from the individual programs and relocated to three dedicated modules:

**D\_OBSTYP** This module defines global identifiers (i. e., unique numbers) and names for different measurement and observation types, carriers, ranging code types, LCs, etc.

The identifiers are used internally by all programs to address specific observations, carriers, and so on. The names are used for output purposes, i. e., for program result files, summaries, and protocols.

**O\_OBSTYP** The module D\_OBSTYP is complemented by module O\_OBSTYP, providing the access and query functions for the observation types. This includes functions to translate the global identifier to an output name and vice versa, and query functions, e. g., whether a specific observation is a phase or code observation or on which carrier wave a ranging code is transmitted.

**D\_FREQ** All frequency-, wavelength-, and LC-related tasks are managed by this module. It is the “heart” of the new observation management system. Frequencies for all carriers of GNSS satellites and the coefficients associated with all LCs are computed as needed and buffered in a module-internal structure. This internal structure can be queried only based on dedicated functions. The functions return the frequency, wavelength, or LC coefficients for a particular epoch, observation type or LC, and satellite.

Module D\_FREQ also provides a function to create LCs of observations, i. e., a record of GNSS observations and an LC type are specified and the function returns the corresponding linear combination of observations.

All arrays and variables related to frequencies, measurements, LCs, and similar items have been completely replaced by the specific query functions throughout the software. This was a profound modification of the BSW. About 30 programs and more than 200 subroutines had to be modified, re-organized, and in some cases even completely rewritten. About 10 programs—main processing programs in particular—and their core subroutines had to be rewritten entirely, implicating a conversion from FORTRAN 77 to Fortran 90. The rewritten programs are labeled in Tab. A.1 with the “◦ → ●” symbol in the F77/F90 columns.

These implementations greatly facilitate the inclusion/use of new carriers, measurement and observation types, or new LCs. The necessary steps are demonstrated taking the implementation of a new LC as example:

1. Assign a new global identifier and a name for the new LC in D\_OBSTYP.
2. Define some basic properties of the LC (e. g., geometry- or ionosphere-free) by setting the corresponding flags in D\_OBSTYP.
3. Define the creation rule of the LC, i. e., code the computation of each LC coefficient in module D\_FREQ.

The new LC is now readily available throughout the software and can be used based on the query functions and the global identifier. The selection of the new LC and LC-specific options must of course be implemented in the GUI and the associated interface

programs. But these implementations are completely independent from the observation and frequency management part of the software.

### 5.2.2 Dynamic Memory Management and Removal of Fixed Limits

The transition from a static to a dynamic memory model was another labor-intensive step in the software update. Many arrays were pre-allocated with a fixed size in the previous versions of the BSW. The maximum dimensions were defined by global parameters, but in several cases the limits were fixed in each program. These predefined limits were not only a problem for memory allocation. The limits also appear in loops as maximum number of cycles (e. g., a loop over two frequencies), in conditional statements, and at many more places.

The definition of maximum dimensions is moved from the programs to modules in the new BSW. The dimensions are provided as global parameters and they are used consistently in all programs. A change of a maximum dimension (e. g., the number of GNSS) must be made only at one defined place and all programs function accordingly.

All problematic fixed-size arrays, e. g., lists of satellites or observations, have been removed. Memory is allocated and released as needed at runtime. This measure takes care of the significant increase in the number of satellites, stations, observations, and parameters to be expected, if new GNSS are included in the software. The dynamic memory management is not only more flexible; it also helps to reduce the memory requirements of programs (compared to the previous versions), because in most cases the maximum dimensions were not really needed.

### 5.2.3 Redesign of File Formats

Several software-specific files of the BSW Version 5 were tailored to two GNSS, two frequencies, and one phase and code type. These restrictions required a redesign of the corresponding formats.

The file definition together with all in-/output, access, and conversion routines were encapsulated in dedicated modules. A redesign of file formats does not only involve the format itself, but implies the modification of many subroutines and programs, such as ASCII–binary converters, converters from old to new formats, or file manipulation and extraction programs. In the end, all processing programs using the files had to be changed and adapted to the new formats, as well.

About 15 file formats had to be changed. The most profound modifications are related to files containing GNSS observations, receiver-specific information, and biases.

The observation file format underwent the most radical change. Code and phase observations were stored in separate files in Version 5. Only two-frequency data could be stored,

detailed information on the observations (e. g., type of code) was not available. The format was obsolete (as, e. g., limited disk space does not play a crucial role nowadays) and did not fulfill the multi-GNSS requirements anymore.

The new observation file is completely redesigned: the separation of measurement-types in dedicated files was dropped, all observations are localized in one file. This is an advantage, if a program needs all measurement types, because a synchronization between the different files is no longer necessary. The administrative effort is significantly reduced. The number of carriers and of code and phase observations per carrier are no longer restricted. This generalization is absolutely necessary if the new signals on more than two carriers shall be used, e. g., for LCs with three or more components. The complete information related to each measurement is stored and allows it to correctly take into account DCBs and other biases.

The receiver file now contains details on the available measurement types and tracking technologies. This information is necessary to apply the correct biases. Moreover, the file defines an observation priority list for each receiver to be used, if more than one comparable observations are available, e. g., if P- and C/A-code observations are available.

The DCB file was redesigned to a more general bias file. The bias type is no longer predefined. Absolute or differential biases are allowed for arbitrary measurement types. The biases may relate to a GNSS, to single satellites, to receivers, or to any combination thereof. They are optionally accompanied by a validity interval. A new bias correction subroutine uses the query functions for the biases and for the LC factors to automatically correct observations or to return all required biases.

### 5.2.4 Source Code Modernization

Outdated program structures and source code parts were consequently modernized by using advanced programming features offered by Fortran 90, like user-defined operators or function overloading. The source code of FORTRAN 77 programs and subroutines was completely rewritten in Fortran 90, if an update was not feasible.

Table 5.1 lists the programming language<sup>2</sup> and the number of programs, subroutines, and modules of the original and updated BSW versions. The overall percentage of Fortran 90 program parts was increased from about 48% to 60%. A total of 10 out of 56 FORTRAN 77 processing programs have been recoded in Fortran 90; four others have been replaced by completely new programs (cf. Tab. A.1). The percentage of Fortran 90 processing programs was increased from about 45% to 60%.

---

<sup>2</sup>All FORTRAN 77 subroutines already contain some Fortran 90 code, e. g., the inclusion of certain general modules. To a large extent, however, the old subroutines do not make use of advanced programming features like dynamic memory allocation.

**Table 5.1:** Number of programs, subroutines, and modules in BSW Versions 5 and 6 (F77: FORTRAN 77, F90: Fortran 90).

Type		Version 5	Removed	New	Version 6
Programs	F77	56	16	–	40
	F90	45	2	16	59
	Sum	101	18	16	99
Subroutines	F77	659	209	–	450
	F90	560	81	89	568
	Sum	1219	290	89	1018
Modules	F77	–	–	–	–
	F90	59	4	29	84
	Sum	59	4	29	84
Overall	F77	715	225	–	490
	F90	664	86	134	712
	Sum	1379	311	134	1202

The number of modules increased by 50%, giving a clear indication of the successful realization of the modularization and encapsulation. The new Version 6 contains about 200 (or about 17%) fewer subroutines than the Version 5, because:

- unused routines were identified and removed;
- routines with a similar purpose were combined in dedicated modules and/or replaced by overloaded functions;
- routines related to file formats (e. g., in-/output or conversion functions) were encapsulated in corresponding modules;
- Fortran 90 intrinsic routines were consequently used to replace “home-made” routines serving the same purpose.

All in all, about 50 of 100 programs and 800 of 1200 subroutines had to be changed in some way in the course of the modernization of the BSW.

### 5.2.5 Secondary Issues

All program output files, summaries, and warning/error messages had to be adapted to the new features. The output formats must be more flexible to deal with an arbitrary number of GNSS, frequencies, LCs, etc. Accordingly, all format statements in the source

OBSERVATION SELECTION	
Satellite system	ALL
Frequency	L3
Elevation cutoff angle	3 degrees

(a) Old BSW.

GNSS SELECTION	<input checked="" type="checkbox"/> GPS	<input checked="" type="checkbox"/> GLONASS	<input checked="" type="checkbox"/> Galileo
Combination	Iono-free	Iono-free	None
Frequencies	L1 L2 L5	None	L1 L5 L7 L8 L6
Measurements	Phase	Iono-free	Phase & Code
Smoothed code	<input type="checkbox"/>	Geometry_free	<input type="checkbox"/>
SLR SELECTION		Widelane	
Observations	R1	Mel-Wuebb	
		GRAPHIC	
		P-C_(None)	
		P-C_(IF)	
		P+C_(GF)	

(b) Redesigned BSW.

**Figure 5.2:** Observation selection in the BSW.

code (about 8000) had to be checked and adapted. The BSW includes several programs to extract information from the program output files in order to create short summaries. Such programs had to be changed to process the updated outputs, as well.

The GUI was updated to make available all new features. Although the programs get more and more complicated, the processing options must be presented to the user in an easy and comprehensible way. Several parts of the GUI (especially concerning the selection of observation types and LCs) had to be fundamentally redesigned, as illustrated by Fig. 5.2.

Further examples of secondary tasks are related to the update of the program help system and the complete revision of the software manual. Much additional work was caused by these updates.

## 5.3 Summary

With several next-generation GNSS, updates of existing systems, and innovations in satellite navigation, a scientific multi-GNSS analysis software package is needed. This need was recognized by the AIUB and BKG. A project was initiated to implement full multi-GNSS capabilities in the Bernese GPS Software.

A list of requirements for a modern GNSS analysis tool was composed. Attention had to be paid not only to scientific, but also to technical issues. The list of requirements is, of course, always subject to change and matures with the software development process and improvements in the field of GNSS data processing and observation modeling. Software design concepts were developed based on the list of requirements. The principles underlying modularization, independence from external formats and factors, and high

flexibility and easy expandability were identified as the key issues of the software design and architecture.

The update of the BSW was a very demanding task. The restriction to two GNSS and two frequencies rendered a straight-forward implementation of real multi-GNSS capability virtually impossible. A radical software redesign and modernization was necessary.

The update comprised tasks like implementing a completely reworked frequency, observation, and LC management system; the update of a multitude of file formats and the corresponding interface, access, and conversion routines; the adaptation of all processing programs to the new formats; the transition from a static to a dynamic memory management; and the modernization of the source code making use of the advanced programming features offered by Fortran 90. Additional work was caused by controlling and updating all program output files, format statements, the help system and the user manual, and the GUI.

In the end, 50 of 100 programs, 800 of 1200 subroutines, 15 file formats, and most GUI panels and output files were changed, updated or recoded. Including the conceptual and design phase, the resulting effort was about six man-years.

The update was a costly, but necessary task. The next generation BSW is now truly multi-GNSS capable. All kinds of GNSS, frequencies, and observation types can be processed. Corresponding biases can be accounted for. The implementation of future systems, new carriers, or new LCs with more than two components is possible in an easy and flexible way with only minor programming work.

## **Part III**

# **Combined Analysis of Observations from GPS and GLONASS**



# 6 Setup of Experiments

## 6.1 Motivation

If highest accuracy is required, the analysis of microwave GNSS data is carried out in the post-processing mode. The observation data is recorded over a certain amount of time and jointly analyzed in processing batches (sessions) of predefined lengths. A session length of 24 hours is widely used. The IGS, e. g., established a daily data processing scheme since its early days for the high quality rapid and final products. This is in particular convenient for the analysis centers and for the user community because a regular product update schedule, synchronized with the business calendar, can be maintained.

Selecting a session length always implies a trade-off between product quality and product latency. More observation data is generally improving the accuracy of the estimated parameters, but increases production time and vice versa. The processing batch length has, however, an additional more profound impact on the analysis.

All GNSS have system inherent repeat cycles as described in Sect. 2.4, e. g., the orbital period of a GPS satellite of half a sidereal day. A batch length close to a system-specific repeat cycle may have a negative (amplification) or positive (averaging out) effect on unmodeled errors and may therefore influence the parameter estimates. Aliasing effects may cause artificial periods in time series of parameter estimates [Ray *et al.*, 2008]. The selection of the processing batch length is in particular important in a combined multi-GNSS data analysis as it may “favor” a particular GNSS and “penalize” another. The well-established 24-hour session length is only about four minutes longer than two revolution periods of the GPS satellites. This averaging period might favor the GPS, but might not be the optimum choice for a multi-GNSS analysis.

The main goals of our study are to: (a) systematically explore the impact of the processing batch (session) length in GNSS data analysis; (b) study the effects of combining observations from GPS and GLONASS observations. A set of different solutions were generated based on four different session lengths, namely on two revolution periods of a GLONASS satellite, on two revolution periods of a GPS satellite, on a synodic day (the well-known 24 hours), and on a length corresponding to neither the GPS nor the GLONASS revolution periods. Single-system (GPS-only, GLONASS-only) and combined solutions were generated for each of the four session lengths. The resulting parameter time series are analyzed and compared.

The computations are based on three years (2008 to 2010) of GPS and GLONASS observation data from a global tracking network. All solutions are based on the same data set and follow the same processing scheme. The resulting orbits are in addition validated using the SLR observation technique.

## 6.2 Design of the Study

### 6.2.1 Data Basis

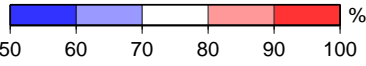
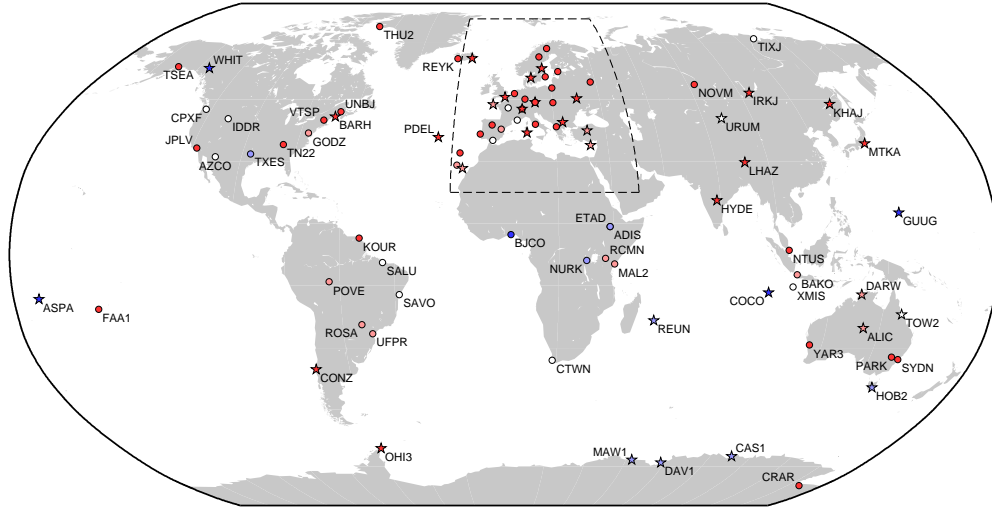
The CODE GNSS observation data archive contains RINEX files for currently more than 350 stations and covers almost 20 years. It is continuously updated and completed. The station information (observations and metadata) is collected from data centers from the IGS, the European permanent network (EPN), and many other sources. The CODE data archive serves as the primary data source for this study.

A network of 92 globally distributed GPS/GLONASS combined tracking stations was selected (Figs. 6.1). The observations cover the years 2008 to 2010. The starting year was mainly dictated by the lack of a reasonable number of GLONASS-capable tracking stations before 2008. Only stations with observations available for more than 75% of the three years were selected for the study in order to guarantee a stable and consistent network and to reduce the influence of the changing network geometry on the results. Exceptions from this rule were made for 16 (isolated) stations to maintain a balanced global station distribution. These stations are mainly located on the southern hemisphere, namely in Africa, Antarctica, and on several islands in the Pacific and the Indian Ocean (Fig. 6.1a). Table A.2 lists the 92 stations with the percentage of available tracking data for each single year. The exceptions of the 75%-rule are marked in gray.

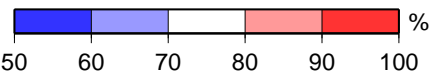
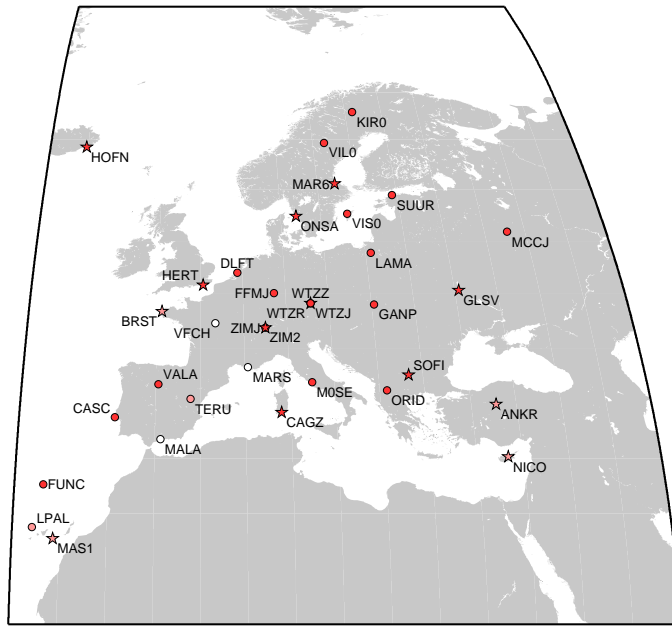
Special care was taken to keep the GPS and GLONASS solutions comparable—to the extent possible. Stations for which a pronounced imbalance between GPS and GLONASS observations was detected, were excluded during data import. Figure 6.2 shows the actual number of stations used in the analysis. The number of stations increases almost linearly in 2008, from a minimum of about 35 to about 80 stations. During the following two years, 2009 and 2010, the number of stations was stable on a level between 80 and 90.

The drop of almost 30% in the number of stations on April 29, 2010 and the following days is interesting. It was caused by a failure in the GLONASS tracking for a specific receiver type. A firmware update solved the problem and a few days later the stations started to track GLONASS normally. Details concerning this event may be found in the IGS station mail, in particular in *Walford* [2010a] and *Walford* [2010b].

Figure 6.3 shows the number of satellites used in the analysis. The number of GPS satellite ranges between 30 and 32 throughout the three years. Numerous daily “drop-outs” of single satellites are caused by repositioning events. Satellites are excluded from processing



(a) Global view of the tracking network.



(b) European region of the tracking network.

**Figure 6.1:** Network of tracking stations and available GPS/GLONASS observations in percent (IGS reference sites are indicated by an asterisk).

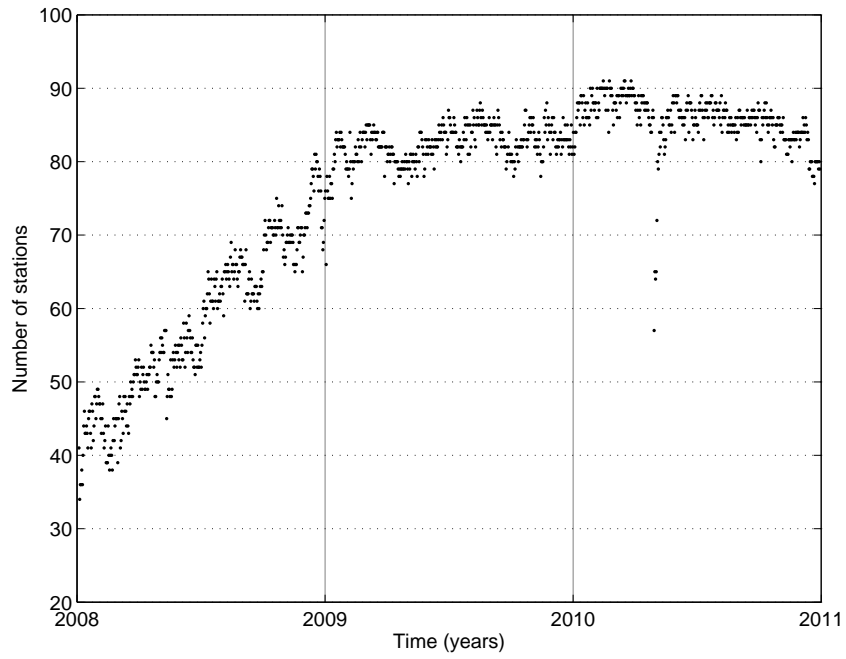


**Figure 6.2:** Number of tracking stations used in the data processing.

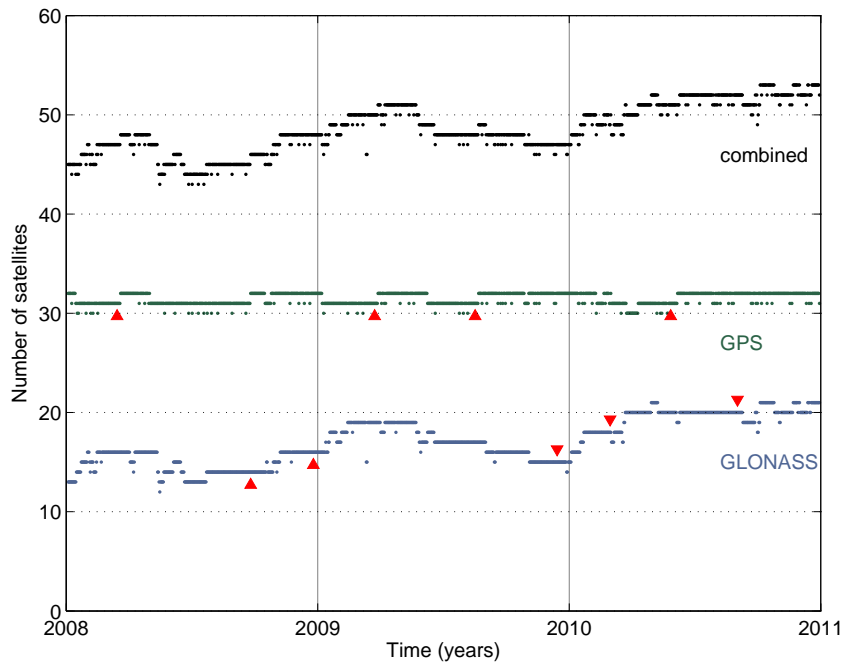


**Figure 6.3:** Number of satellites used in the data processing (triangles indicate satellite launches).

**Table 6.1:** Session identifiers, characteristics, and resulting number of sessions.

ID	Adapted to	Session length in		# sessions
		sidereal days	h, min, s	
LNG	–	$18/17$	25 h 21 min 00 s	1037
DAY	one synodic day	–	24 h 00 min 00 s	1096
GPS	GPS	$17/17$	23 h 56 min 30 s	1097
GLO	GLONASS	$16/17$	22 h 32 min 00 s	1166

during these events. Such frequent maneuvers are dictated by the deep (2:1)-resonance of the GPS satellites' orbital revolution period with the Earth's rotational period, the sidereal day (see Sect. 2.4.1). The number of GLONASS satellites increased from initially 14 to 21 during the three years. The triple-satellite launch concept followed by Russia to complete the GLONASS constellation can be nicely observed in the figure (satellite launches are marked by triangles), e. g., at the beginning of 2010, where two times three satellites became active (in January and in March). The GLONASS satellites do not need to be repositioned for constellation-keeping purposes after an initial positioning into the correct orbital slot, because the GLONASS satellites' orbital periods are not commensurable with the sidereal day.

## 6.2.2 Characteristics of Computed Solutions

### Processing batch length

The three years of observations are analyzed in four different data processing lines. Each processing line consists of exactly the same steps (as outlined in Sect. 6.2.3), but is based on a different batch length. Two session lengths are commensurable with the orbital periods of GPS and GLONASS, respectively, one is the customary (solar) daily session, and the last one is far from the revolution periods of both GNSS.

Two requirements constrained the session length: (a) The session boundaries should always fall on integer 30 second boundaries, as the RINEX data was sampled at 30 second intervals. (b) All session lengths should be integer multiples of a common basic time interval  $\Delta T$ . This time interval was used to set up the nodal points of the piece-wise linear parameter representations in the analysis. The sampling of the corresponding parameters (e. g., troposphere parameters) was therefore the same for all session types, resulting in consistent and comparable solutions.

An interval length of  $\Delta T = 1 \text{ h } 24 \text{ min } 30 \text{ s}$  was found to be suitable, based on the averaged actual orbital revolution periods for all GPS ( $\bar{T}_G = 11 \text{ h } 58 \text{ min } 01 \text{ s}$ ) and all GLONASS ( $\bar{T}_R = 11 \text{ h } 15 \text{ min } 43 \text{ s}$ ) satellites. This interval agrees with  $1/17$  of the length of a sidereal day ( $d_*$ ) on the level of a few seconds, and will be treated as equivalent, i. e.,  $\Delta T = 1/17 d_*$ .

**Table 6.2:** Solution identifiers and characteristics.

ID	Characteristic
GPS	GPS-only
GLO	GLONASS-only
CMB	GPS/GLONASS, one constant ISB per session
NEQ	GPS/GLONASS combined on NEQ level, epoch-wise ISBs

Note that it was not possible to use the same interval for the daily solution:  $\Delta T = 1$  h 30 min was used instead. Table 6.1 summarizes the characteristics of the four session lengths.

The GLO and GPS sessions correspond almost precisely to two orbital revolutions of a GLONASS and a GPS satellite, respectively. The long LNG session, with a batch size of 25 hours 21 minutes, corresponds to neither of the systems. The daily session DAY, although very similar to the GPS session length, was included for reference.

The GPS and GLO sessions contain exactly two revolutions of a satellite of the respective GNSS. A GPS satellite completes 32 revolutions in 17 GLO sessions and 36 revolutions in 17 LNG sessions. A GLONASS satellite completes 17 full revolutions in 8 GPS and 9 revolutions in 4 LNG sessions, respectively.

### Solution types

Four different solutions are made for each of the four session lengths, namely a GPS-only solution, a GLONASS-only solution, and two combined GPS/GLONASS solutions. The two combined solutions differ in the handling of the inter-system biases between GPS and GLONASS:

- One constant ISB per session is set up in the first solution. The ISB is realized by prohibiting cross-system ambiguity resolution.
- One ISB is allowed per epoch in the second solution. This is realized by combining (stacking) the GPS-only and GLONASS-only NEQ systems as outlined in Sect. 3.5.2. The single-system solutions are assumed to be uncorrelated.

Table 6.2 list the four solution types and the corresponding identifiers. Combining the four session lengths with the four solution types gives all in all 16 different solutions; each is uniquely identified by its solution ID and session ID.

### 6.2.3 Data Processing

All solutions in this study are based on the same processing scheme. A consistent set of station coordinates, troposphere parameters, orbits, and Earth rotation parameters

(ERPs) is generated for each of the 16 solutions. Although the session lengths vary, the time resolution of sub-daily parameters (e. g., troposphere parameters) is always the same, namely  $1/17$  d\*. The results are generated in a multi-step process:

1. The observations are imported from RINEX files and preprocessed (including ambiguity resolution).
2. NEQ systems are set up for each solution type.
3. The NEQ systems are combined to create 3-year coordinate sets, ERPs, and GCCs.
4. Troposphere parameters and orbits are estimated using (keeping fixed) the previously combined 3-year coordinates and ERPs.
5. SLR residuals are generated for all orbits for validation.

All calculations were performed with an advanced version of the BSW. Extensive use was made of the automation features offered by the software. Up-to-date models were used and the processing closely followed the processing scheme used by CODE for its contributions to the IGS final orbit product. Table 6.3 lists the most important background models and processing options used in our experiments. Products from CODE were used wherever possible. The computations were carried out on the Linux cluster of the University of Bern, Switzerland. At the time of this study, the Linux cluster comprised about 170 nodes equipped mainly with 8-core processors and memory ranging from 8 to 24 GiB.

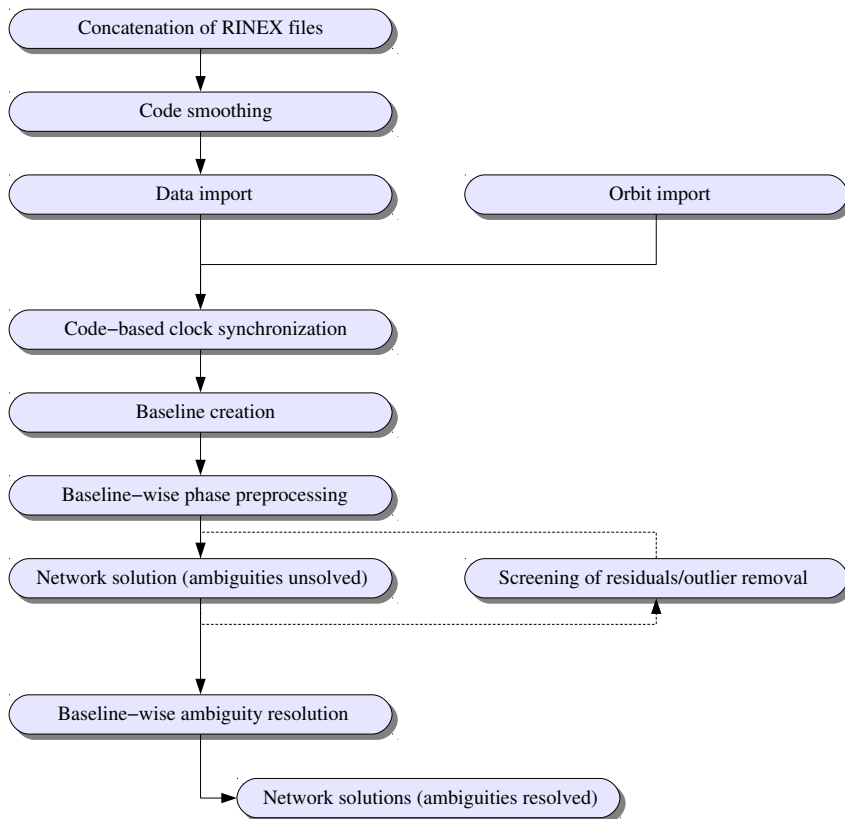
### Setup of solution-specific NEQ systems

Figure 6.4 shows the flow chart of the processing steps necessary to set up the NEQ systems for a particular solution. The processing starts with the data conversion and the data import step. The daily RINEX observation files are concatenated and cut to the validity interval of the selected session. Code observations are smoothed [*Springer, 2000*] and written back to the RINEX files, thus replacing the original code. Eventually, the RINEX phase and code observations are converted to the BSW observation file format. Orbits and ERPs are imported from the CODE processing.

The data import is followed by a preparatory and preprocessing part. A code-based ZD solution provides the receiver clock corrections for clock synchronization. A linearly independent set of baselines, i. e., station SDs as given by the observation equations (3.11), is created using an algorithm maximizing the number of resulting SD observations. The subsequent preprocessing of phase measurements runs in a baseline-wise mode using the triple-difference observations (3.17b). Different linear combinations are used to identify and correct cycle slips. Bad observations are removed and new ambiguities are set up if a cycle slip could not be corrected reliably. In the next step, a first ambiguity-float network solution is computed based on the ionosphere-free LC of the phase DD observations (3.15b). Post-fit residuals are generated, screened, and outliers are removed.

**Table 6.3:** Processing details.

Measurement model	Description
Basic observation	DDs of ionosphere-free LC of carrier phases
Data sampling rate	180 s
Elevation angle cutoff	3°
Elevation-dependent weighting	$1/\cos^2 z$
Geodetic datum definition	$2 \times 3$ no-net translation and rotation conditions on IGS08 reference sites [Rebischung, 2011] ( <i>multi-year solution</i> ); all stations fixed on multi-year results ( <i>final solution</i> ); geocenter constrained to zero
Mathematical correlations	Modeled correctly
Ionosphere	2nd-order, 3rd-order, and ray path bending effects modeled [Schaer et al., 2010]
Troposphere a priori model	Vienna mapping function (VMF) with meteorological data from a weather model [Böhm et al., 2006b; Kouba, 2008]
Estimated parameters	Description
Station coordinates	One set of coordinates per session
Velocities	Linear (only in <i>multi-year solution</i> )
Geocenter coordinates	Set up but heavily constrained to zero
Phase ambiguities	Resolved ambiguities introduced as known
Troposphere	Zenith delay corrections in intervals of 1 h 24 min 30 s (1 h 30 min for session DAY), mapped with VMF; one set of horizontal troposphere gradients per session
Orbital parameters	6 osculating orbital elements plus 5 solar radiation pressure coefficients (constant in D-, Y-, and X-direction, periodic terms in X-direction [Beutler et al., 1994b]) per satellite
Earth rotation parameters	X- and Y-coordinates of pole, UT1-UTC as piecewise-linear functions with 1 h 24 min 30 s (1 h 30 min) spacing. The first UT1-UTC parameter is fixed to the a priori value from IERS C04 [Gambis, 2004]
Background models	Description
Antenna phase center model	Absolute IGS08 model
Gravity field model	JGM3 [Tapley et al., 1996]
Solar radiation pressure model	Updated CODE model for GPS satellites [Springer, 2000; Dach et al., 2009]; no a priori model for GLONASS
Nutation model	IAU2000 [Mathews et al., 2002]
Sub-daily pole model	IERS2003 [McCarthy and Petit, 2004]
Solid Earth tide model	IERS2003 [McCarthy and Petit, 2004]
Ocean tidal loading	FES2004 [Lyard et al., 2006]
Pole tide model	IERS2003 [McCarthy and Petit, 2004]
Atmospheric tidal loading	Model by Ray and Ponte [2003]
Atmospheric pressure loading	Model by Petrov and Boy [2004]



**Figure 6.4:** Flow chart of the processing steps to set up the NEQ systems.

Ambiguities are resolved baseline by baseline for GPS as well as for GLONASS. Four strategies are applied depending on the baseline length, up to a maximum of 9000 km for GPS and up to 3000 km for GLONASS. The GPS/GLONASS ISB is realized by the unresolved cross-system ambiguities. More details concerning the features of GLONASS ambiguity resolution are provided in [Schaer *et al.*, 2009].

Finally, the full NEQ systems are set up. The most important options are listed in Tab. 6.3. Three solutions are generated in parallel, namely the GPS-only, the GLONASS-only, and the GPS/GLONASS combined solution CMB. The fourth solution (NEQ) requires no additional computations on the observation level. The GPS- and GLONASS-only solutions have parameters in common (e. g., coordinates) but are otherwise completely decorrelated by the epoch-wise ISBs. The two solutions may therefore be combined on the NEQ level to yield the NEQ solution.

The resulting NEQ systems are stored. Size-reduced NEQs are created as well, by pre-eliminating all orbit and troposphere parameters. These smaller NEQs allow it to very efficiently generate multi-year combinations.

### Multi-year solutions

Cumulative 3-year solutions are created following the sequential LSE approach as outlined in Sect. 3.5.2. The computations are based on the session-specific size-reduced NEQs from the previous step.

The coordinate time series from a preliminary combination are analyzed with the BSW program FODITS [Ostini *et al.*, 2008] to identify outliers and discontinuities. The list of detected events is taken into account for the following solutions. Four different solutions are generated:

1. The main solution to generate station coordinates, velocities, and coordinate time series, i. e., session-specific coordinate residuals w. r. t. the combined solution. The geodetic datum is defined by imposing 3 no-net translation and 3 no-net rotation conditions on a subset of 35 IGS08 reference stations contained in the network (indicated by an asterisk in Fig. 6.1). The IGS08 coordinates and velocities are used as a priori information.
2. An ERP solution where the 3-year combined coordinates and velocities are introduced as known, and no-net translation and rotation conditions are imposed on all stations. The ERPs are resampled to the particular session length.
3. The same ERP solution as previously described, but the ERPs are resampled to 23 h 56 min 30 s. This resampling was possible only for the GLO, GPS, and LNG session lengths due to the common parameter sampling interval of  $\Delta T = 1 \text{ h } 24 \text{ min } 30 \text{ s}$ .
4. A solution to create a time series of GCCs, again with introduced 3-year coordinates/velocities and 3 no-net translation and 3 no-net rotation conditions on all stations. The GCCs are set up as constant for each individual session, i. e., one set of GCC parameters was estimated per session.

### Final products generation

The session-wise final orbit parameters are based on the full NEQ systems created in the first processing part. The geodetic datum is defined by introducing the 3-year coordinate/velocity results from the previous step and imposing tight constraints on all stations. A very stable and self-consistent datum definition closely related to IGS08 is obtained in that way. The ERPs from the multi-year solution, which are resampled to the session length, are introduced as known.

The GPS/GLONASS solution NEQ is created in this step as well, by stacking the corresponding GPS-only and GLONASS-only NEQ systems.

### SLR residuals

Orbits, which were derived from microwave observation data, do not allow it to assess the true (outer) orbit accuracy, because technique-specific biases (modeling errors) are not

detectable. The orbits may, however, be validated by using observations from a different space geodetic technique—like SLR [Springer, 2000; Flohrer, 2008].

We have computed time series of SLR residual for all 16 orbit solutions. The observations and meteorological data were converted from the SLR normal point format [ILRS, 2004] to the BSW format. Subsequently, the range residuals were derived from the comparison of the SLR ranges with computed ranges based on the orbits derived from microwave observations and on the ITRF08 station coordinates for the SLR observatories.

### 6.3 Summary and Key Figures

An ensemble of  $4 \times 4 = 16$  solutions was generated in our study. The solutions are based on three years of observation data from a global network of 92 GPS/GLONASS tracking stations. The data set was analyzed four times independently, each time with a different processing batch length (Tab. 6.1): two session lengths corresponding precisely to two orbital revolutions of a GPS and GLONASS satellite, respectively, the “classical” 24-hour session length, and one session length not corresponding to either of the two GNSS. Four solutions were generated for each session length (Tab. 6.2): a GPS-only, a GLONASS-only, a GPS/GLONASS solution with one ISB per session, and a GPS/GLONASS solution combined on the NEQ level with epoch-wise ISBs.

A total of 4396 sessions was processed and 17 584 session-specific solutions were generated. Table 6.4 shows the average computation time requirements for different parts of the processing. Creating the NEQ systems for each session was the most time consuming task. The compilation of the final results is a very rapid and efficient process, because it is solely based on NEQ information. The comparatively short runtime of the complete 3-year series could only be achieved by consequently using the parallel processing capabilities of the BSW and the Linux cluster.

Table 6.5 provides statistical information averaged over all solutions. More than 45 satellites have been observed on the average. The lower ambiguity resolution rate for GLONASS (about 50%) as compared to GPS (90%) is a direct result of the applied

**Table 6.4:** Average runtime requirement of the processing parts.

Processing part	Runtime needed for	
	one session	a full 3-year series
NEQ system setup	2 hours	10 days
Multi-year combination	–	1 hour
Final results generation	2 minutes	4 hours
Computation of SLR residuals	30 seconds	1 hour

**Table 6.5:** Averaged processing statistics for one session.

Average number of	GPS	GLONASS	Total
Stations	–	–	75
Satellites	31	16	47
Observations	300 000	145 000	445 000
Parameters	–	–	2500
Ambiguities	4500	2750	7250
Resolved ambiguities	90%	48%	74%

strategies. Due to software restrictions, no attempt was made to resolve GLONASS ambiguities for very long baselines between 3000 km and 9000 km.

## 6.4 Geometry-induced Variations in the Observation Material

Figure 6.5 illustrates the number of observations per satellite and session for each of the four different session lengths. The numbers refer to available observations after preprocessing. The number of observations apparently gets smaller when comparing the panels from top (LNG) to bottom (GLO). This effect is caused by the fact that the single sessions get shorter (from  $^{18}/_{17}$  to  $^{16}/_{17}$  sidereal days). However, the smaller number of observations per session is compensated by the increasing number of processed sessions (1037 LNG sessions as compared to 1166 GLO sessions). The overall number of observations is (almost) the same for all four solutions. The different number of sessions is not visible in Fig. 6.5, as the four graphs have slightly different scales. The massive drop in available observations end of April 2010, was explained by a receiver problem in Sect. 6.2.1.

A change in the network (e. g., if a station stops tracking) causes an overall variation in the number of observations affecting all satellites in a similar way. These network changes are visible in Fig. 6.5 as a pattern of vertical lines affecting all satellites. Apart from these “color changes” caused by stations, the observation graphic shows GNSS-specific periodic variations.

Figure 6.6 shows the number of observations per satellite relative to the mean number of observations per satellite and per session in percent, i. e., the performance of the single satellites relative to the mean performance. This rescaling suppresses the variations caused by the network changes and accentuates the periodic variations. Variations which affect all satellites (vertical lines) indicate phases where the number of weakly observed satellites varies. The GPS satellites show variations especially in the LNG and GLO sessions, the GLONASS satellites in the LNG, GPS, and DAY sessions.

Figures 6.7a and 6.7b show the stacked (i. e., averaged over all satellites) amplitude spectra of the available observations for GPS and GLONASS and confirm the presence of periodic

6.4 Geometry-induced Variations in the Observation Material

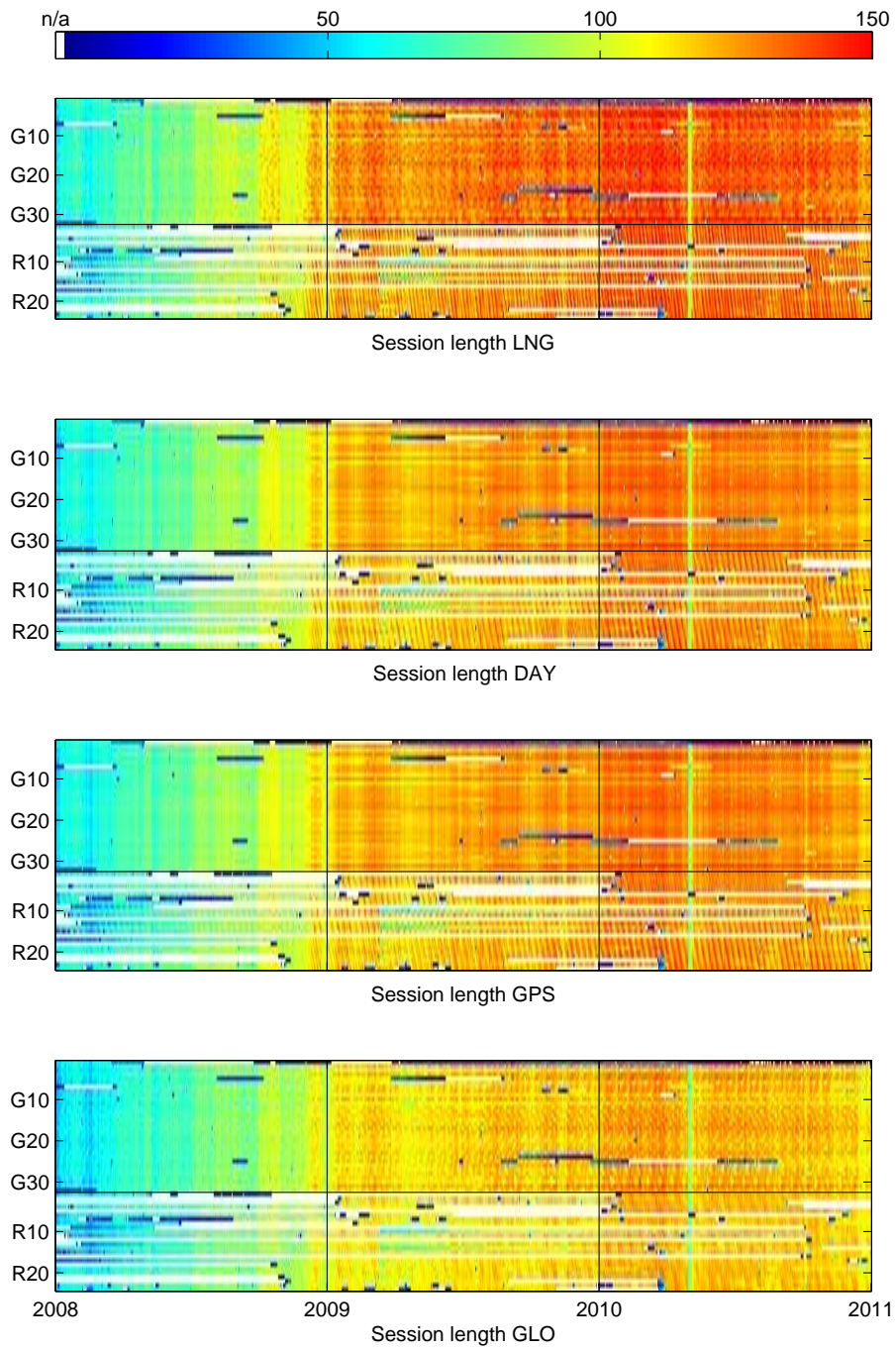
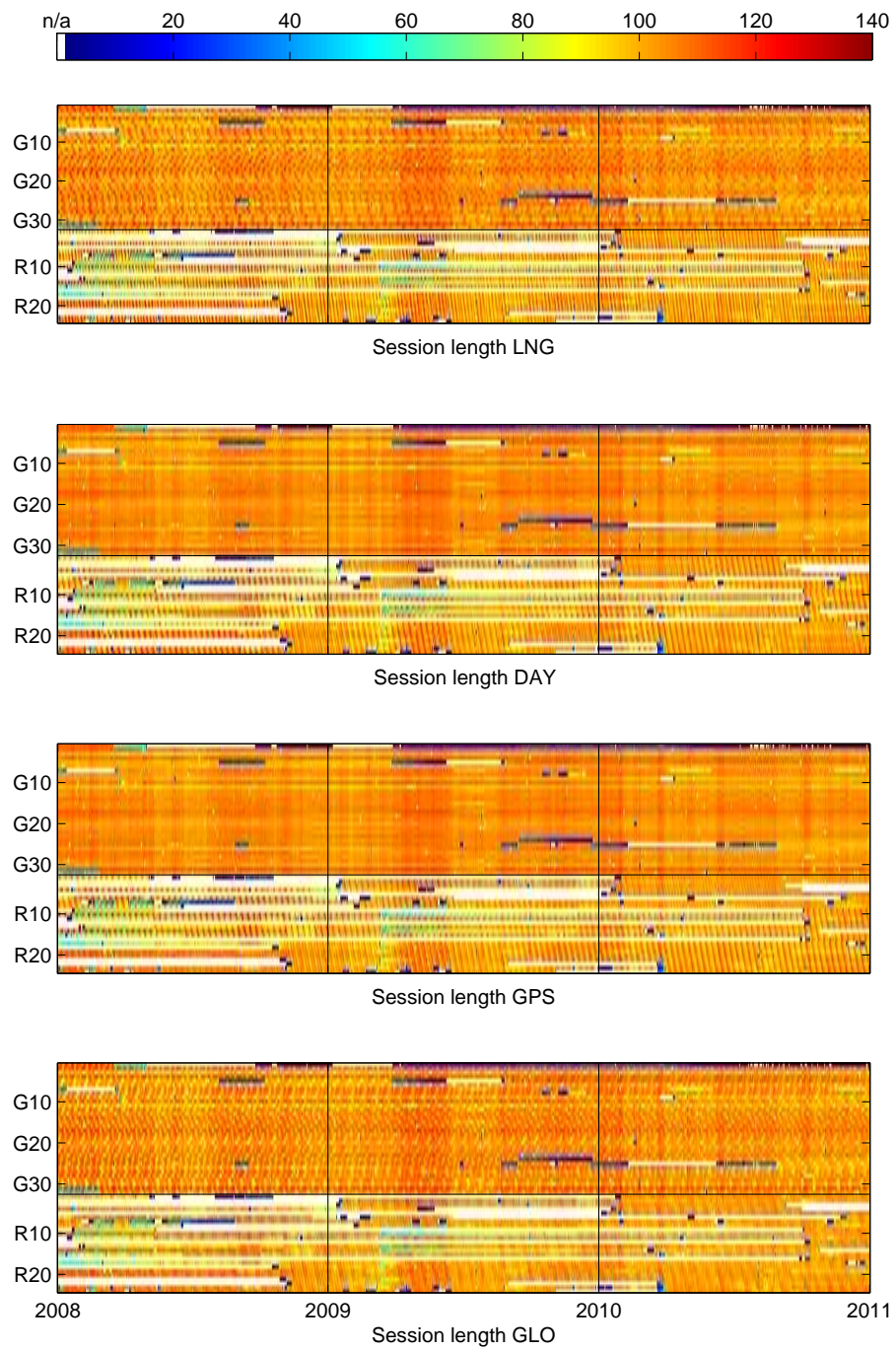
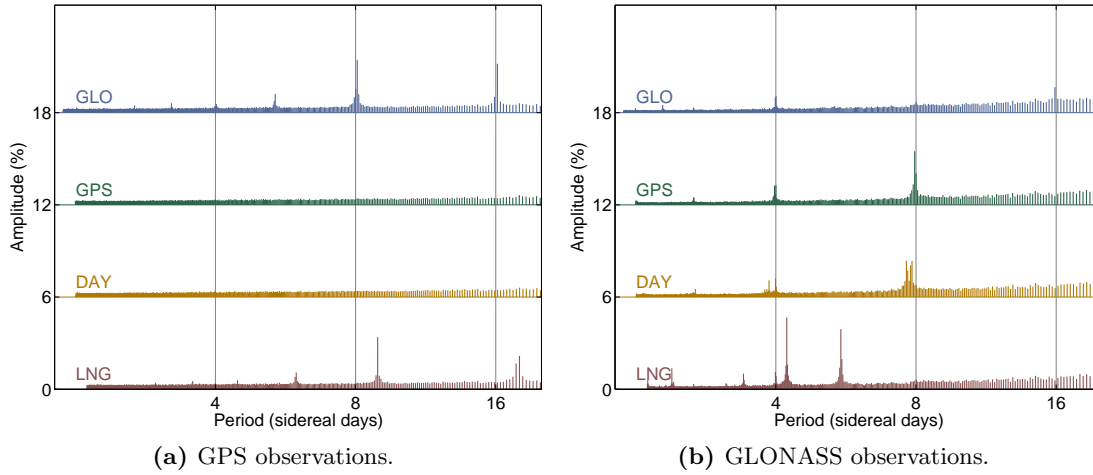


Figure 6.5: Number of observations per satellite (in units of 1000).



**Figure 6.6:** Number of observations per satellite relative to the mean number of observations per satellite (in percent).



**Figure 6.7:** Stacked amplitude spectra of available observations in percent (relative to the mean number of observations per satellite).

**Table 6.6:** Main periods of the variations in the processed observation data.

ID	Session length	Periods (in $d_*$ )	
		GPS	GLONASS
LNG	18/17 $d_*$	18, 9	5.5, 4.2
DAY	one synodic day	–	7.8 7.6
GPS	17/17 $d_*$	–	8
GLO	16/17 $d_*$	16, 8	–

variations. Table 6.6 summarizes the most important periods. No pronounced variations are visible for either GNSS in the respective GNSS-specific session, neither for GPS in the GPS and DAY sessions nor for GLONASS in the GLO session. This behavior was expected, because the satellite constellation repeats after every session. The orientation of the Earth is not necessarily the same at the beginning of each session but this has almost no effect if the stations are well distributed in longitude.

The prominent periods for GPS in the LNG session are 18 and 9 sidereal days. The periods for the GLO sessions are 16 and 8 sidereal days. These periods correspond to the sampling of the orbital revolution period of a GPS satellite with the corresponding session length. This sampling of the orbital period with the session length would in principle also lead to periodic variations for the DAY session. The period would, however, be about 350 days and cannot be seen in Fig. 6.7a.

The sampling of the orbital revolution period of a GLONASS satellite with the respective session length yields the periods for the GPS and DAY sessions and the peak at 4.2 sidereal

days in the LNG session. The remaining peak at 5.5 sidereal days cannot be explained by a simple sampling of the revolution periods.

The amplitude spectra in Fig. 6.7 show that the decision on a particular processing session length may introduce periodic variations in the number of available observations per session. The variations are in the range of about 3% to 5% w. r. t. the mean number of observations per satellite or about 1500 observations peak-to-peak in absolute numbers. The periods are purely geometric in nature and may appear in the final results, as well.

# 7 Results and Discussion

## 7.1 Station Coordinates

### 7.1.1 Assessment of Coordinate Time Series

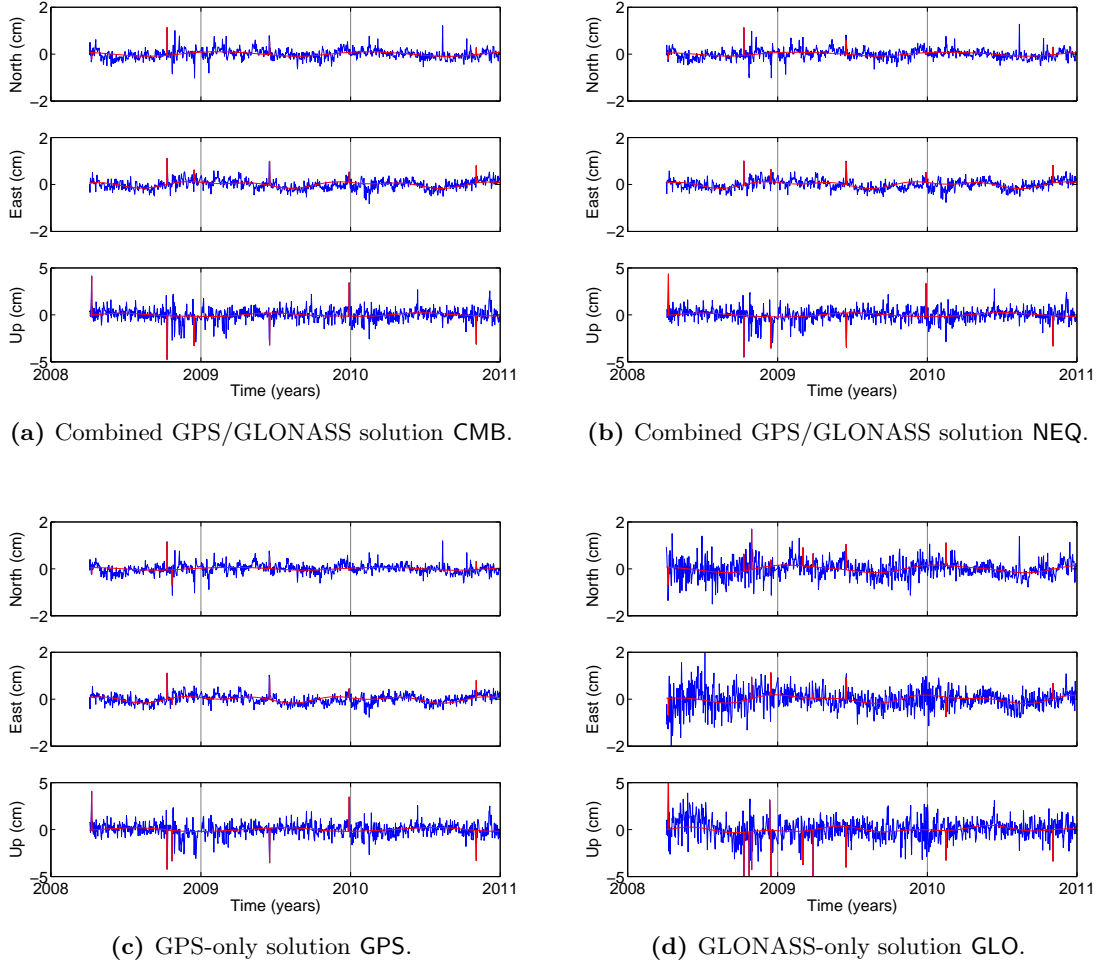
Station coordinates and velocities are computed individually for each of the 16 solutions based on a multi-year combination of NEQ systems. The time series of coordinate residuals are generated by comparing session-specific coordinates with the combined 3-year solution. These series of residuals are screened for outliers and discontinuities. The BSW program FODITS is used for this task in a fully automated way. The program represents the time series of coordinates by a functional model, which contains parameters for discontinuities, outliers, velocity changes, and periodic functions. Parameters are added to the functional model step-by-step until further elements do not significantly improve the representation of the time series anymore [Ostini *et al.*, 2008].

Table 7.1 shows the number of detected outliers and discontinuities for the 16 solutions. The two combined solutions and the GPS-only solution show comparable numbers of detected events. An inspection of the corresponding time series confirms that the same problems were identified. An example of a coordinate time series is given in Fig. 7.1. The panels show the coordinate residuals (in blue) for all four solutions for the 24-hour session for the station Funchal, Portugal. The functional model determined by the screening program FODITS is shown in red color. The spikes indicate detected outliers.

Comparing the three solutions CMB, NEQ, and GPS (Figs. 7.1a to 7.1c) shows that the same events have been detected for the three solutions. The GLONASS-only solution GLO (Fig. 7.1d) shows a significantly higher noise than the other three solutions. This is

**Table 7.1:** Total number of detected events in the coordinate time series.

Session	Number of discontinuities				Number of outliers			
	CMB	NEQ	GPS	GLO	CMB	NEQ	GPS	GLO
LNG	7	8	6	21	154	163	161	352
DAY	7	7	10	23	184	187	187	356
GPS	7	7	15	31	175	180	174	377
GLO	7	7	6	23	192	203	212	391



**Figure 7.1:** Time series of coordinates (blue) for station Funchal, Portugal, and FODITS model (red) for all four solutions (session length DAY).

mainly caused by the smaller number of GLONASS satellites and, as a consequence, by a smaller number of observations. Other reasons are a less stable satellite tracking and the smaller number of successfully resolved phase ambiguities (about 50% as compared to 90% for GPS) affecting in particular the East component. The noise gets smaller in the course of the three years thanks to the increasing number of GLONASS satellites and stations.

The higher number of detected outliers (Tab. 7.1) for the GLONASS-only solutions is mainly caused by the larger noise of the residuals. It would be advisable to increase the outlier detection threshold (as a function of the noise) for the GLO session length, although an average of 6 removed outliers per station in a 3-year time series does not pose a problem.

The number of detected outliers decreases with increasing processing batch length. The factor of improvement agrees quite well with a theoretical factor obtained from the square-root-law applied to the number of available observations. However, as soon as GPS is involved, the GPS session length gives significantly fewer outliers than the DAY session length although both differ only by 4 minutes. This behavior indicates that station-specific unmodeled effects, like multipath, are mitigated if the station–satellite geometry repeats strictly every session.

### 7.1.2 Coordinate Consistency

The 16 sets of 3-year coordinates can be compared by applying a Helmert transformation between them. The resulting root mean square (RMS) error is an indicator of the coordinate consistency. A 6-parameter Helmert transformation, allowing for 3 translations and 3 rotations, was used to compare all solutions for each particular session length. The transformation parameters were estimated based on all stations but outliers were removed to prevent single stations from biasing the results. A total of 11 outliers were detected in the 24 comparisons with a maximum of 3 outliers in the GPS/GLO comparison for session length GPS. All estimated translations and rotation angles are close to zero and may be neglected.

The overall RMS errors of the Helmert transformations between the different solutions for each session length are listed in Tab. 7.2. The two combined solutions CMB and NEQ are most consistent for each session length (sub-millimeter overall consistency).

Comparing the two combined solutions with the GPS-only solution shows that the NEQ-level combinations (i. e., the solution where epoch-wise ISBs were estimated) are more consistent with the GPS-only solutions (more “GPS-like”) than the CMB solutions. On the other hand, the CMB solutions are closer to GLONASS-only than the NEQ solutions. The influence of the GLONASS observations on the results is stronger, if one constant ISB is estimated per session.

**Table 7.2:** RMS errors of Helmert transformations between different solutions.

Sol 1	Sol 2	Session length			
		LNG	DAY	GPS	GLO
CMB	NEQ	0.38	0.42	0.38	0.46
CMB	GPS	1.40	1.38	1.32	1.45
CMB	GLO	2.61	2.61	2.81	2.47
NEQ	GPS	1.25	1.14	1.18	1.18
NEQ	GLO	2.78	2.87	2.98	2.60
GPS	GLO	3.37	3.42	3.37	3.31

The least consistent results are obtained by the GPS-only and GLONASS-only solutions as they are completely independent solutions based on different observations. They still agree on the level of a few millimeters, however.

### 7.1.3 Coordinate Repeatabilities

The coordinate repeatability is a good indicator for the quality of a coordinate solution. The repeatability is computed as the overall RMS error of all coordinate residuals of a particular station w. r. t. the 3-year solution.

Table 7.3 lists the median repeatabilities in North-, East-, and Up-direction, and the overall repeatability for each particular session. The best results for each session length are obtained with the combined GPS/GLONASS solutions CMB and NEQ. The GLONASS-only solution shows the highest values in all cases. This is not surprising as the noise of the GLONASS coordinate time series is significantly larger than that achieved with the other solutions (Fig. 7.1d). The quality of the GPS-only solution is significantly better than that of the GLONASS-only solution, but not as good as that for the combined GPS/GLONASS solutions.

The expected improvements of the coordinate repeatability may be estimated by applying the square-root-law to the number of observations used for a particular solution. Table 7.4 lists the mean achieved factors (computed from the average of the total repeatabilities of all session lengths) and the expected factors in percent. These two types of factors agree quite well, although the actual improvement is always better than expected, if GLONASS is involved. The reason for this behavior is not known. The corresponding factors for the ambiguity float solutions, however, prove that the different percentage of

**Table 7.3:** Median of station repeatabilities in North-, East-, Up-direction, and total (in mm).

Solution	Session LNG				Session DAY			
	N	E	U	Total	N	E	U	Total
CMB	2.2	2.1	5.4	3.6	2.1	2.1	5.6	3.6
NEQ	2.1	2.1	5.5	3.7	2.1	2.1	5.6	3.6
GPS	2.2	2.1	5.7	3.9	2.2	2.2	5.8	4.0
GLO	4.5	5.4	9.9	7.1	4.6	5.7	9.7	7.3
Solution	Session GPS				Session GLO			
	N	E	U	Total	N	E	U	Total
CMB	2.1	2.1	5.6	3.7	2.2	2.1	5.6	3.7
NEQ	2.1	2.1	5.6	3.7	2.2	2.1	5.6	3.8
GPS	2.2	2.2	5.8	3.9	2.3	2.1	6.0	4.0
GLO	4.7	5.5	10.2	7.5	4.8	5.7	10.6	7.7

**Table 7.4:** Mean observed and expected improvement of coordinate repeatability.

	CMB/GPS	CMB/GLO	GPS/GLO
Observed	10%	100%	80%
Expected	25%	80%	45%

successfully resolved ambiguities of the GPS and GLONASS solutions is not responsible for this discrepancy.

#### 7.1.4 Periodic Variations in the Coordinate Residuals

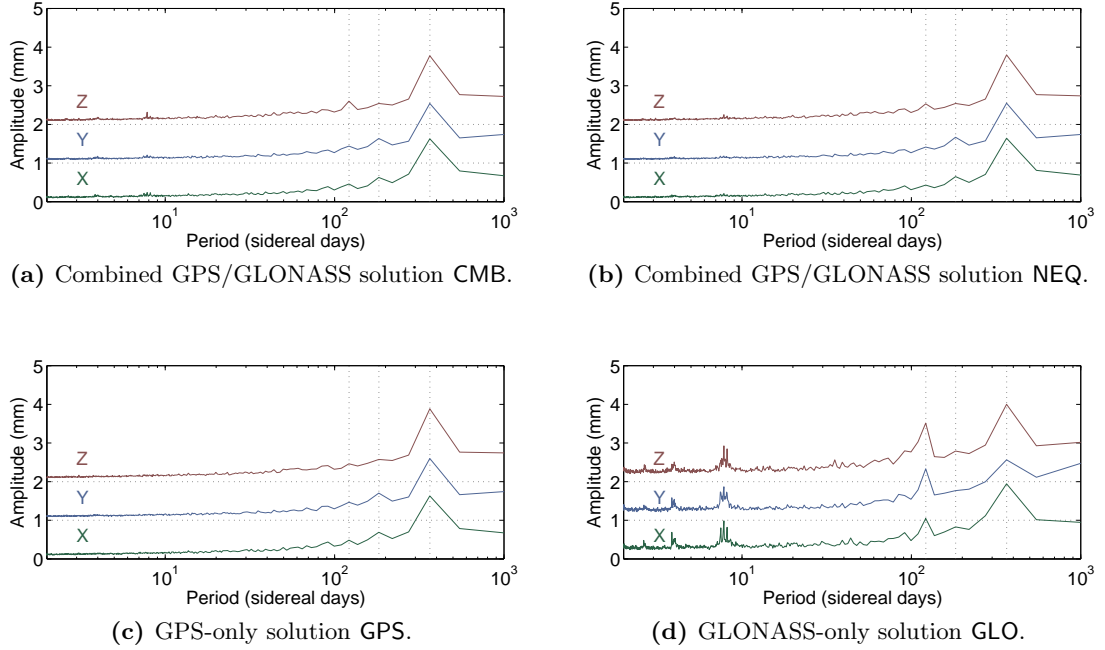
Let us now inspect the time series for periodic variations in the coordinate residuals. Amplitude spectra were computed for all 16 coordinate time series. The spectra of all stations for each particular solution are averaged to obtain mean (or stacked) spectra. These mean spectra mainly show the periods affecting the complete network in a similar way. Station-specific periods are minimized. The spectra are computed in geocentric equatorial Cartesian coordinates.

Figure 7.2 shows the spectra for all solutions for the session length DAY. The vertical lines mark the annual period and the second and third harmonic thereof. The single spectra are shifted (by 1 mm) for display purposes. The spectra look very much alike for all different session lengths, so we only discuss the daily solutions DAY.

All spectra show a dominating annual signal. The presence of an annual signal in GNSS-derived coordinate time series is well known [Dong *et al.*, 2002]. Whether the signal is truly annual or has the period of the draconitic GPS or GLONASS year (as listed in Tab. 2.2) cannot be decided with a data set of only three years.

The GPS-only solution does not show any significant periods apart from the annual signal (Fig. 7.2c). The GLONASS-only solution (Fig. 7.2d) on the other hand, shows significant peaks, namely around 120 days, 8.2 days, 7.8 days, and 7.6 days. The same peaks appear in all solutions independently of the session length. This kind of periodic signals is therefore not caused by aliasing effects due to the session length. The resolution of the time series is not good enough to decide whether the 120 day period is a third of a tropical year (365.25 days) or of a draconitic GLONASS-year (353.2 days).

The three periods around 7.8 days are probably associated with the repeat periods of the station–satellite geometry, the basic GLONASS ground track repeat cycle being 8 sidereal days (7.98 days). The period of  $1/3$  year might be associated with the three orbital planes of GLONASS. The GLONASS-specific periods almost completely vanish for the two combined solutions as shown in Figs. 7.2a and 7.2b.



**Figure 7.2:** Stacked amplitude spectra of coordinate residuals for session length DAY (the vertical lines mark the periods of 1, 1/2, and 1/3 year).

## 7.2 Orbits and Geocenter

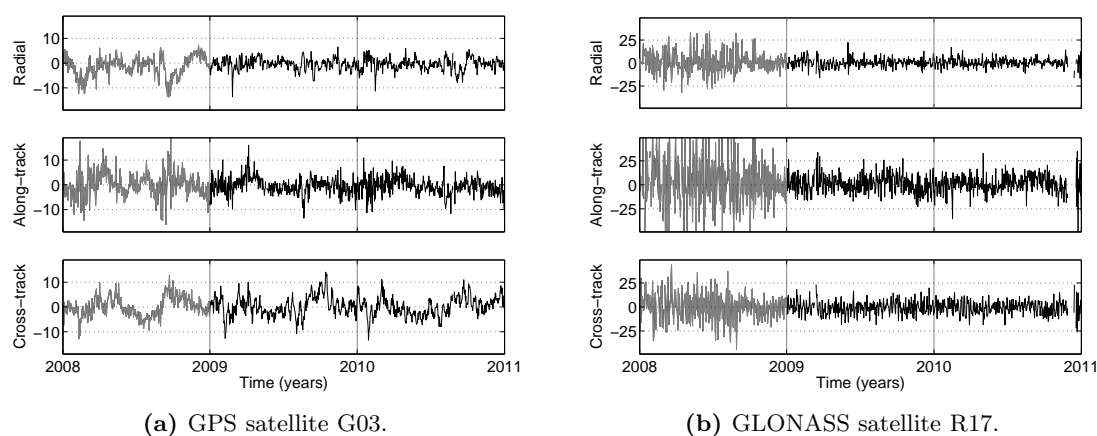
A total of 32 GPS and 24 GLONASS satellites have been observed during the three years of our study. The results presented in this section are, however, based on a subset of the available satellites. Satellites were not considered if they were only observed during a small portion of the three years or if they were repositioned in the constellation. This “screening” was necessary in order to obtain reliable and representative results. Table 7.5 lists the accepted satellites, the corresponding orbital planes, and the maximum elevation angle  $\beta_0$  of the Sun above each orbital plane.

The position difference at session boundaries computed from two subsequent orbits, i. e., the difference  $\mathbf{r}_i(t) - \mathbf{r}_{i+1}(t)$  for two subsequent sessions  $i$  and  $i+1$  at session boundary  $t$ , is a good measure for the quality of the estimated orbits. These orbit overlap differences may either be projected in the satellites’ radial, along-track, and cross-track directions, or the absolute value of the overlap difference may be used (3-D position overlap).

Figure 7.3 shows the orbit overlap differences in the radial, along-track, and cross-track directions for a GPS satellite (G03) and a GLONASS satellite (R17). The differences are taken from the single-system solutions of the 24-hour session. The overlap differences of these two satellites are representative for all solution types. In the case of GLONASS, the differences are rather large at the beginning of the study and successively decrease

**Table 7.5:** Used satellites, planes, and maximum elevation  $\beta_0$  of the Sun above the orbital plane.

GPS						GLONASS								
Plane	$\beta_0$	Satellites				Plane	$\beta_0$	Satellites						
A	45°	8	9	27	31	1	67°	2	7	8				
B	67°	12	16	28	30	2	55°	10	11	13	14	15		
C	77°	3	6	17	19	3	88°	17	18	19	20	21	23	24
D	75°	2	4	11	21									
E	61°	10	18	20	22									
F	40°	13	14	15	23									

**Figure 7.3:** Orbit overlap differences in radial, along-track, and cross-track directions (in cm).

during 2008 until they reach a stable level. This behavior is caused by the small numbers of GLONASS satellites and tracking stations in 2008. The first year of orbit overlap differences is therefore not used for the computations (mean values, standard deviations) in the following section. The neglected time interval is marked in gray in Fig. 7.3. Outliers were removed from the time series.

### 7.2.1 Overlap Differences at Session Boundaries

Table 7.6 lists the mean 3-D position overlap differences for all solutions. The values are computed separately for GPS and GLONASS satellites. The combined GPS/GLONASS solution CMB is clearly the best one (showing the smallest mean differences) for all session lengths, followed by the combination with epoch-wise ISBs, and the single-system solutions. Comparing the combined to the single-system solutions, the improvement is about 5% for GPS satellites and about 30% for GLONASS satellites. The improvements for GPS, as well as for GLONASS, are in the limits of the expected factors (derived from the square-root-law) listed in Tab. 7.4. Although GLONASS gains significantly more, the

**Table 7.6:** Mean orbit 3-D position overlap difference (in cm).

Session	GPS satellites			GLONASS satellites		
	CMB	NEQ	GPS	CMB	NEQ	GLO
LNG	5.2	5.3	5.5	8.7	10.2	10.9
DAY	5.4	5.5	5.6	8.8	10.6	11.6
GPS	5.2	5.3	5.5	8.9	10.7	11.6
GLO	5.3	5.4	5.6	9.3	11.3	12.2

satellite orbits of both systems benefit from a combined analysis. It is interesting to note that the best GPS-derived station coordinates were achieved not in the CMB solution, but in the NEQ solution (compare Tab. 7.3).

Tables 7.7 and 7.8 list the standard deviations of the orbit overlap differences projected onto the satellites' radial, along-track, and cross-track directions for GPS and GLONASS. For both GNSS, the along-track direction shows the biggest differences, followed by the cross-track and radial components. Note that the cross-track component of the overlap differences profits the most from a combination in the case of GPS: about 8% as compared to 5% and 3% for the radial and along-track component, respectively. The improvements in the case of GLONASS are about the same (25% to 30%) for all three components.

The transition from the shortest to the longest session length improves the 3-D position differences (Tab. 7.6) in the case of GLONASS: the shortest session yields the largest overlap differences; the GPS and DAY session lengths—differing only by about 4 minutes—give the same results; and the long session LNG gives the best results. The improvements are about 5% from solution to solution. This is in good agreement with the theoretically expected improvements. The square-root-law applied to the difference in session lengths suggests an improvement of about 3%. The mean 3-D position overlap differences of the GPS satellites do, however, not show a clear dependence on the session length.

Inspecting the single components of the differences for GPS (Tab. 7.7) and GLONASS (Tab. 7.8) shows that the radial component profits significantly more from longer sessions than the other two components. The along-track component is about the same for all session lengths with the exception of the longest session: session length LNG yields the largest along-track differences for GPS but the smallest for GLONASS. The differences of the cross-track components profit from longer sessions only in the case of GLONASS.

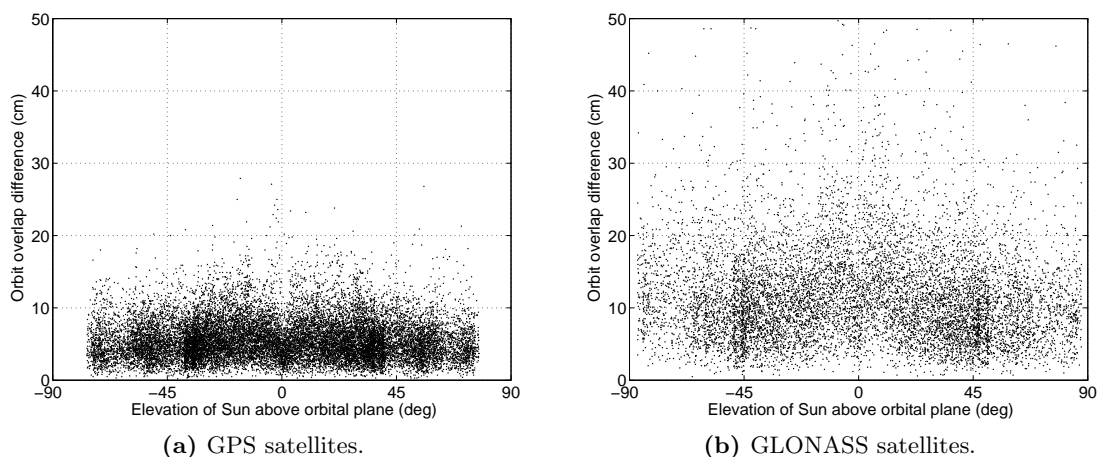
Figure 7.4 shows the 3-D position overlap differences as a function of the elevation angle  $\beta_0$  of the Sun above the orbital planes. The displayed differences are obtained from the single-system solutions computed with the 24-hour session length (the other solutions are very similar). The overlap differences for GLONASS are about a factor of 2 larger than the differences for the GPS (compare also Tab. 7.6). The overlap differences do not show a strong dependency on the angle  $\beta_0$ .

**Table 7.7:** Standard deviations of orbit overlap differences for GPS (in cm).

Session	Radial			Along-track			Cross-track		
	CMB	NEQ	GPS	CMB	NEQ	GPS	CMB	NEQ	GPS
LNG	2.1	2.2	2.2	4.3	4.4	4.4	3.4	3.5	3.7
DAY	2.8	2.9	2.9	3.9	4.0	4.1	3.6	3.7	3.9
GPS	2.8	2.9	3.0	4.0	4.0	4.1	3.3	3.4	3.6
GLO	3.2	3.2	3.3	4.0	4.0	4.1	3.2	3.3	3.4

**Table 7.8:** Standard deviations of orbit overlap differences for GLONASS (in cm).

Session	Radial			Along-track			Cross-track		
	CMB	NEQ	GLO	CMB	NEQ	GLO	CMB	NEQ	GLO
LNG	3.4	4.0	4.3	7.8	9.2	9.9	5.5	6.5	6.8
DAY	3.8	4.4	4.7	8.0	9.5	10.5	5.6	6.7	7.3
GPS	3.9	4.6	4.9	8.1	9.7	10.7	5.6	6.7	7.0
GLO	4.8	5.8	6.1	8.0	9.4	10.5	5.7	6.8	7.2

**Figure 7.4:** 3-D position overlap differences w. r. t. the elevation  $\beta_0$  of the Sun above the orbital plane (based on single-system solutions, session length DAY).

## 7.2.2 Periodic Variations in the Overlap Differences

Figure 7.5 shows the stacked amplitude spectra of the GPS-only and GLONASS-only 3-D position orbit overlap differences for all four session lengths (the single spectra are shifted by 1.5 cm). The spectra for the two combined solutions CMB and NEQ are similar and included in Appendix B (Fig. B.1).

The maximum amplitudes in the the GPS spectra (Fig. 7.5a) are about 5 mm and in general at least a factor of 2 smaller than the GLONASS amplitudes (Fig. 7.5b). All four GPS solutions show a period of about half a year. The periods of 18, 9, and 4.5 sidereal days in the LNG session correspond to the basic repeat cycle (and harmonics thereof) of the station–satellite geometry: after 17 LNG sessions, i. e., after 18 sidereal days, a GPS satellite has completed exactly 36 full revolutions. The geometry exactly repeats after 17 sessions. In the case of the GLO session length, the geometry also repeats after 17 sessions corresponding to 16 sidereal days. This period, together with its harmonics, appears in the spectrum for the GLO session length. These periods were already mentioned in Sect. 6.4 and listed in Tab. 6.6. The spectra for the DAY and the GPS session lengths look similar, but the GPS spectrum is the cleanest one.

The amplitudes in the GLONASS spectra (Fig. 7.5b) are of the size of 1 cm. All four session lengths show at least one pronounced peak. There is no completely flat spectrum as in the case of GPS. The sampling of the orbital revolution period of a GLONASS satellite with the corresponding session length yields exactly the periods from the LNG, DAY, and GPS session lengths. These periods are listed in Tab. 6.6. The 16 day peak in the GLO session reflects the repetition of the station–satellite geometry: a GLONASS satellite completes 34 full revolutions in 17 GLO sessions, i. e., in 16 sidereal days. With the exception of the 16 day period in the GLONASS spectrum of session length GLO, all periods already appeared in the spectra of the number of available observations in Sect. 6.4.

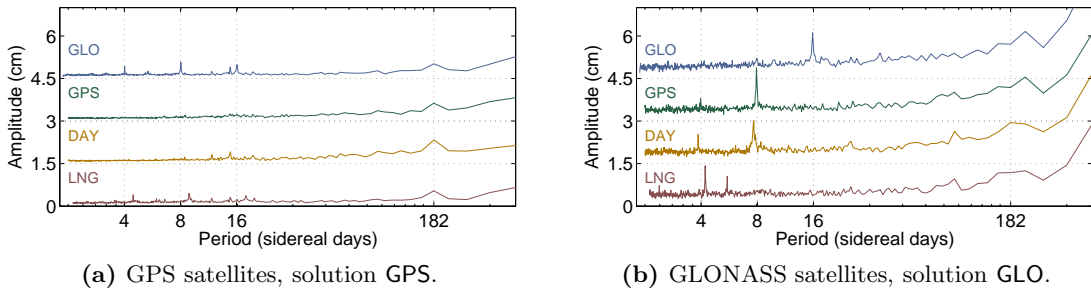


**Figure 7.5:** Stacked amplitude spectra of 3-D position overlap differences for all four session lengths (single-system solutions).

### 7.2.3 Geocenter Coordinates

The geocenter is the center of mass of the Earth. It is the origin of the natural reference frame the equations of motions (2.3) for Earth orbiting satellites refer to. The geocenter coordinates (GCCs) define the offset of the geocenter w. r. t. the point of origin of the reference stations. The geocenter varies w. r. t. the Earth's crust due to mass redistributions in (and on) the Earth [Dong *et al.*, 1999].

The results computed in our study all refer to solutions, where the geocenter coordinates were assumed to be zero, i. e., where the center of mass was assumed to coincide with the center of figure. We computed a full set of solutions with estimated geocenter coordinates, however, to study the impact of the different solution types on the GCC estimates. The results are very much the same for all session lengths, which is why we discuss the results for the 24-hour session, only.

Figure 7.6 shows the estimated GCCs and the elevation angle  $\beta_0$  of the Sun above the orbital planes (six for GPS and three for GLONASS). The GCCs derived from GPS-only solutions (Fig. 7.6a) vary in the range of a few centimeters. The X- and Y-components show a clear seasonal (annual and semi-annual) signal. This is confirmed by the corresponding amplitude spectra in Fig. 7.7a. Apart from the seasonal signal, however, the spectra for these two components are very clean. The Z-component does not show a clear seasonal variation. Inspecting the corresponding spectrum, however, reveals several pronounced periods. The largest spectral lines correspond to a semi-annual signal and to odd harmonics of a year, namely to  $1/3$ ,  $1/5$ , and  $1/7$  years. Our time series are not long enough to precisely determine the periods. These particular periods in the GPS GCC time series were also detected by Flohrer [2008]. The origin of these spectral lines is unknown.

The GCC time series derived from GLONASS solutions (Fig. 7.6b) show a different behavior. The X- and Y-components are of the size of several centimeters. Apart from a seasonal signal in the X-component, the X- and Y-component both show a spectral line at about 8 sidereal days. This line was already detected in the spectra of GLONASS-only coordinate time series (Fig. 7.2d) and is probably caused by the repeat cycle of the station–satellite geometry. The Z-component of the GLONASS geocenter shows large variations with a peak-to-peak size of about 30 cm. In addition, the variations show a striking correlation with the angles  $\beta_0$  w. r. t. the three orbital planes. The corresponding spectral line in Fig. 7.7b lies at  $1/3$  GLONASS year with an amplitude of 9 cm. This variation has nothing to do with a mass redistributions in the Earth's body. In addition to this dominating spectral line, the spectrum shows, similar to GPS, pronounced peaks at odd harmonics of the draconitic GLONASS year, namely at  $1/5$ ,  $1/7$ , and  $1/13$  GLONASS years.

The reason for these large variations in Z-direction of the GLONASS-derived geocenter coordinates is not yet understood. The clear relation to the elevation of the Sun above the orbital planes implies a correlation with the orbital parameters, in particular with

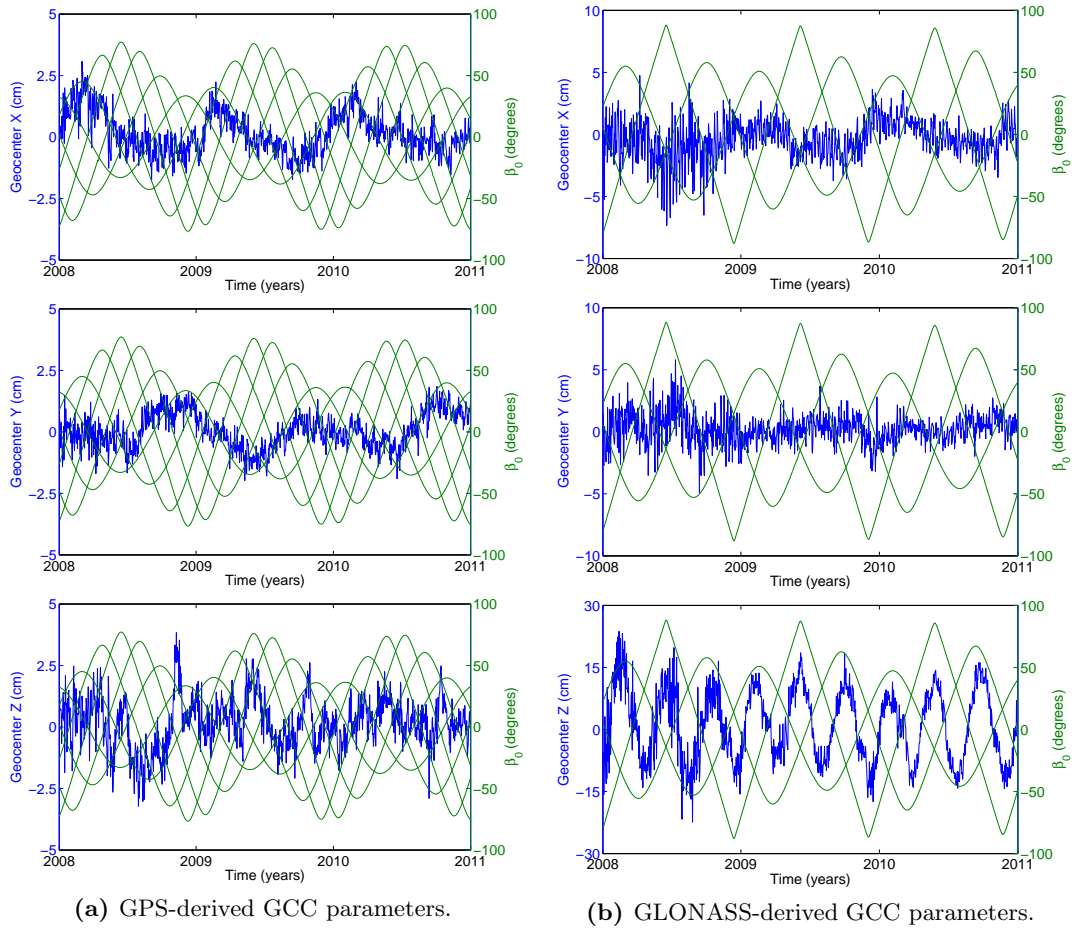


**Figure 7.6:** Geocenter coordinates derived from GPS and GLONASS observations and elevation  $\beta_0$  of the Sun above the orbital planes (session length DAY).

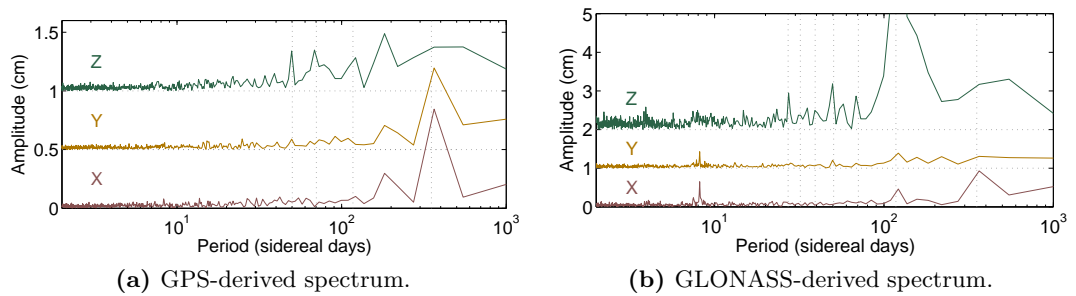


**Figure 7.7:** Amplitude spectra of GCC parameters for session length DAY (the vertical lines mark the draconitic GNSS year and the odd harmonics thereof, i.e.,  $1/3$ ,  $1/5$ , ... year).

the parameters of the radiation pressure model. The Earth's rotation decorrelates the X- and Y-components of the geocenter and the orbital parameters. No large variations and no dependency on the angle  $\beta_0$  is visible for these components. In contrast, the GCC Z-component is not decorrelated as the Earth rotates approximately around the Z-axis.

Studies of the error characteristics of the estimated orbital parameters did not show a clear correlation between orbital and GCC parameters (Sect. 7.2.4). A test solution revealed, however, that the deletion of the constant and periodic radiation pressure parameters in the satellite-fixed X-direction reduces the geocenter Z-component by a factor of 2. Although the amplitude of the Z-component is still large (about 10 cm) it is remarkable that it can be significantly reduced by changing the setup of the orbital parameters.

The presence of such large variations confirms that no-net translation conditions on the set of reference stations are mandatory, in particular if orbit parameters are estimated.

#### 7.2.4 Error Characteristics of Orbital Parameters

Each satellite orbit is represented by six osculating elements referring to the initial epoch  $t_0$  of an arc (as introduced in Sect. 2.3.1) and a limited number of empirical dynamical parameters defining the acceleration of a satellite due to the solar radiation pressure. We have applied the extended orbit model [Beutler *et al.*, 1994b]:

$$\mathbf{a}_{\text{rpr}} = \mathbf{a}_{\text{rpr},0} + D(u) \mathbf{e}_D + Y(u) \mathbf{e}_Y + X(u) \mathbf{e}_X \quad (7.1)$$

with

$$\begin{aligned} D(u) &= D_0 + D_c \cos u + D_s \sin u \\ Y(u) &= Y_0 + Y_c \cos u + Y_s \sin u \\ X(u) &= X_0 + X_c \cos u + X_s \sin u, \end{aligned} \quad (7.2)$$

where

- $\mathbf{a}_{\text{rpr}}$  is the acceleration of a satellite due to solar radiation pressure,
- $\mathbf{a}_{\text{rpr},0}$  is the acceleration derived from an a priori model,
- $\mathbf{e}_D$  is the unit vector pointing from the satellite to the Sun,
- $\mathbf{e}_Y$  is the unit vector along the satellite's solar panel axis,
- $\mathbf{e}_X$  is defined by  $\mathbf{e}_D \times \mathbf{e}_Y$ ,
- $u$  is the argument of latitude of the satellite,
- $D_0, Y_0, X_0$  are constant accelerations in the D-, Y-, and X-directions, and
- $D_{c/s}, Y_{c/s}, X_{c/s}$  are periodic (once per revolution) terms in the D-, Y- and X-directions.

The updated empirical CODE solar radiation pressure model [Springer, 2000; Dach et al., 2009] is used as a priori model for GPS satellites launched before November 2006. The a priori model is set to zero for all GLONASS satellites and for the 8 GPS satellites launched later than November 2006. Only the three constant accelerations ( $D_0$ ,  $Y_0$ , and  $X_0$ ) and the two periodic terms in the X-direction ( $X_c$  and  $X_s$ ) were estimated, which results in 11 estimated orbital parameters per satellite and arc.

Figure 7.8 shows the RMS errors of the semi-major axis  $a$  and the five dynamical parameters ( $D_0$ ,  $Y_0$ ,  $X_0$ ,  $X_c$ , and  $X_s$ ) for the GLONASS satellite R20 together with the elevation of the Sun above the orbital planes. The semi-major axis is included as an example of the six Keplerian elements and because  $a$  also defines the mean motion. The figures for the other orbit parameters are included in Appendix B (Fig. B.4). The RMS errors show a strong correlation with the angle  $\beta_0$ . The RMS errors for the GPS satellites show a comparable behavior. The corresponding figures for the GPS satellite G06 are included for reference in Appendix B (Figs. B.5 and B.6).

The correlation of the RMS errors with the angle  $\beta_0$  arises because the unit vectors  $\mathbf{e}_D$ ,  $\mathbf{e}_Y$ , and  $\mathbf{e}_X$  assume a fundamentally different meaning in the orbit reference frame (defined by the radial, along-track, and cross-track directions) depending on the angle  $\beta_0$ :

- Sun almost perpendicular to the orbital plane ( $\beta_0 \approx \pm 90^\circ$ ):  $\mathbf{e}_D$  is perpendicular to the orbital plane and  $\mathbf{e}_Y$  points in along-track direction;
- Sun in orbital plane ( $\beta_0 = 0^\circ$ ):  $\mathbf{e}_D$  lies in the orbital plane;  $\mathbf{e}_Y$  is normal to the orbital plane and changes from the “North pole” of the orbital plane to the “South pole” and vice-versa, when  $\mathbf{r}$  is collinear with  $\mathbf{e}_D$ .

This behavior is a fundamental property of our radiation pressure model. All satellites from a particular plane show a similar magnitude and signature of the RMS errors. The solution type (single-system oder combined) and the session length do not significantly change the error characteristics. The RMS errors are almost the same no matter whether GCCs are estimated or not.

### 7.3 Earth Rotation Parameters

Session-specific Earth rotation parameters (ERPs) are not comparable due to the different session lengths. This is why the polar coordinates  $x_p$ ,  $y_p$ , and the difference UT1-UTC were estimated in the 3-year combination step as piecewise linear, continuous functions and subsequently resampled to one sidereal day. The sampling rate of one sidereal day was selected in order to mitigate the influence of the sub-daily pole model on the resulting time series. The resampling was, however, not possible for the 24-hour session length, which is why the daily session is not included in our comparisons. The differences of the estimated ERPs are studied relative to the IERS C04 pole series [Gambis, 2004].

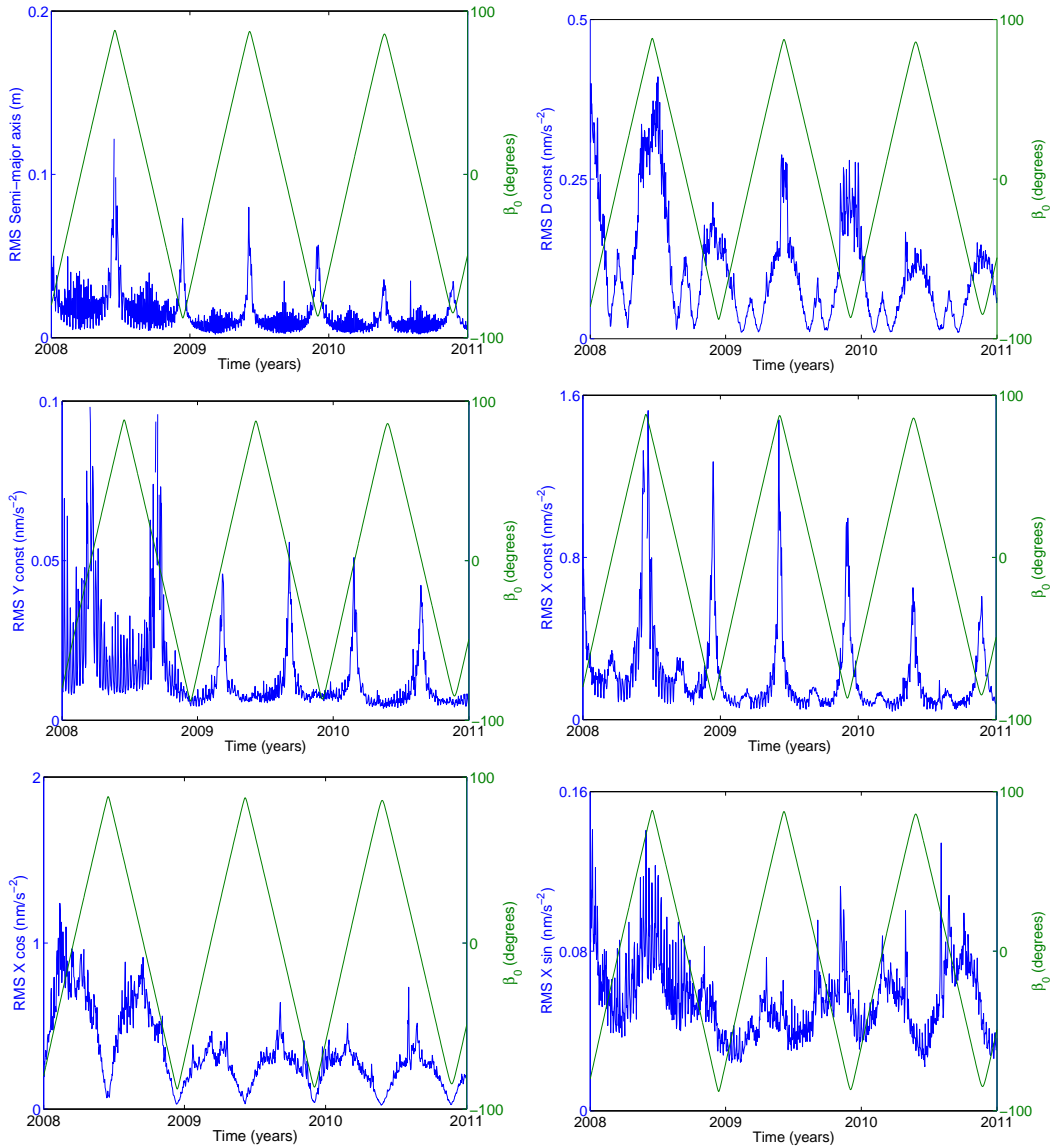


**Figure 7.8:** RMS errors of 6 orbit parameters ( $a$ ,  $D_0$ ,  $Y_0$ ,  $X_0$ ,  $X_c$ ,  $X_s$ ) for GLONASS satellite R20 and elevation  $\beta_0$  of the Sun above the orbital plane (GLONASS-only solution, 24-hour session length).

**Table 7.9:** Mean of X- and Y-pole differences w. r. t. IERS C04 (in  $\mu\text{as}$ ).

Session	X-Pole				Y-Pole			
	CMB	NEQ	GPS	GLO	CMB	NEQ	GPS	GLO
LNG	-44	-44	-47	-79	25	18	14	36
GPS	-49	-50	-51	-66	23	19	6	19
GLO	-49	-48	-48	-75	24	17	10	38

**Table 7.10:** Standard deviations of X- and Y-pole differences w. r. t. IERS C04 (in  $\mu\text{as}$ ).

Session	X-Pole				Y-Pole			
	CMB	NEQ	GPS	GLO	CMB	NEQ	GPS	GLO
LNG	93	92	94	179	87	86	88	186
GPS	99	97	98	189	88	88	89	198
GLO	96	96	98	197	88	87	90	201

Table 7.9 shows the mean values of the ERP differences. Systematic biases of about  $-50 \mu\text{as}$  for  $x_p$  and about  $20 \mu\text{as}$  for  $y_p$  are visible. The  $x_p$  differences obtained from the GLONASS-only solutions are by a factor of about 1.5 higher when compared to all other solutions, the errors in  $y_p$  by about a factor of 2. The  $x_p$  errors for the other solutions do not show a clear dependency on the particular type of the solution. The  $y_p$  errors, on the other hand, show a very systematic behavior w. r. t. the solution type: the values derived from the GPS-only solutions are always the smallest, followed by the values from the two combined solutions. There is no pronounced dependency on the session length. The comparison is problematic, however, because GPS-only solutions were used to establish the IERS C04 series.

The standard deviations of the X- and Y-pole time series are listed in Tab. 7.10. The standard deviations are around  $90 \mu\text{as}$  for the X- as well as for the Y-component (the Y-component being slightly better). The GLONASS-only values are a factor of about 2 larger than all other standard deviations. Apart from that, the solutions do not show a dependency on the solution type or on the session length (although there seems to be a small positive tendency towards the longest session).

Figures 7.9a and 7.9b show the time series of the  $x_p$  and  $y_p$  differences to the IERS C04 series for the session length LNG as an example. The other session lengths give similar results and show the same characteristics. The corresponding figures are provided in Appendix B (Fig. B.7). The UT1-UTC differences, shown in Fig. 7.9c, reveal an interesting behavior. The differences drift away from zero, i. e., the estimate drifts away from the IERS C04 series. This is not surprising, as UT1 is not accessible by GNSS due to the correlations with the orbital parameters  $\Omega$ . Only the first derivative of the difference can be determined reliably. As a consequence, the UT1-UTC estimates must be

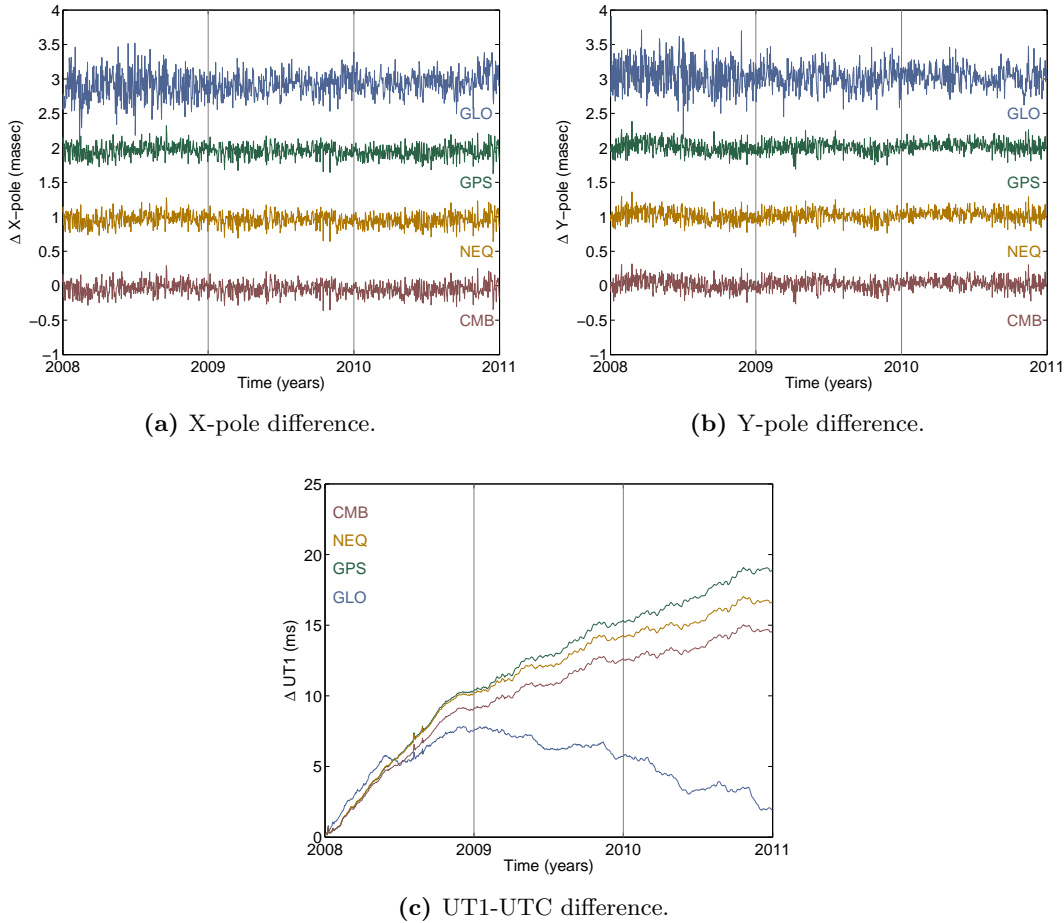


**Figure 7.9:** Difference of ERPs to IERS C04 for all solutions (session length LNG).

constrained to a priori. For our experiments, the first parameter of the 3-year solution was constrained to the IERS C04 value. The drift in the UT1-UTC series derived from GPS observations is well known [Thaller, 2008]. The UT1-UTC series from the GLONASS-only solutions show a different characteristic. The estimates show the same drift values as GPS in the year 2008 and then change direction and slowly return almost to zero during the following two years. This behavior is basically the same for all session lengths (see also Figs. B.7a and B.7b in Appendix B). The different characteristics for GPS and GLONASS UT1-UTC estimates is probably caused by the different a priori models for solar radiation pressure (Sect. 7.2.4).

A spectral analysis of the estimated  $x_p$  and  $y_p$  parameters for all solutions did not show any system-specific periods. All solution-specific spectra are identical to the spectrum of the IERS C04 series.

## 7.4 Orbit Validation with Satellite Laser Ranging

The orbit validation procedure is based on the comparison of SLR range measurements with the computed distances between the observing sites and the satellites using the microwave orbit [Flohner, 2008]. The estimated satellite orbits and the (ITRF08) station coordinates are introduced as known. The differences “observed minus computed” are called range residuals. They are primarily an indicator for the orbit quality in radial direction. Note that the computed differences may contain SLR range biases as no parameters are estimated when the residuals are generated. The mean values of the range residuals may therefore not be interpreted in a meaningful way.

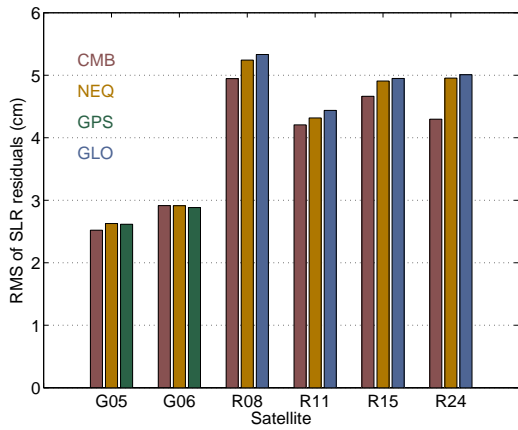
We use SLR observations from station Zimmerwald to the two GPS satellites G05 and G06, which are equipped with reflectors, and to four GLONASS satellites (R08, R11, R15, and R24). Table 7.11 lists the number of SLR measurements for each satellite. Figure 7.10 shows the overall RMS errors of the range residuals for all different solutions. A mean range residual was subtracted before computing the RMS errors in order to eliminate the influence of potential range biases. In general, the GLONASS residuals are about a factor of 1.5 larger than the GPS residuals.

The GLONASS orbits obtained from the combined data analysis are significantly better than the GLONASS-only orbits. The orbits are better if a constant ISB is estimated per session. The improvement in the case of GLONASS is about 10%. The RMS errors related to the GPS satellite G06 do not change significantly for different solutions. In the case of G05, the combined solutions CMB are slightly better than the GPS-only solutions. The improvement ranges between 3% and 7%.

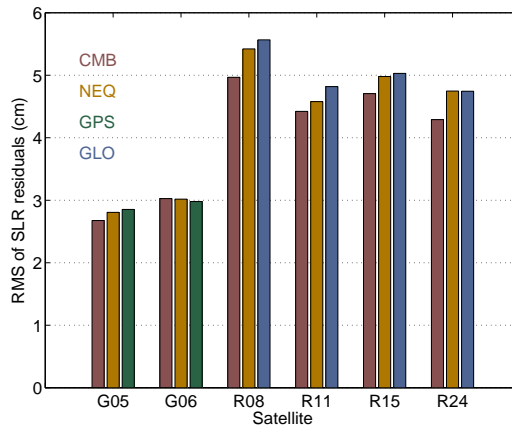
These results confirm that not only the inner accuracy (or consistency) but also the true accuracy of the orbits improves in the combined GPS/GLONASS analysis.

**Table 7.11:** Number of SLR measurements (station Zimmerwald).

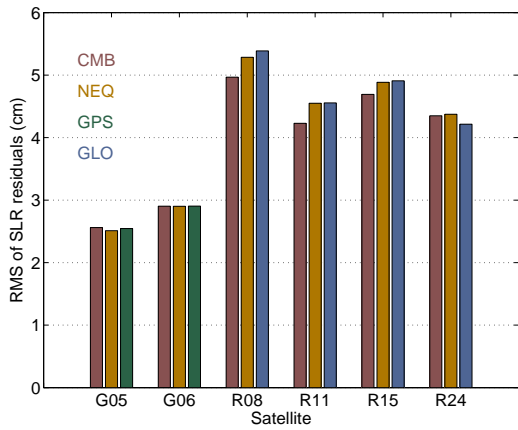
GPS satellites		GLONASS satellites			
G05	G06	R08	R11	R15	R24
1127	1762	3059	3308	3967	1203



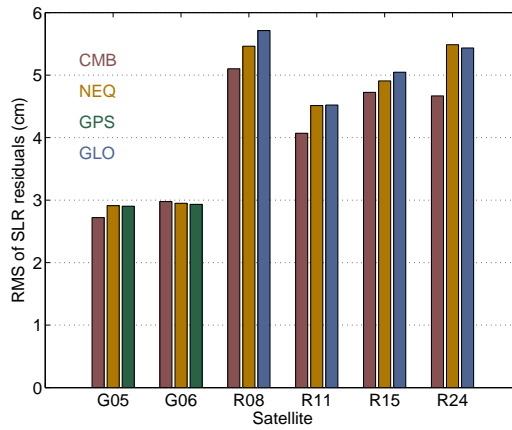
(a) Session length LNG.



(b) Session length DAY.



(c) Session length GPS.



(d) Session length GLO.

**Figure 7.10:** RMS errors of SLR range residuals for 2 GPS satellites (G05, G06) and 4 GLONASS satellites (R08, R11, R15, R24) observed by station Zimmerwald.



## 8 Summary and Conclusions

The combined analysis of observations from different GNSS as well as the development of a full multi-system capable analysis software package stood in the center of this work. Although all GNSS are based on the same navigation principles, they differ in the details of implementation. The individual design of the space segment, the satellite constellation, is of a particular interest. The satellites of a GNSS move around the Earth in (almost) circular orbits in the MEO region and the characteristics of the orbits define the satellite–observer geometry. The time it takes a satellite to reappear at the same spot in the sky for a particular observer is a key aspect. It defines the repeatability of the ground track. A GPS satellite, e. g., repeats its ground track each sidereal day, a GLONASS satellite every eight sidereal days.

The quality of a (high-rate) positioning solution is mainly governed by the number of simultaneously observable satellites and by a good distribution of the satellites in the sky. These two factors are crucial in particular under unfavorable conditions with a restricted horizon visibility. For a mid-latitude station, 6 GPS satellites are visible on the average at the same time above  $25^\circ$  elevation. The average number of visible satellites rises to 16—almost three times as many satellites as in the GPS-only case—as soon as GLONASS and Galileo are added. Not only the satellite number grows but the observation geometry improves significantly in a multi-GNSS scenario. The PDOP, an indicator for the quality of the instantaneous observation geometry, improves by about 40% for a multi-GNSS solution as compared to a single-system solution. The users interested in kinematic positioning will profit considerably from using all available GNSS, especially in regions with a restricted view of the sky.

For scientific purposes, a major benefit results from the additional navigation signals provided by modernized and new GNSS. Innovations in data processing, like new linear combinations of observations, will improve the results. The combination of observations from systems with substantially different (orbit) characteristics will offer the opportunity to identify modeling deficiencies and may help to develop and sophisticate system- or satellite-specific models.

The observation equations get more and more complicated when the characteristics and peculiarities of different systems have to be taken into account correctly. A coherent, easy-to-read formalism is indispensable for that purpose. Our notation, which is based on few simple principles, avoids extensive indexing. It allows us to provide the full equations for undifferenced observations and for all kinds of single-, double-, and triple-differences.

Special attention must be paid to the various types of biases that must be taken into account correctly in a consistent multi-system data analysis.

A single difference bias term appears as soon as observations with different carrier wavelengths are combined. It destroys the integer nature of DD phase ambiguities and makes ambiguity resolution very demanding for FDMA-based systems like GLONASS. Moreover, cross-system ambiguity resolution becomes feasible only if both systems share at least one frequency (and if no large inter-system biases are present). The second type of observation biases is due to signal delays caused by the receiver and satellite hardware. They depend on the characteristics of the measurement, e. g., on the carrier frequency or the code type. Phase and code biases can be estimated on a differential level, distinguishing inter-system, inter-frequency, and inter-code biases. These parameters are of interest, in particular if observations from different GNSS are combined. A correct and consistent treatment of all relevant bias parameters is one of the main challenges in a multi-GNSS data processing.

The combination of different GNSS does not only generate high demands concerning the theoretical background models but also concerning the analysis software packages. The Bernese GPS Software Version 5 is capable of processing dual-frequency data from GPS as well as from GLONASS. In 2005, the AIUB and the BKG initiated a project to implement full multi-GNSS capabilities into the software package. About 50 out of 100 programs, 800 out of 1200 subroutines, 15 file formats, most output files, and the GUI were changed, updated, or recoded in this project. The effort represents about 6 man-years. The next-generation BSW is now truly multi-GNSS capable and well prepared for future developments in the field of GNSS.

After laying out the theoretical foundation and after realizing a multi-GNSS capable software, we conducted a study to investigate: (a) the impact of the session length on GNSS data post-processing and (b) the performance of single-system solutions as compared to multi-GNSS solutions. We analyzed three years (2008–2010) of data from a global network of 92 GPS/GLONASS-capable tracking stations. Several solutions were computed based on four different session lengths, namely two revolutions of a GLONASS satellite ( $16/17$  sidereal days), two revolutions of a GPS satellite ( $17/17$  sidereal days),  $18/17$  sidereal days (favoring neither GPS nor GLONASS), and 24 hours. A GPS-only, a GLONASS-only, and two GPS/GLONASS-combined solutions were generated for each of the four session lengths leading to an overall of 16 different solutions. The two combined solutions differ in the way the GPS/GLONASS inter-system biases are handled: only one constant ISB is estimated per session when combining the systems on the observation level (the ISB is actually realized by the unresolved cross-system ambiguities), whereas one ISB per epoch is estimated when combining the separately established GPS and GLONASS normal equations.

Based on time series of coordinate repeatabilities we found that the combined analysis of GPS and GLONASS observations is always better than the solutions based on only one system. The best results are obtained from the combined GPS/GLONASS solution

---

with one constant ISB. The achieved improvement (about 100% w.r.t. GLONASS-only and 10% w.r.t. GPS-only solutions) is in quite good agreement with the factors expected from the square-root law. The GLONASS-specific periodic variations in the coordinate time series were almost completely suppressed in the combined solutions. The different session lengths have no significant impact on the resulting coordinate time series.

Orbit overlap differences at the session boundaries were used to compare the quality of the estimated satellite orbits. The orbits from the combined analysis were always better than those obtained from single-system analyses. The improvement is about 30% in the case of GLONASS, and 5% in the case of GPS. The best results for GPS were obtained with a session length corresponding precisely to two orbital revolutions of a GPS satellite; the best GLONASS orbit were obtained from the longest session (18/17 sidereal days). The selection of the optimum session length in a multi-GNSS analysis is therefore not trivial. The stacked amplitude spectra of the orbit overlap errors reveal the presence of significant periodic variations ranging between 4 and 18 sidereal days. These periods are different for GPS and GLONASS and for the various session lengths. The observed periods in the spectra are caused by the repeat cycles of the station–satellite geometry.

The GCC time series reveal an interesting systematic for the GLONASS-only solutions. The Z-component of the geocenter shows large periodic variations (of about 30 cm peak-to-peak) and a striking correlation to the elevation angle  $\beta_0$  of the sun above/below the orbital planes. This indicates a correlation of the geocenter Z-component with some of the orbital elements. Experiments showed that the particular selection of parameters related to solar radiation pressure substantially changes the GCC variations in Z-direction. An inspection of the error characteristics of the estimated orbital elements did, however, not explain the coupling mechanism, despite the fact that the errors of the orbital elements show a strong correlation with angle  $\beta_0$ , as well.

The comparison of the UT1-UTC estimates with the IERS C04 pole series shows a different behavior for GPS and GLONASS. The parameters drift continuously away from the IERS C04 series if GPS is involved. The GLONASS-only results drift in the same direction as the GPS solutions in the first year and then the reconstructed UT1-UTC series slowly approach the IERS C04 values again. The polar coordinates  $x_p$  and  $y_p$  do not show any periodic variations specific to the different session lengths.

In summary, the best coordinate and orbit solutions are obtained from the combined analysis of GPS and GLONASS observations. Both systems profit from the combined analysis, although GLONASS benefits significantly more than GPS. This finding is supported by the validation of the different orbits with SLR measurements. We consider the quality of the combined GPS/GLONASS solutions as very promising and are encouraged to consequently follow the combined multi-GNSS analysis approach when striving for highest accuracy.



**Part IV**  
**Appendices**



## A Tables

**Table A.1:** Bernese GPS Software Version 6 program overview. Changes w. r. t. the old Version 5 are marked in gray (deleted, new, or rewritten programs).

Program name	F77	F90	Year	Purpose/remark
Transfer and conversion part				
ABBO2N		•	2003	Convert old station abbreviation table to new format
ATX2PCV		•	2007	Convert ANTEX to BSW format
BV3RXN	•		1989	Convert BSW broadcast data to RINEX
BV3RXO	•		1989	Deleted; replaced by OBSRNX
CCRINEXG	•		1997	Cut/concatenate GLONASS RINEX navigation files
CCRINEXN	•		1990	Cut/concatenate GPS RINEX navigation files
CCRINEXO	○ →	•	1990	Cut/concatenate RINEX observation files
CCRNXC		•	2000	Combine/manipulate RINEX clock data
CHOPRE		•	2001	Convert CHAMP orbit format to SP3
CPFSP3		•	2005	Convert SLR CPF format to SP3
FMTOBS		•	2002	Convert observation files from ASCII to binary format
FMTRES		•	1999	Convert residual files from ASCII to binary format
FMTSTD	•		1991	Convert BSW standard orbits from ASCII to binary
IRV2STV		•	2005	Convert IRV or precise orbits to state vectors
LEOAUX		•	2000	Read/convert CHAMP auxiliary file
NEQ2ASC		•	1998	Convert NEQ files between ASCII and binary format
NEQ2NQ0		•	1998	Deleted; obsolete
NEQFMT	•		1993	Deleted; obsolete
OBSFMT		•	2002	Convert binary observation files to ASCII format
OBSO2N		•	2006	Convert observation files from V 5 to V 6 format
OBSRNX		•	2010	Create RINEX files from binary observation files
PHCCNV	•		1996	Convert phase center corrections to BSW format
POEPRE		•	2002	Deleted; obsolete
QLRINEXO		•	2003	Convert SLR quick-look format to RINEX
RESFMT		•	1999	Convert binary residual files to ASCII
RNX2STA		•	2003	Extract station information from RINEX files
RNXOBS		•	2007	Create BSW binary observation files from RINEX
RXMBV3	•		1989	Convert RINEX meteo data to BSW format
RXNBV3	•		1989	Convert RINEX broadcast data to BSW format
RXNPRES	•		1997	Convert GPS/GLONASS broadcast files to SP3 format
RXOBV3	•		1989	Deleted; replaced by RNXOBS
SATFCNV		•	2005	Downgrade satellite info file from new to old format

*continued on next page*

Table A.1: Bernese GPS Software Version 6 program overview (*continued*).

Program name	F77	F90	Year	Remark
SIGO2N		•	2001	Upgrade old sigma and FIX files to new format
SNX2NQ0		•	1998	Convert SINEX files to NEQ format
SNX2SLR		•	2009	Extract SLR information from SINEX files
SNX2STA		•	2003	Extract station information from SINEX files
SP3CPF		•	2005	Create CPF file from SP3
STA2STA		•	2010	Convert between station information file formats
STAMERGE		•	2007	Merge station information files
STAO2N		•	2003	Upgrade old station information file to new format
STDFMT	•		1991	Convert binary standard orbit format to ASCII
TBLO2N		•	2001	Extract station information from translation tables
TROTRO		•	2001	Manipulation of troposphere SINEX files
Orbit part				
BRDTAB	•		1987	Transform broadcast to tabular orbits
BRDTST	•		1988	Check broadcast orbits
CCPREORB	•		1994	Concatenate SP3 orbit files
DEFXTR	•		1992	Summarize ORBGEN output
KINPRE		•	2002	Create SP3 file from kinematic positions
ORBCMP	•		1992	Comparison of different SP3 files
ORBGEN	•		1987	Generate/update standard orbits
POLUPD	•		1994	Reformat/update pole files
POLXTR	•		1992	Extract continuous pole from series of single files
PRETAB	•		1986	Convert SP3 format to tabular orbits
PREWEI	•		1994	Change accuracy codes in SP3 files
SATCLK	•		1988	Extract satellite clocks from broadcast files
SATGRA	○ → •		1988	Visualize satellite observations
STDDIF	•		1988	Compare standard orbit files
STDELE	•		1995	Compare osculating elements
STDPRE	•		1986	Create SP3 file from standard orbits
Data Processing				
ADDNEQ2		•	1997	Combination of NEQ files
CLKEST	○ → •		1999	Interpolate clock corrections
CODSPP	○ → •		1987	Code-based clock synchronization, single-point positioning
CODXTR	•		1995	Summarize CODSPP output
ERPEST	•		1997	Analyze pole files
GPSEST	○ → •		1987	Parameter estimation and NEQ file creation
GPSXTR	○ → •		1992	Summarize ADDNEQ2 and GPSEST outputs
IONEST	○ → •		1988	Estimate ionosphere models
LEOKIN		•	1999	Deleted; obsolete
MAUPRP	•		1988	Phase preprocessing
MPRXTR	•		1992	Summarize MAUPRP output
OBSSMT		•	2008	Smooth code observations, clean data

*continued on next page*

**Table A.1:** Bernese GPS Software Version 6 program overview (*continued*).

Program name	F77	F90	Year	Remark
RNXSMT	•		1996	Deleted; replaced by OBSSMT
SNGDIF	○ → •		1987	Form single-difference observations
Simulation part				
GPSSIM	•		1988	Deleted; replaced by SIMOBS
SIMOBS		•	2007	Simulate observation data
Service part				
AMBCHK	•		1994	Compare resolved ambiguities
BASLST		•	2001	Create lists of baselines
CHGHED		•	2000	Change header of observation files
CODCHK	•		1988	Deleted; obsolete
COMPAR	•		1989	Compare series of station coordinate files
COOSYS	•		1989	Helmert transformation of coordinates
COOVEL	•		1992	Propagate coordinates with velocity field
CRDMERGE		•	2003	Merge station coordinate and velocity files
ETRS89	•		1996	Transform coordinates to ETRS89 system
FODITS		•	2010	Find outliers and discontinuities in time series
HELMR1	•		1988	Helmert transformation between coordinate files
MKCLUS		•	2002	Create clusters of observation files
NUVELO	•		1996	Compute NUVEL1/1A velocities
OBSSPL	•		1989	Split observation files
POLINT	•		1995	Concatenate pole information
QLRSUM		•	2003	Create SLR summary
RCVTST		•	2002	Assess receiver performance
REDISP		•	2001	Display residuals
RESCHK		•	2000	Detect misbehaving stations and satellites
RESRMS	○ → •		1993	Find outliers in observation residuals
RNXGRA	○ → •		1992	Create simple graphics from RINEX observation files
SATMRK		•	2002	Mark observations in observation files
SUBDIF	•		1998	Compare sub-daily pole models
VELDIF	•		1992	Compare velocity files
Auxiliary programs				
MENUAUX		•	2000	Interface program to GUI
GETKEY		•	2000	BPE utility program
GTALLKEY		•	2000	BPE utility program
PUTKEYW		•	2001	BPE utility program
SETDAY	•		1990	BPE utility program
SETWEEK	•		1993	BPE utility program
STA2ID		•	2001	BPE utility program

**Table A.2:** Tracking stations and data completeness (stations with a data availability < 75% are marked in gray).

Station name	Data availability (in %)			
	2008	2009	2010	Overall
ADIS 31502M001	77	39	81	66
ALIC 50137M001	70	97	96	88
ANKR 20805M002	66	97	99	87
ASPA 50503S006	0	55	100	52
AZCO 49454M001	54	85	96	78
BAKO 23101M002	83	92	83	86
BARH 49927S001	95	100	96	97
BJCO	0	71	98	56
BRST 10004M004	48	99	99	82
CAGZ 12725M004	92	98	99	96
CAS1 66011M001	4	96	95	65
CASC 13909S001	81	100	98	93
COCO 50127M001	0	63	99	54
CONZ 41719M002	100	100	99	100
CPXF 49642S001	95	76	67	79
CRAR 66001M004	99	99	99	99
CTWN	39	90	98	76
DARW 50134M001	81	91	92	88
DAV1 66010M001	0	97	96	64
DLFT 13502M006	100	100	100	100
ETAD 31503M001	86	72	25	61
FAA1 92201M012	99	99	100	99
FFMJ 14279M001	97	100	100	99
FUNC 13911S001	72	100	100	91
GANP 11515M001	99	100	100	100
GLSV 12356M001	97	100	99	99
GODZ 40451M123	66	100	96	87
GUUG 82301M001	0	50	96	50
HERT 13212M010	100	100	99	100
HOB2 50116M004	6	98	96	67
HOFN 10204M002	100	100	100	100
HYDE 22307M001	98	99	93	97
IDDR 49451M001	55	88	85	76
IRKJ 12313M002	100	99	99	99
JPLV	81	95	93	90
KHAJ 12361M001	99	100	99	99
KIRO 10422M001	100	100	100	100
KOUR 97301M210	96	99	98	98
LAMA 12209M001	100	100	99	100
LHAZ 21613M002	99	96	99	98
LPAL 81701M001	48	100	98	82

*continued on next page*

---

**Table A.2:** Tracking stations and data completeness (*continued*).

Station name	Data availability (in %)			
	2008	2009	2010	Overall
MOSE 12772M001	100	97	99	99
MAL2 33201M003	45	95	100	80
MALA 13443M001	37	95	98	77
MAR6 10405M002	100	100	100	100
MARS 10073M008	43	96	97	79
MAS1 31303M002	48	100	98	82
MAW1 66004M001	0	94	94	63
MCCJ	95	94	99	96
MTKA 21741S002	98	90	95	94
NICO 14302M001	55	98	100	84
NOVM 12367M002	100	100	99	100
NTUS 22601M001	94	83	96	91
NURK 34001M001	7	99	90	65
OH13 66008M006	99	99	100	99
ONSA 10402M004	100	100	100	100
ORID 15601M001	93	93	98	95
PARK 50108M001	98	99	99	99
PDEL 31906M004	72	100	99	90
POVE 41628M001	48	100	94	81
RCMN 33203M001	88	86	85	86
REUN 97401M003	22	65	100	62
REYK 10202M001	96	100	98	98
ROSA 41632M001	68	97	91	85
SALU 41640M001	45	100	85	77
SAVO 41643M001	47	98	91	79
SOFI 11101M002	100	99	92	97
SUUR 10601M001	96	98	99	98
SYDN 50124M003	98	99	98	98
TERU 13487M001	62	98	99	86
THU2 43001M002	99	100	99	99
TIXJ 12360M002	99	43	80	74
TN22 49450M001	96	100	99	98
TOW2 50140M001	25	99	93	72
TSEA 49448S001	88	90	95	91
TXES 49512M001	83	73	24	60
UFPR 41610M002	46	99	94	80
UNBJ 40146M002	100	100	100	100
URUM 21612M001	29	95	100	75
VALA 13463M002	77	93	100	90
VFCH 10046M001	49	99	79	76
VILO 10424M001	100	100	93	98
VISO 10423M001	100	100	100	100

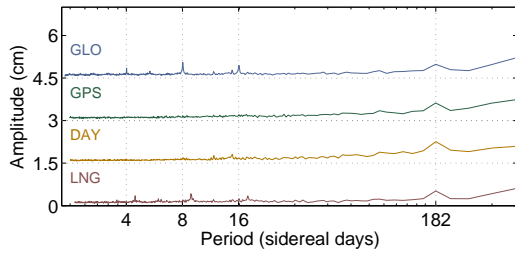
---

*continued on next page*

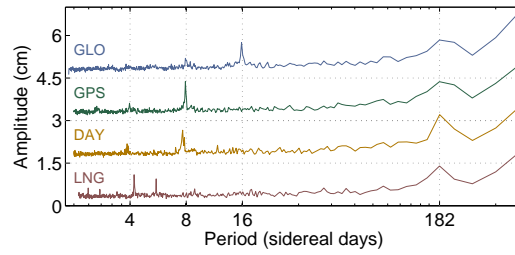
**Table A.2:** Tracking stations and data completeness (*continued*).

Station name	Data availability (in %)			
	2008	2009	2010	Overall
VTSP 49449M001	95	100	100	98
WHIT 40136M001	0	58	100	53
WTZJ 14201M012	99	100	82	94
WTZR 14201M010	99	100	99	99
WTZZ 14201M014	100	100	100	100
XMIS 50183M001	43	98	96	79
YAR3 50107M008	83	95	97	92
ZIM2 14001M008	100	100	100	100
ZIMJ 14001M006	98	100	80	93

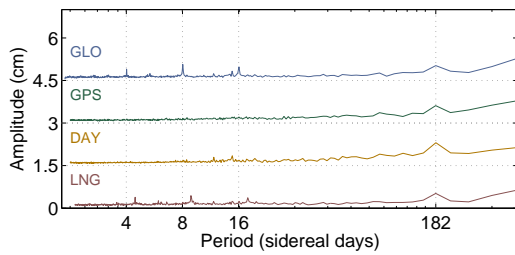
## B Figures



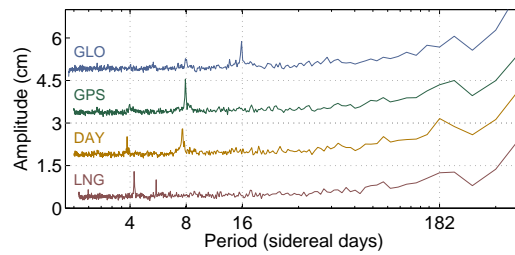
(a) GPS satellites, solution CMB.



(b) GLONASS satellites, solution CMB.



(c) GPS satellites, solution NEQ.



(d) GLONASS satellites, solution NEQ.

**Figure B.1:** Stacked amplitude spectra of 3-D position overlap differences for all four session lengths (solutions CMB and NEQ).

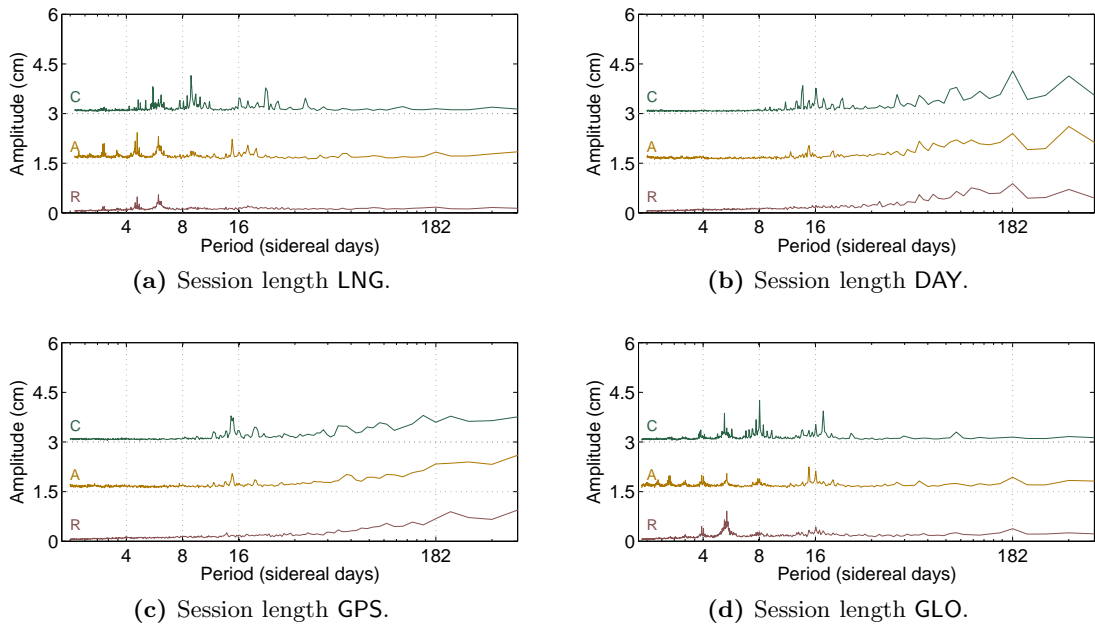


**Figure B.2:** Stacked amplitude spectra of GPS-only orbit overlap differences in radial (R), along-track (A), and cross-track (C) directions.

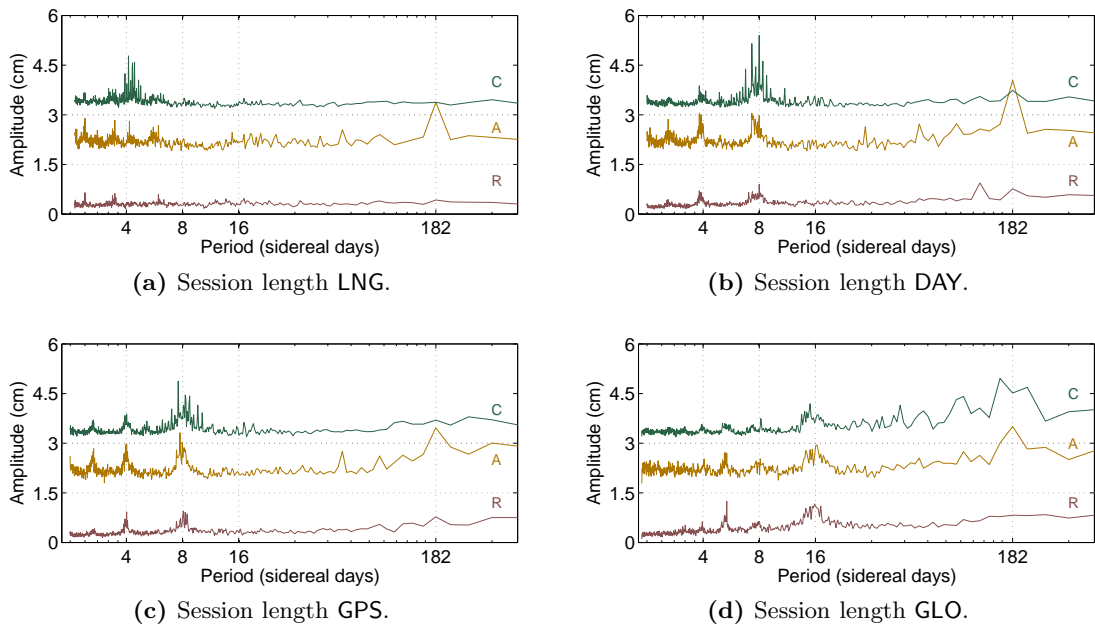


**Figure B.3:** Stacked amplitude spectra of GLONASS-only orbit overlap differences in radial (R), along-track (A), and cross-track (C) directions.

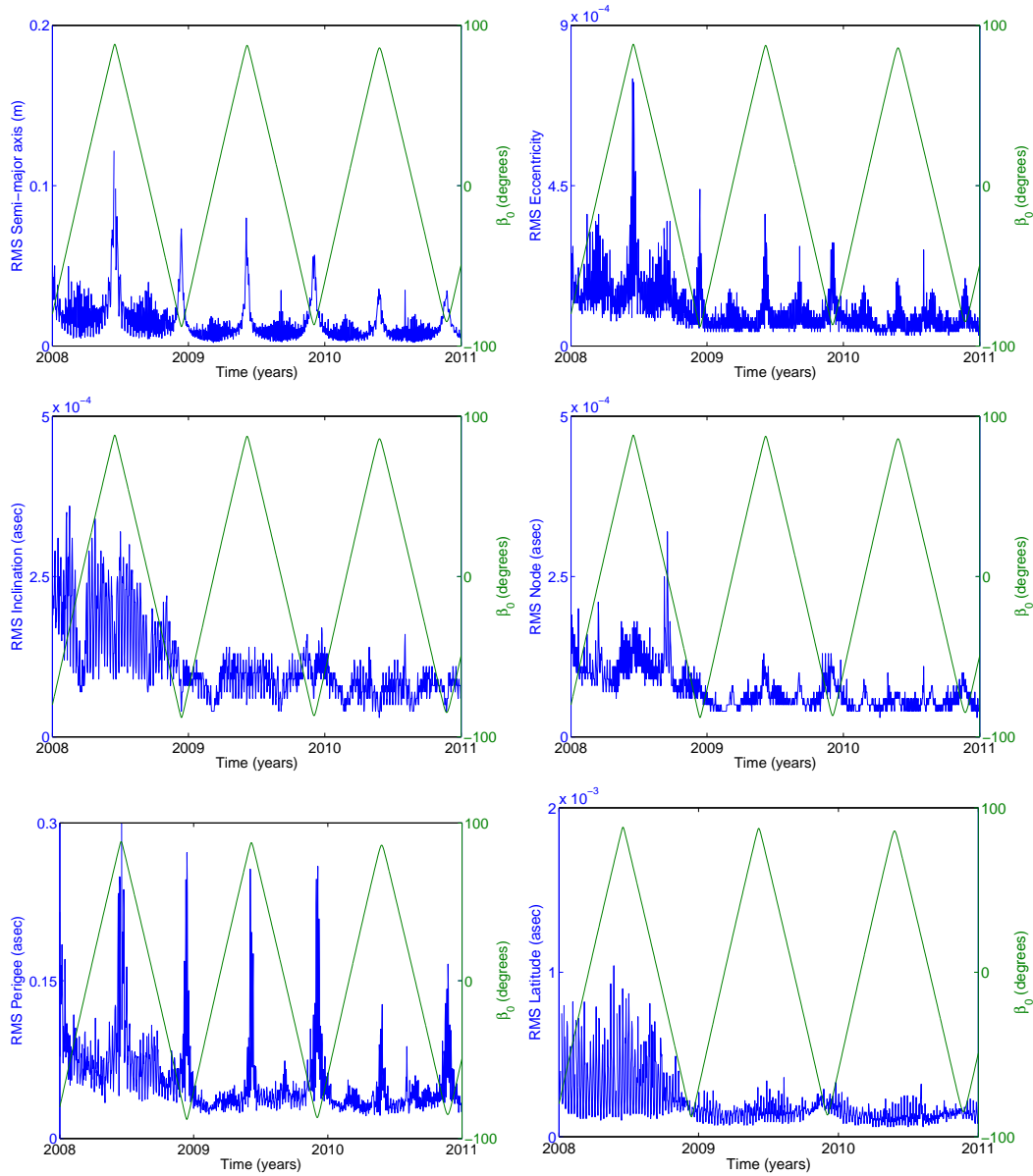


**Figure B.4:** RMS errors of the 6 orbital elements ( $a$ ,  $e$ ,  $i$ ,  $\Omega$ ,  $\omega$ ,  $u_0$ ) and elevation  $\beta_0$  of the Sun above the orbital plane (satellite R20, GLONASS-only solution, 24-hours session length).

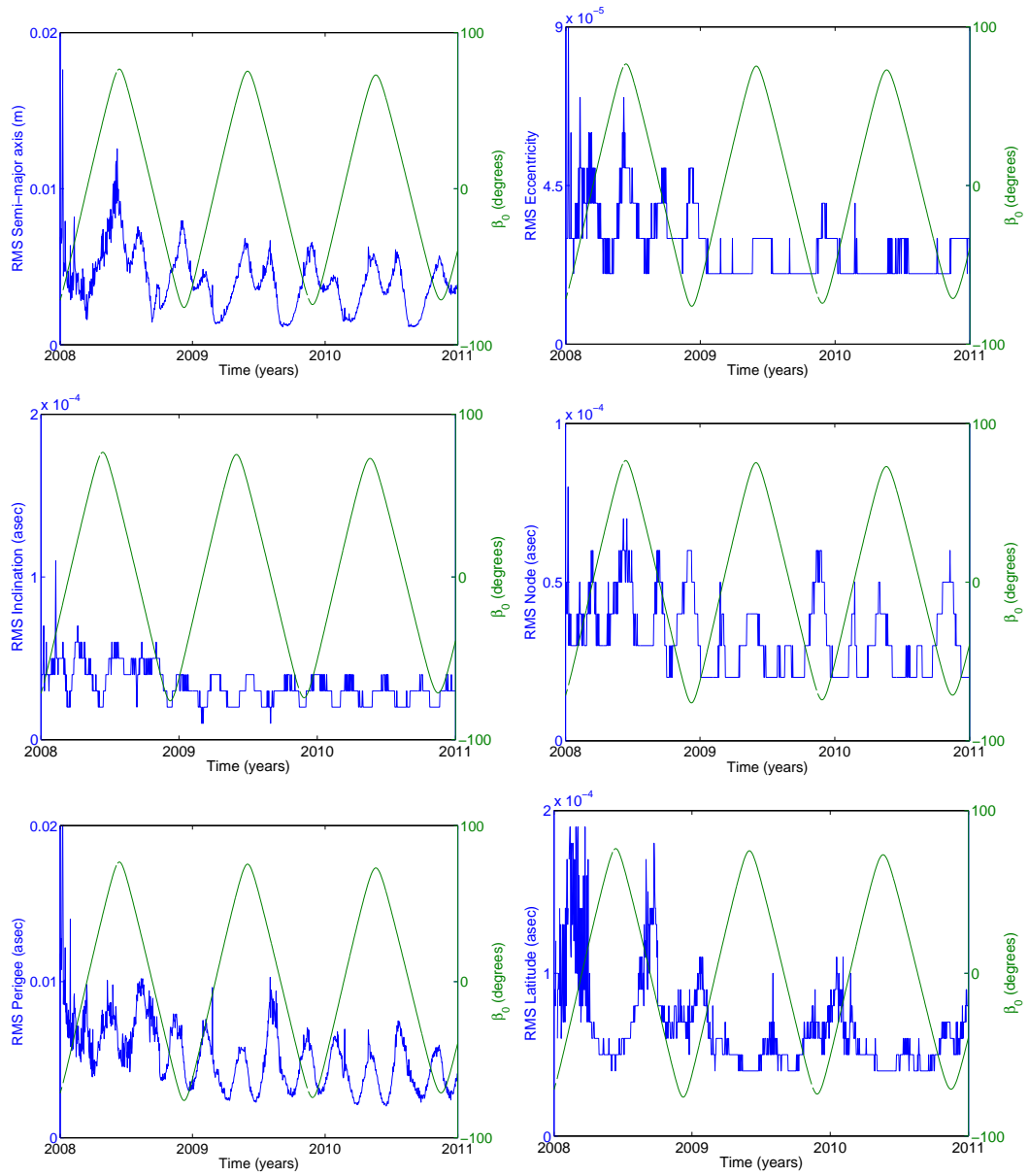


**Figure B.5:** RMS errors of the 6 orbital elements ( $a$ ,  $e$ ,  $i$ ,  $\Omega$ ,  $\omega$ ,  $u_0$ ) and elevation  $\beta_0$  of the Sun above the orbital plane (satellite G06, GPS-only solution, 24-hours session length).

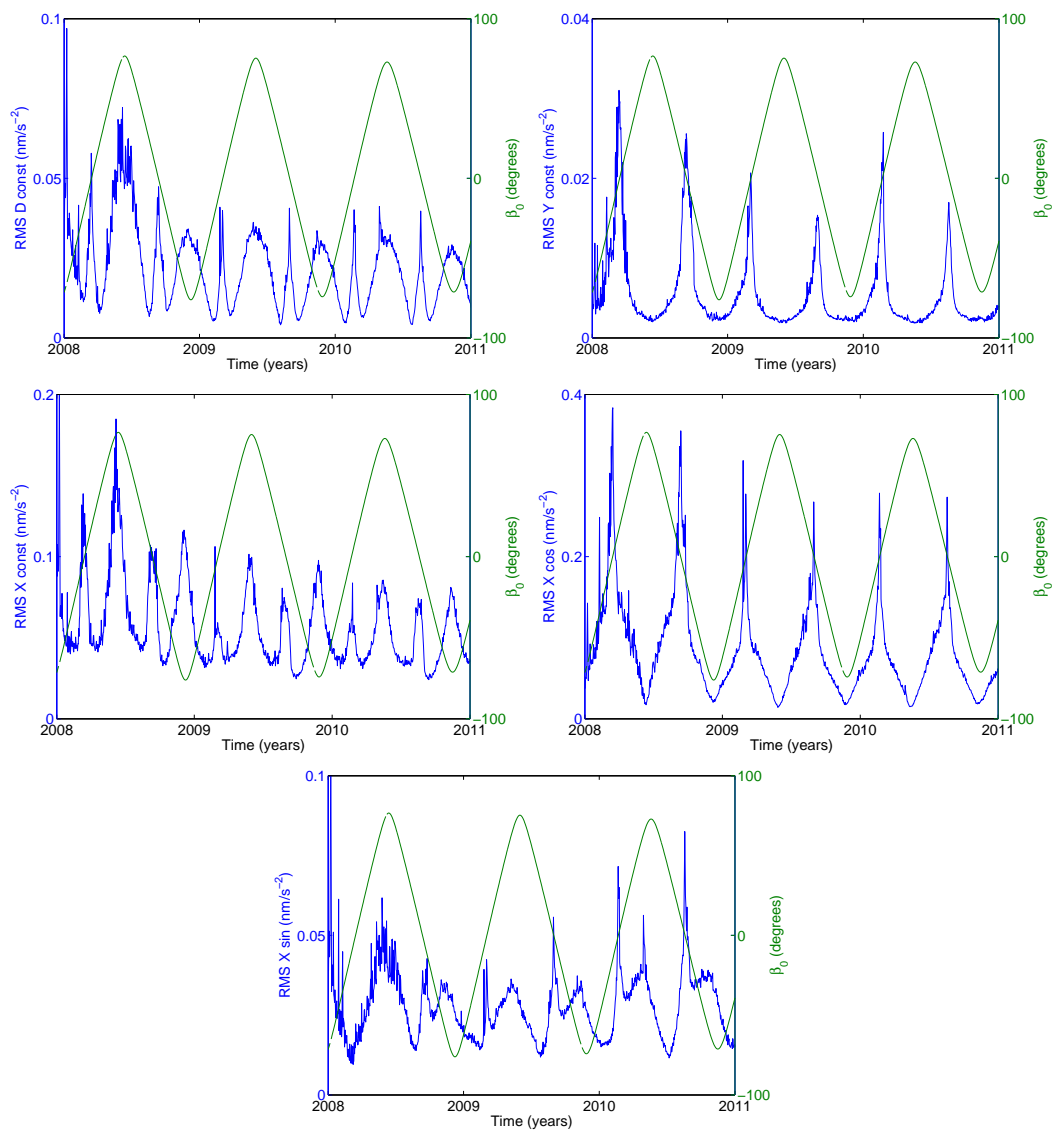


**Figure B.6:** RMS errors of the 5 dynamical parameters ( $D_0$ ,  $Y_0$ ,  $X_0$ ,  $X_c$ ,  $X_s$ ) and elevation  $\beta_0$  of the Sun above the orbital plane (satellite G06, GPS-only solution, 24-hours session length).

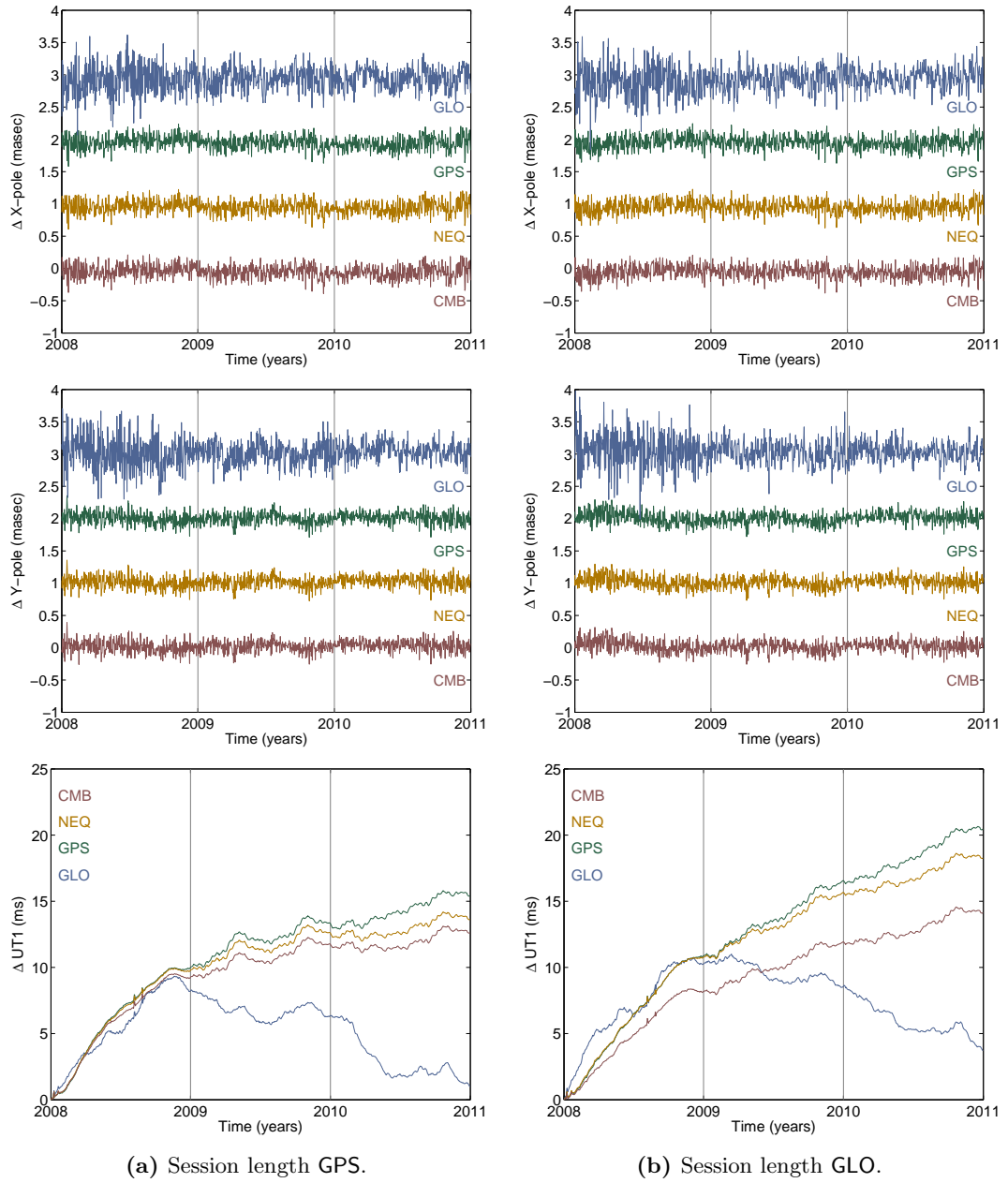


**Figure B.7:** Difference of ERPs to IERS C04 (from top: X-pole, Y-pole, UT1-UTC) for session lengths GPS and GLO.

## Bibliography

- ANSI (1978), *American National Standard programming language, FORTRAN: ANSI X3.9-1978*, American National Standards Institute, available at <http://www.ansi.org> (accessed June 2011).
- ANSI (1992), *American National Standard for programming language, FORTRAN—extended: ANSI X3.198-1992*, American National Standards Institute, available at <http://www.ansi.org> (accessed June 2011).
- Ashby, N. (2003), Relativity in the Global Positioning System, *Living Reviews in Relativity*, **6**(1), <http://www.livingreviews.org/lrr-2003-1> (accessed June 2011).
- Ballard, A. H. (1980), Rosette Constellations of Earth Satellites, *IEEE Transactions on Aerospace and Electronic Systems*, **16**(5), 656–673.
- Banville, S., R. Santerre, M. Cocard, and R. B. Langley (2008), Satellite and Receiver Phase Bias Calibration for Undifferenced Ambiguity Resolution, in *Proceedings of the 2008 National Technical Meeting of the Institute of Navigation*, pp. 711–719, San Diego, USA.
- Beutler, G. (2005a), *Methods of Celestial Mechanics I: Physical, Mathematical, and Numerical Principles*, Vol. I, Springer-Verlag, Berlin, Germany, ISBN 3-540-40749-9.
- Beutler, G. (2005b), *Methods of Celestial Mechanics II: Application to Planetary System, Geodynamics and Satellite Geodesy*, Vol. II, Springer-Verlag, Berlin, Germany, ISBN 3-540-40750-2.
- Beutler, G., D. A. Davidson, R. B. Langley, R. Santerre, P. Vaníček, and D. E. Wells (1984), *Some Theoretical and Practical Aspects of Geodetic Positioning Using Carrier Phase Difference Observations of GPS Satellites*, Vol. 14 of *Mitteilungen der Satelliten-Beobachtungsstation Zimmerwald*, University of Bern, Bern, Switzerland.
- Beutler, G., I. Bauersima, W. Gurtner, and M. Rothacher (1987), Correlations between simultaneous GPS double difference carrier phase observations in the multistation mode: Implementation considerations and first experiences, *Manuscripta Geodaetica*, **12**, 40–44.
- Beutler, G., I. I. Mueller, and R. E. Neilan (1994a), The International GPS Service for Geodynamics (IGS): Development and Start of Official Service on January 1, 1994, *Bulletin Géodésique*, **68**(1), 39–70.

- Beutler, G., E. Brockmann, W. Gurtner, U. Hugentobler, L. Mervart, and M. Rothacher (1994b), Extended Orbit Modeling Techniques at the CODE Processing Center of the International GPS Service for Geodynamics (IGS): Theory and Initial Results, *Manuscripta Geodaetica*, **19**, 367–386.
- Beutler, G., M. Rothacher, S. Schaer, T. A. Springer, J. Kouba, and R. E. Neilan (1999), The International GPS Service (IGS): An Interdisciplinary Service in Support of Earth Sciences, *Advances in Space Research*, **23**(4), 631–653.
- Bilich, A., and K. M. Larson (2009), It's Not All Bad: Understanding and Using GNSS Multipath, *GPS World*, **20**(10), 31–39.
- Blewitt, G., Y. Bock, and J. Kouba (1994), Constructing the IGS Polyhedron by Distributed Processing, in *IGS workshop on Densification of the IERS Terrestrial Reference Frame through regional GPS Networks*, edited by J. F. Zumberge and R. Liu, pp. 21–37, [http://igscb.jpl.nasa.gov/igscb/resource/pubs/zumberge\\_94a.pdf](http://igscb.jpl.nasa.gov/igscb/resource/pubs/zumberge_94a.pdf) (accessed June 2011), 30 November–2 December, 1994, Pasadena, USA.
- Böhm, J., A. Niell, P. Tregoning, and H. Schuh (2006a), Global Mapping Function (GMF): A new empirical mapping function based on numerical weather model data, *Geophysical Research Letters*, **33**(L07304), doi: 10.1029/2005GL025546.
- Böhm, J., B. Werlo, and H. Schuh (2006b), Troposphere mapping functions for GPS and very long baseline interferometry from European Centre for MediumRange Weather Forecasts operational analysis data, *Journal of Geophysical Research*, **111**(B02406), doi: 10.1029/2005JB003629.
- Brockmann, E. (1997), *Combination of Solutions for Geodetic and Geodynamic Applications of the Global Positioning System (GPS)*, Vol. 55 of *Geodätisch-geophysikalische Arbeiten in der Schweiz*, Schweizerische Geodätische Kommission, Zürich, Switzerland.
- Capitaine, N., D. Gambis, D. D. McCarthy, G. Petit, J. Ray, B. Richter, M. Rothacher, M. Standish, and J. Vondrak (eds.) (2002), Proceedings of the IERS Workshop on the Implementation of the New IAU Resolutions, *IERS Technical Note 29*, Observatoire de Paris, Paris, France, available at <http://www.iers.org> (accessed June 2011), April 18–19, 2002, Paris, France.
- Dach, R., U. Hugentobler, P. Fridez, and M. Meindl (eds.) (2007), *Bernese GPS Software Version 5.0*, Astronomical Institute, University of Bern, Bern, Switzerland, <http://www.bernese.unibe.ch/docs/DOCU50.pdf> (accessed June 2011).
- Dach, R., E. Brockmann, S. Schaer, G. Beutler, M. Meindl, L. Prange, H. Bock, A. Jäggi, and L. Ostini (2009), GNSS Processing at CODE: Status Report, *Journal of Geodesy*, **83**(3–4), 353–366, doi: 10.1007/s00190-008-0281-2.
- Dach, R., S. Schaer, S. Lutz, M. Meindl, and G. Beutler (2010), Combining Observations from different GNSS, in *Proceedings of EUREF 2010 Symposium*, June 2–5, 2010, Gävle, Sweden.

- 
- Dong, D., J. O. Dickey, Y. Chao, and M. K. Cheng (1999), Geocenter Variations Caused by Mass Redistribution of Surface Geophysical Processes, *IERS Technical Note*, **25**, 47–54.
- Dong, D., P. Fang, Y. Bock, M. K. Cheng, and S. Miyazaki (2002), Anatomy of apparent seasonal variations from GPS-derived site position time series, *Journal of Geophysical Research*, **107**(B4), doi: 10.1029/2001JB000573.
- Dow, J. M., R. E. Neilan, and C. Rizos (2009), The International GNSS Service in a changing landscape of Global Navigation Satellite Systems, *Journal of Geodesy*, **83**(3–4), 191–198, doi: 10.1007/s00190-008-0300-3.
- Elósegui, P., J. Davis, R. Jaldehag, J. Johansson, A. Niell, and I. Shapiro (1995), Geodesy using the Global Positioning System: The effects of signal scattering on estimates of site position, *Journal of Geophysical Research*, **100**(B6), 9921–9934, doi: 10.1029/2007JB004949.
- Flohrer, C. (2008), *Mutual Validation of Satellite-Geodetic Techniques and its Impact on GNSS Orbit Modeling*, Vol. 75 of *Geodätisch-geophysikalische Arbeiten in der Schweiz*, Schweizerische Geodätische Kommission, Zürich, Switzerland, ISBN 978-3-908440-19-2.
- Gambis, D. (2004), Monitoring Earth orientation using space-geodetic techniques: State-of-the-art and perspective, *Journal of Geodesy*, **78**(4–5), 295–303.
- Ge, M., G. Gendt, M. Rothacher, C. Shi, and J. Liu (2008), Resolution of GPS carrier-phase ambiguities in Precise Point Positioning (PPP) with daily observations, *Journal of Geodesy*, **82**, 389–399, doi: 10.1007/s00190-007-0187-4.
- Görres, B., J. Campbell, M. Becker, and M. Siemes (2006), Absolute calibration of GPS antennas: laboratory results and comparison with field and robot, *GPS Solutions*, **10**(2), 136–145, doi: 10.1007/s10291-005-0015-3.
- Grelier, T., A. Ghion, J. Dantepal, L. Ries, A. DeLatour, J.-L. Issler, J.-Á. Ávila-Rodríguez, S. Wallner, and G. W. Hein (2007), Compass Signal Structure and First Measurements, in *Proceedings of the 20th International Technical Meeting of the Satellite Division of The Institute of Navigation*, pp. 3015–3024, ISBN 978-1-605600-69-7, September 25–28, 2007, Fort Worth, USA.
- Gurtner, W., and L. Estay (2009), RINEX: The Receiver Independent Exchange Format (Version 3.01), <ftp://igs.cb.jpl.nasa.gov/igs/data/format/rinex301.pdf> (accessed June 2011).
- Gurtner, W., and G. L. Mader (1990), Receiver Independent Exchange Format Version 2, *GPS Bulletin of the Commission VIII of the International Coordinates of Space Techniques for Geodesy and Geodynamcis (CSTG)*, **3**(3).

- Gurtner, W., G. Beutler, I. Bauersima, and T. Schildknecht (1985), Evaluation of the GPS carrier difference observations: The BERNESE second generation software package, in *Proceedings 1st International Symposium on Precise Positioning with the Global Positioning System*, edited by C. Goad, US Department of Commerce, Rockville, USA.
- Gurtner, W., R. Noomen, and M.R. Pearlman (2004), The international laser ranging service: current status and future developments, *ASR*, **36**, 327–332.
- Habrich, H. (1999), *Geodetic Applications of the Global Navigation Satellite System (GLONASS) and of GLONASS/GPS Combinations*, Ph.D. thesis, Astronomical Institute, University of Bern, Bern, Switzerland.
- Hein, G.W., J.-Á. Ávila-Rodríguez, S. Wallner, B. Eissfeller, T. Pany, and P. Hartl (2007a), Envisioning a Future GNSS System of Systems, Part 1, *Inside GNSS*, **2**(1), 58–67.
- Hein, G.W., J.-Á. Ávila-Rodríguez, S. Wallner, B. Eissfeller, T. Pany, and P. Hartl (2007b), Envisioning a Future GNSS System of Systems, Part 2, *Inside GNSS*, **2**(2), 64–72.
- Hilla, S. (2010), The Extended Standard Product 3 Orbit Format (SP3-c), <http://igsceb.jpl.nasa.gov/igsceb/data/format/sp3c.txt> (accessed June 2011).
- Hofmann-Wellenhof, B., H. Lichtenegger, and E. Wasle (2008), *GNSS—Global Navigation Satellite Systems: GPS, GLONASS, Galileo & more*, Springer-Verlag, Berlin, Germany, ISBN 978-3-211-73012-6.
- Hugentobler, U., M. Meindl, G. Beutler, H. Bock, R. Dach, A. Jäggi, C. Urschl, L. Mervart, M. Rothacher, S. Schaer, E. Brockmann, D. Ineichen, A. Wiget, U. Wild, G. Weber, H. Habrich, and C. Boucher (2006), CODE IGS Analysis Center Technical Report 2003/2004, in *IGS 2004 Technical Reports*, edited by K. Gowey *et al.*, IGS Central Bureau, Pasadena, USA.
- ICD (2008), *Global Navigation Satellite System (GLONASS) Interface Control Document, Navigational Radiosignal in Bands L1, L2*, 5th ed., Russian Institute of Space Device Engineering, [http://rniikp.ru/en/pages/about/publ/ICD\\_GLONASS\\_eng.pdf](http://rniikp.ru/en/pages/about/publ/ICD_GLONASS_eng.pdf) (accessed June 2011).
- ICD (2010), *European GNSS (Galileo) Open Service: Signal In Space Interface Control Document*, European Union, [http://ec.europa.eu/enterprise/policies/space/files/galileo/galileo\\_os\\_sis\\_icd\\_revised\\_2\\_en.pdf](http://ec.europa.eu/enterprise/policies/space/files/galileo/galileo_os_sis_icd_revised_2_en.pdf) (accessed June 2011).
- IGS (2008), *International GNSS Service Strategic Plan 2008–2012*, IGS Central Bureau, Pasadena, USA, available at <http://www.igs.org> (accessed June 2011).
- ILRS (2004), ILRS Normal Point Format, [http://ilrs.gsfc.nasa.gov/products\\_formats\\_procedures/normal\\_point/np\\_format.html](http://ilrs.gsfc.nasa.gov/products_formats_procedures/normal_point/np_format.html) (accessed June 2011).

- IS-GPS (2010a), *Navstar GPS Space Segment/Navigation User Interfaces, Interface Specification IS-GPS-200*, rev. ed., Science Applications International Corporation, <http://www.gps.gov/technical/icwg/IS-GPS-200E.pdf> (accessed June 2011).
- IS-GPS (2010b), *Navstar GPS Space Segment/User Segment L5 Interfaces, Interface Specification IS-GPS-705*, rev. ed., Science Applications International Corporation, <http://www.gps.gov/technical/icwg/IS-GPS-705A.pdf> (accessed June 2011).
- Kaplan, E. D., and C. J. Hegarty (eds.) (2006), *Understanding GPS: Principles and Applications*, 2nd ed., Artech House Inc., Boston, USA, ISBN 1-58053-894-0.
- Koch, K. R. (1999), *Parameter estimation and hypothesis testing in linear models*, 2nd ed., Springer-Verlag, Berlin, Germany, ISBN 978-3540652571.
- Kouba, J. (2004), Improved relativistic transformations in GPS, *GPS Solutions*, **8**(3), 170–180, doi: 10.1007/s10291-004-0102-x.
- Kouba, J. (2008), Implementation and testing of the gridded Vienna Mapping Function 1 (VMF1), *Journal of Geodesy*, **82**, 193–205, doi: 10.1007/s00190-007-0170-0.
- Langley, R. B. (1999), Dilution of Precision, *GPS World*, **10**(5), 52–59.
- Lyard, F., F. Lefevre, T. Letellier, and O. Francis (2006), Modelling the global ocean tides: modern insights from FES2004, *Ocean Dynamics*, **56**, 394–415, ISSN 1616-7341, doi: 10.1007/s10236-006-0086-x.
- Mader, G. L. (1999), GPS Antenna Calibration at the National Geodetic Survey, *GPS Solutions*, **3**(1), 50–58, doi: 10.1007/PL00012780.
- Mathews, P. M., T. A. Herring, and B. A. Buffet (2002), Modeling of nutation-precession: New nutation series for nonrigid Earth, and insights into the Earth’s interior, *Journal of Geophysical Research*, **107**(B4), doi: 10.1029/2001JB000390.
- McCarthy, D. D., and G. Petit (eds.) (2004), IERS Conventions (2003), *IERS Technical Note 32*, IERS Conventions Centre, Frankfurt am Main, Germany, available at <http://www.iers.org> (accessed June 2011).
- Mervart, L. (1995), *Ambiguity Resolution Techniques in Geodetic and Geodynamic Applications of the Global Positioning System*, Vol. 53 of *Geodätisch-geophysikalische Arbeiten in der Schweiz*, Schweizerische Geodätische Kommission, Zürich, Switzerland.
- Ostini, L., R. Dach, M. Meindl, S. Schaer, and U. Hugentobler (2008), FODITS: A New Tool of the Bernese GPS Software, in *Proceedings of EUREF 2008 Symposium*, edited by J. A. Torres and H. Hornik, June 18–21, 2008, Brussels, Belgium.
- Parkinson, B. W., and S. T. Powers (2010a), The Origins of GPS, *GPS World*, **21**(5), 30–41, available at <http://www.gpsworld.com> (accessed June 2011).
- Parkinson, B. W., and S. T. Powers (2010b), Fighting to Survive, *GPS World*, **21**(6), 8–18, available at <http://www.gpsworld.com> (accessed June 2011).

- Pearlman, M. R., J. J. Degnan, and J. M. Bosworth (2002), The International Laser Ranging Service, *Advances in Space Research*, **30**(2), 135–143, doi: 10.1016/S0273-1177(02)00277-6.
- Petit, G., and B. Luzum (eds.) (2010), IERS Conventions (2010), *IERS Technical Note 36*, IERS Conventions Centre, Frankfurt am Main, Germany, available at <http://www.iers.org> (accessed June 2011).
- Petrie, E. J., M. Hernandez-Pajares, P. Spalla, P. Moore, and M. A. King (2011), A Review of Higher Order Ionospheric Refraction Effects on Dual Frequency GPS, *Surveys in Geophysics*, **32**(3), 197–253, doi: 10.1007/s10712-010-9105-z.
- Petrov, L., and J.-P. Boy (2004), Study of the atmospheric pressure loading signal in Very Long Baseline Interferometry observations, *Journal of Geophysical Research*, **109**(B03405), doi: 10.1029/2003JB002500.
- Ray, J. (2000), New pseudorange bias convention, IGS Mail No. 2744, IGS Central Bureau, March 2000, <http://igscb.jpl.nasa.gov/pipermail/igsmail/2000/002818.html> (accessed June 2011).
- Ray, J., Z. Altamimi, X. Collilieux, and T. van Dam (2008), Anomalous harmonics in the spectra of GPS position estimates, *GPS Solutions*, **12**(1), 55–64, doi: 10.1007/s10291-007-0067-7.
- Ray, R. D., and R. M. Ponte (2003), Barometric tides from ECMWF operational analyses, *Annales Geophysicae*, **21**(8), 1897–1910, doi: 10.5194/angeo-21-1897-2003.
- Rebischung, P. (2011), Upcoming switch to IGS08/igs08.atx, IGS Mail No. 6354, IGS Central Bureau, March 2011, <http://igscb.jpl.nasa.gov/pipermail/igsmail/2011/006346.html> (accessed June 2011).
- Rothacher, M. (1992), *Orbits of Satellite Systems in Space Geodesy*, Vol. 46 of *Geodätisch-geophysikalische Arbeiten in der Schweiz*, Schweizerische Geodätische Kommission, Zürich, Switzerland.
- Rothacher, M., and G. Mader (2003), Receiver and Satellite Antenna Phase Center Offsets and Variations, in *Towards Real-Time: Network, Data, and Analysis Centre 2002 Workshop, Proceedings*, edited by P. Tétreault *et al.*, pp. 141–152, IGS Central Bureau, Pasadena, USA, [http://igs.org/igscb/resource/pubs/02\\_ott/session\\_8.pdf](http://igs.org/igscb/resource/pubs/02_ott/session_8.pdf) (accessed June 2011).
- Rothacher, M., and D. Thaller (2006), SINEX Version 2.02, IERS Message No. 103, IERS Central Bureau, available at <http://www.iers.org> (accessed June 2011).

- Rothacher, M., W. Gurtner, S. Schaer, R. Weber, W. Schlüter, and H. O. Hase (1996), Azimuth- and Elevation-Dependent Phase Center Corrections for Geodetic GPS Antennas Estimated from GPS Calibration Campaigns, in *GPS Trends in Precise Terrestrial, Airborne, and Spaceborne Applications*, Vol. 115 of *IAG Symposium*, edited by G. Beutler *et al.*, pp. 333–338, Springer-Verlag, ISBN 3-540-60872-9.
- Santerre, R. (1991), Impact of GPS Satellite Sky Distribution, *Manuscripta Geodaetica*, **16**, 28–53.
- Schaer, S. (1999), *Mapping and Predicting the Earth's Ionosphere Using the Global Positioning System*, Vol. 59 of *Geodätisch-geophysikalische Arbeiten in der Schweiz*, Schweizerische Geodätische Kommission, Zürich, Switzerland, ISBN 3-908440-01-7.
- Schaer, S., W. Gurtner, and J. Feltens (1998), IONEX: The IONosphere Map EXchange Format Version 1, in *Proceedings of the IGS Analysis Center Workshop*, edited by J. M. Dow *et al.*, pp. 233–247, <ftp://igscb.jpl.nasa.gov/igscb/data/format/ionex1.pdf> (accessed June 2011), February 9–11, 1998, Darmstadt, Germany.
- Schaer, S., R. Dach, and M. Meindl (2008), CODE Analysis Strategy Summary, <http://www.aiub.unibe.ch/download/CODE/CODE.ACN> (accessed June 2011).
- Schaer, S., R. Dach, and S. Lutz (2010), CODE analysis model changes (VMF/HOI), IGS Mail No. 6287, IGS Central Bureau, October 2010, <http://igscb.jpl.nasa.gov/pipermail/igsmail/2010/006279.html> (accessed June 2011).
- Schaer, S. C., E. Brockmann, M. Meindl, and G. Beutler (2009), Rapid Static Positioning Using GPS and GLONASS, in *Proceedings of EUREF 2009 Symposium*, edited by J. Ihde and H. Hornik, May 27–30, 2009, Florence, Italy.
- Schmid, R., and R. Khachikyan (2010), Update: *rcvr\_ant.tab*, *antex14.txt*, IGS Mail No. 6259, IGS Central Bureau, September 2010, <http://igscb.jpl.nasa.gov/pipermail/igsmail/2010/006250.html> (accessed June 2011).
- Schmid, R., and M. Rothacher (2003), Estimation of elevation-dependent satellite antenna phase center variations of GPS satellites, *Journal of Geodesy*, **77**(7–8), 440–446, doi: 10.1007/s00190-003-0339-0.
- Springer, T. A. (2000), *Modeling and Validating Orbits and Clocks Using the Global Positioning System*, Vol. 60 of *Geodätisch-geophysikalische Arbeiten in der Schweiz*, Schweizerische Geodätische Kommission, Zürich, Switzerland, ISBN 3-908440-02-5.
- Springer, T. A., and R. Dach (2010), GPS, GLONASS and More, *GPS World*, **21**(6), 48–58, <http://www.nxtbook.com/nxtbooks/questex/gps0610/index.php#/44> (accessed June 2011).

- Tapley, B. D., M. M. Watkins, J. C. Ries, G. W. Davis, R. J. Eanes, S. R. Poole, H. J. Rim, B. E. Schutz, C. K. Shum, R. S. Nerem, F. J. Lerch, J. A. Marshall, S. M. Klosko, N. K. Pavlis, and R. G. Williamson (1996), The Joint Gravity Model 3, *Journal of Geophysical Research*, **101**(B12), 28029–28049.
- Teunissen, P. J. G., and A. Kleusberg (eds.) (1998), *GPS for Geodesy*, 2nd ed., Springer-Verlag, Berlin, Germany, ISBN 3-540-63661-7.
- Thaller, D. (2008), Inter-technique combination based on homogeneous normal equation systems including station coordinates, Earth orientation and troposphere parameters, *Scientific Technical Report STR08/15*, Deutsches GeoForschungsZentrum, available at <http://www.gfz-potsdam.de> (accessed June 2011).
- Walford, J. (2010a), Leica GRX1200 GG Pro Receivers, IGS Station Mail No. 3684, IGS Central Bureau, April 2010, <http://igs.cb.jpl.nasa.gov/pipermail/igsstation/2010/002828.html> (accessed June 2011).
- Walford, J. (2010b), Leica GRX1200 GG Pro Receivers - resolution, IGS Station Mail No. 3699, IGS Central Bureau, April 2010, <http://igs.cb.jpl.nasa.gov/pipermail/igsstation/2010/002842.html> (accessed June 2011).
- Walker, J. G. (1971), Some Circular Orbit Patterns Providing Continuous Whole Earth Coverage, *Journal of the British Interplanetary Society*, **24**, 369–384.
- Walker, J. G. (1984), Satellite Constellations, *Journal of the British Interplanetary Society*, **37**, 559–571.
- Wu, J. T., C. Wu, G. A. Hajj, W. I. Bertiger, and S. M. Lichten (1993), Effects of antenna orientation on GPS carrier phase, *Manuscripta Geodaetica*, **18**, 91–98.

**“Geodätisch-geophysikalische Arbeiten in der Schweiz”**  
**(Fortsetzung der Publikationsreihe “Astronomisch-geodätische Arbeiten in der Schweiz”)**  
**der Schweizerischen Geodätischen Kommission ([www.sgc.ethz.ch](http://www.sgc.ethz.ch))**

- 61 2001 Spatial and Temporal Distribution of Atmospheric Water Vapor using Space Geodetic Techniques. Lars Peter Kruse, 128 Seiten.
- 62 2001 Solar Spectrometry for Determination of Tropospheric Water Vapor. Bernd Sierk, 212 Seiten.
- 63 2001 Analysis of refraction influences in geodesy using image processing and turbulence models. Philipp Flach, 175 Seiten.
- 64 2003 INS/GPS Integration for Pedestrian Navigation. V. Gabaglio, 161 Seiten.
- 65 2003 Efficient Methods for Determining Precise Orbits of Low Earth Orbiters Using the Global Positioning System. Heike Bock, 214 Seiten.
- 66 2003 Capteurs et Algorithmes pour la Localisation Autonome en Mode Pédestre. Quentin Ladetto, 121 Seiten.
- 67 2004 GPS based Determination of the Integrated and Spatially Distributed Water Vapor in the Troposphere. Marc Troller, 172 Seiten.
- 68 2005 Geodetic Mobile Solar Spectrometer. Alexander Somieski, 205 Seiten.
- 69 2005 Absolute Airborne Gravimetry. Henri Baumann, 142 Seiten.
- 70 2006 The *Swiss Trolley* – A Modular System for Track Surveying. Ralph Glaus, 184 Seiten.
- 71 2006 Development of a Robotic Mobile Mapping System by Vision-Aided Inertial Navigation: A Geomatics Approach. Fadi Atef Bayoud, 157 Seiten.
- 72 2007 Das neue Landeshöhennetz der Schweiz LHN95. Andreas Schlatter, 373 Seiten.
- 73 2007 Pseudo-Stochastic Orbit Modeling of Low Earth Satellites Using the Global Positioning System. Adrian Jäggi, 214 Seiten.
- 74 2008 Cartographie Mobile en Temps Réel. Hervé Gontran, 162 Seiten.
- 75 2008 Mutual Validation of Satellite-Volume 75 Geodetic Techniques and its Impact on GNSS Orbit Modeling. Claudia Flohrer, 198 Seiten.
- 76 2009 High-resolution GPS tomography in view of hydrological hazard assessment. Simon Lutz, 202 Seiten.
- 77 2009 Trajectory Determination and Analysis in Sports by Satellite and Inertial Navigation. Adrian Wägli, 175 Seiten.
- 78 2009 GPS Based Dynamic Monitoring of Air Pollutants in the City of Zurich. Philippe Kehl, 156 Seiten.
- 79 2010 In-flight Quality Assessment and Data Processing for Airborne Laser Scanning. Philipp Schaer, 166 Seiten.
- 80 2010 Sea Surface Topography and Marine Geoid by Airborne Laser Altimetry and Shipborne Ultrasound Altimetry. Philippe Limpach, 207 Seiten.
- 81 2010 Global Gravity Field Determination Using the GPS Measurements Made Onboard the Low Earth Orbiting Satellite CHAMP. Lars Prange, 213 Seiten.
- 82 2011 Analysis of long-term GPS observations in Greece (1993-2009) and geodynamic implications for the Eastern Mediterranean. Michael D. Müller, 186 Seiten.
- 83 2011 Combined Analysis of Observations from Different Global Navigation Satellite Systems. Michael Meindl, 150 Seiten.